UNIVERSITY OF CALIFORNIA

Los Angeles

Parametric Study of Liquid Contact Line Dynamics: Adhesion vs. Hydrodynamics

A dissertation submitted in partial satisfaction

of the requirements for the degree

Doctor of Philosophy in Aerospace Engineering

by

Alireza Mohammad Karim

2015

ABSTRACT OF THE DISSERTATION

Parametric Study of Liquid Contact Line Dynamics: Adhesion vs. Hydrodynamics

by

Alireza Mohammad Karim

Doctor of Philosophy in Aerospace Engineering

University of California, Los Angeles, 2015

Professor Hossein Pirouz Kavehpour, Chair

There are tremendous interests regarding the wettability of solid surfaces and controlling the wettability on the solid surfaces in industry, technology such as efficiency of oil recovery, micro-fluidics and nano-fluidics, drag reduction on airplane wings, efficient power plants and many other applications. To resolve such challenges, it is required to enhance the knowledge more deeply to understand the underlying physics of fluid/solid interaction at the liquid contact line that describes the dynamics of spreading.

Hence, in this research, experimental techniques have been performed to investigate parametric study about the dynamics of the liquid contact line (i.e. three-phase contact line) with consideration on molecular-kinetic theory (which concentrates on the adhesion of molecules at

the vicinity of the liquid contact line) and the hydrodynamics theory (which focuses on the bulk motion of the liquid on the solid surface).

Over half a century, there have been many experimental/numerical investigations of the moving contact line in forced and spontaneous spreading. Surprisingly, there have been no experimental studies comparing these for the same solid/liquid/vapor system. In the present research such experiments have been performed on identical liquid-solid systems. It has been found out that there exists a huge distinction between experimental results obtained from spontaneous and forced spreading. For spontaneous spreading, excellent agreement has been found using the hydrodynamics theory, as expected. For forced spreading it was shown that hydrodynamic theory does not apply, but instead the molecular-kinetic theory does. This distinction between spontaneous and forced systems has never been noted before. Moreover, this research has provided a hypothesis for predicting the more appropriate model to describe the contact line dynamics for spontaneous and forced systems.

The forced spreading dynamics on low-energy surfaces (i.e. hydrophobic, ultra-hydrophobic glass surfaces, and micro-textured Teflon surfaces) has been investigated. The dynamics of spreading of several Polyethylene Glycol/Water (PEG/water) mixtures, with different weight ratios signifying the effect of the viscous force on spreading, on Teflon substrates (i.e. hydrophobic surfaces), ultra-hydrophobic sprayed glass substrates, and micro-textured Teflon plates have been investigated using Wilhelmy plate method with Tensiometer. It has been found out that spreading dynamics of the PEG/water mixtures on hydrophobic surfaces, ultra-hydrophobic glass surfaces, and micro-textured Teflon substrates are described more appropriately with molecular-kinetic theory.

The wettability of emulsions is a prominent factor with a broad impact in an extensive variety of industrial applications ranging from the petroleum to cosmetic industries. Surprisingly, there is no comprehensive study of emulsion spreading to date. In this research, the spreading of water/silicone oil emulsions on glass substrates was investigated. The time dependent variation of dynamic contact angle, base diameter, and the spreading rate of the emulsion droplets were studied. The effect of water/silicone oil weight percentage as well as the droplet size and dispersed phase bubble size were also investigated. The weight percentage of water/silicone oil emulsion and droplet size did not have a significant impact on the spreading dynamics; however the dispersed phase bubble size affected the spreading dynamics substantially. The coarsening of the dispersed phase bubbles was the key factor in the distinct spreading behavior of emulsions compared to pure liquids.

The only disadvantage of the Tensiometer is the fact of neglecting the viscous force in force measurement method applied on the plate's surface during advancing and receding motion in the pool of highly viscous liquid. This neglect makes the Tensiometer to loose its extent of flexibility for being used for experiments with highly viscous liquids and for large liquid contact line speeds. To address this challenge, a viscous model for dynamic contact angle measurement using force-balance method with Tensiometer has been proposed.

The dissertation of Alireza Mohammad Karim is approved.

Joseph M. Teran

Chang-Jin Kim

Jeffrey D. Eldredge

Hossein Pirouz Kavehpour, Committee Chair

University of California, Los Angeles

2015

This PhD dissertation is lovingly dedicated to my mother, Shayesteh Torabi.

Without your continuous support, encouragement, and love,

I never would have been able to accomplish my goals.

TABLE OF CONTENTS

LIST OF FIGURES

LIST OF TABLES

ACKNOWLEDGEMENTS

I would like to express my great and sincere appreciation to my adviser, Professor H. Pirouz Kavehpour, for his priceless advice and support in every step during the coarse of my PhD study in both my research and my future career path. I am so grateful to Professor Kavehpour for his inspiration, which made me motivated in the field of fluid mechanics since I took the fundamental course in fluid mechanics at UCLA with him. I am so thankful for his precious advices, which have helped me to become an independent research scientist. I also would like to appreciate Professor Kavehpour for his unrelenting effort to find me the necessary support to go through my PhD study.

I also would like to appreciate Professor Jeff Eldredge, Professor C. J. Kim, and Professor Joseph Teran for serving as my PhD committee members. I am also very grateful to Professor Robert Shahram Shaefer for his emotional support and his valuable advice since beginning of my study at UCLA as an undergraduate student until now.

Words are not able to express the level of my appreciation to my parents for all their encouragement and support in every aspect of my life thus far. Without your consistent encouragement, inspirations and prayers I would not be able to go through any of the steps pursuing my education. I consider myself the most fortunate person to have you in my life.

I would like to thank Angie Castillo, Abel Lebon, Samantha Becker, Evgenia Grigorova, Lance Kono, Annie Lee, Miguel Lozano, and Duy Dang for all their administrative/technical services.

I would like to thank all my friends: Mohsen Chitsaz, Farshid Roumi, Mahshid Roumi, Ayaboe Edoh, Hai Le, Rommina Vedad Ghavami, Gabriela Bran-Anleu, Sammy Houssainy, Elaheh Alizadeh Birjandi which have made my student life enjoyable.

VITA

1998: High School Diploma, Danesh High School, Tehran, Iran;

1999:Pre-University Diploma, Shahid Avini Pre-University, Tehran, Iran;

2001-2004: Student, Saddleback Community College, Mission Viejo, CA;

2004-2007: Undergraduate Student, Mechanical and Aerospace Engineering Department, University of California, Los Angeles (UCLA), Los Angeles, CA;

2007: B.S. (Mechanical Engineering), UCLA.

2007-2008: Graduate Student, Graduate Aeronautical Laboratory California Institute of Technology (CALCIT), Californian Institute of Technology (Caltech), Pasadena, CA.

2008: M.S. (Aerospace Engineering), Caltech.

2009-2010: Graduate Research Assistant, GALCIT, Caltech;

2010-2011: Research Assistant, Department of Geology and Planetary Science, Caltech;

2011-2015: Graduate Student Researcher, Complex Fluids and Interfacial Physics Laboratory, Department of Mechanical and Aerospace Engineering (MAE Department), UCLA;

2012-2015: Teaching Assistant/Associate/Fellow, MAE Department, UCLA, taught Elementary Fluid Mechanics, Fluid Mechanics and Aerodynamics Laboratory, Introduction to Computer-Aided Design and Drafting, and Basic Mechanical Engineering Laboratory.

2014: M.S. (Mechanical Engineering), UCLA.

PUBLICATIONS

A. Mohammad Karim and H. P. Kavehpour "Spreading of Emulsions on a Solid Substrate" *J. Coat. Technol. Res.,* **11** (1): 103-108, 2014; A. Mohammad Karim and H. P. Kavehpour "Dynamics of Spreading on Ultra-hydrophobic Surfaces" *J. Coat. Technol. Res.,* **12** (5): 959-964, 2015; A. Mohammad Karim, J. P. Rothstein, and H. P. Kavehpour "Partial Wetting on

Rough Surfaces" *J. Fluid Mech.*, 2015 (In preparation); A. Mohammad Karim, S. H. Davis, and H. P. Kavehpour "Forced vs Spontaneous Spreading of Liquids" *Langmuir*, 2015 (Submitted).

CONFERENCE PROCEEDINGS

A. Mohammad Karim and H. P. Kavehpour "Spreading of Emulsions on Glass Substrates" *65th Annual Meeting of the American Physical Society Division of Fluid Dynamics*, San Diego, CA, 2012; A. Mohammad Karim and H. P. Kavehpour "Spreading of Emulsions on Solid Substrate" *The 16th International Coating Science and Technology Symposium*, Atlanta, GA, 2012; A. Mohammad Karim, J. Kim, J. Rothstein, and H. P. Kavehpour "Dynamics of Wetting of Ultra-hydrophobic Surfaces" *66th Annual Meeting of the American Physical Society Division of Fluid Dynamics*, Pittsburgh, PA, 2013; A. Mohammad Karim and H. P. Kavehpour "Spreading of Emulsions on a Solid Substrate" *SO CAL FLUIDS VIII*, UCLA, Los Angeles, CA, 2014; A. Mohammad Karim and H. P. Kavehpour "Parametric Study of the Dynamics of Partial Wetting" *The 17th International Coating Science and Technology Symposium*, San Diego, CA, 2014; A. Mohammad Karim and H. P. Kavehpour "Laws of spreading: why Tanner, Hoffman, Voinov, Cox and de Gennes were wrong, generally speaking" *67th Annual Meeting of the American Physical Society Division of Fluid Dynamics*, San Francisco, CA, 2014.

HONORS AND AWARDS

Saddleback College: Dean's Honor List, Fall 2002 and Spring 2004; President's Honor List, Spring 2002, Fall 2002, Fall 2003; Student of the Year in the Division of Science, Math and Engineering, 2004; National Dean's List, 2005; Mathematics Scholarship, 2004.

UCLA: Engineering Dean's Honor List, Spring 2005; The Boeing Outstanding Undergraduate Student Award, 2006; Tau Beta Pi Engineering Honor Society member, 2005-present.

Caltech: The JPL (Jet Propulsion Laboratory) Space Fellowship, 10/2007-06/2008.

CHAPTER 1

Introduction

Wettability of solid surfaces and controlling the wettability on the solid surfaces has extensive variety of applications in industry, technology, and nature. We face with different sorts of examples of the spreading of liquids on solid surfaces in daily life in both small scales and large scales [1]. At small scales, wettability has important effect in ink-jet printing, microfluidics and nanofluidics, etc [1]. Some of prominent roles of wettability in industry and technology at large scales are in efficient oil recovery, painting, drag reduction on air-plane wings, efficient satellite communications, increasing the efficiency of power plants, increasing the effect of the pesticides depositing on the leaves, etc [1]. Wettability has also an important role in nature such as walking of water striders on the water, self-cleaning effect of the lotus leaves, etc. These broad applications require enhancing our insight on the area of wettability.

To be able to obtain to enhance the knowledge in the area of spreading, it is prominent to investigate deeply on the physics of spreading and enrich the insight on the dynamics of spreading which can enable us to control the wettabiliby of solid surfaces for achieving goals in response to the demands in technology and industry that have been just mentioned. Despite to this broad spectrum of roles of spreading phenomena in every aspect of our daily life, there have

not been sufficient investigations on the dynamics of spreading of liquids on solid surfaces.

The present work considers on the dynamics of spreading using experimental tools. Attention is given to the available models of spreading dynamics that are hydrodynamics theory and molecular-kinetic theory by looking deeply on the validity of their applications in the area of spreading dynamics for different mechanisms of spreading and wide range of choices of solid surfaces and liquids.

1.1 Spreading Phenomena

Spreading phenomena is the process of displacement of one fluid (e.g. generally a liquid phase) over another fluid (e.g. generally a gas phase) on a solid surface until the energy of the total surface area of the system of the solid/liquid/gas reaches the minimum value [1,2]. Once the liquid droplet is deposited on the solid surface forms a line, where liquid phase, solid phase, and vapor phase coexist simultaneously. This line is called three-phase contact line or liquid contact line or contact line.

When a pure liquid droplet is deposited on a solid substrate, it spreads until it reaches the thermodynamic equilibrium state [2,3]. Based on the mechanical point of view, the equilibrium state of liquid on a solid substrate is reached when the forces applied on the three-phase contact line (where all three phases of solid, liquid, and vapor coexist) are balanced. When the liquid droplet reaches its equilibrium state on the solid surface where the velocity of three-phase contact line (i.e. liquid contact line) is zero, the liquid droplet forms a spherical cap on the solid surface. Here, at the three-phase contact line (i.e. liquid contact line), the equilibrium contact angle (θ_0), that is the angle between the liquid/vapor interface and solid/liquid interface forms as

shown in figure 1.1. The equilibrium contact angle (θ_0) can be measured at the three-phase (Solid/Liquid/Vapor) boundary line by considering the balance of forces being applied at the three-phase contact line. These forces at the three-phase contact line are the interfacial tensions of solid/liquid (σ_{SL}), solid/vapor (σ_{SV}), and liquid/vapor (σ_{LV}). The balance of interfacial forces at the liquid contact line was first formulated by Thomas Young [2].

$$\sigma_{SV} = \sigma_{SL} + \sigma_{LV}\cos\theta_0 \tag{1.1}$$

Equation 1.1 shows the force balance for describing the equilibrium condition of a small, axi-symmetric sessile liquid drop on a flat, horizontal, smooth, homogeneous, isotropic, and rigid solid surface [2].

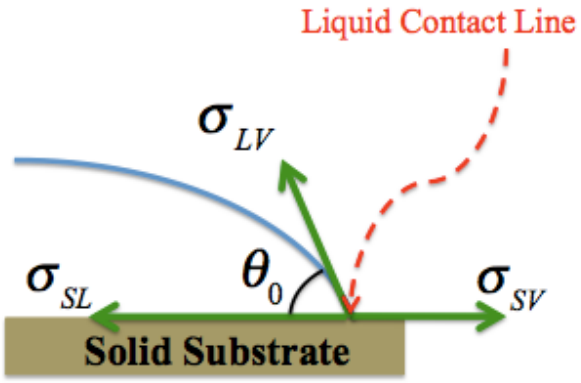

Figure 1.1: Schematic representation of droplet sitting on a solid substrate with interfacial forces acting on it forming contact angle at the three-phase contact line (i.e. liquid contact line) [2].

Based on the thermodynamics point of view, Gibbs' theoretical analysis [4] and Johnson analysis [5] introduced the relation between equilibrium contact angle and the Helmholtz free

energy per unit surface areas of interfaces (e.g. solid/liquid, liquid/vapor, solid/vapor) by applying the principle of minimization of free energy of the interfaces.

$$\cos\theta_0 = \frac{\left(\gamma_{SV} - \gamma_{SL}\right)}{\gamma_{LV}} \tag{1.2}$$

where γ_{SV}, γ_{SL}, and γ_{LV} are Helmholtz free energy per unit surface area for solid/vapor, solid/liquid, and liquid/vapor interfaces, respectively. The equation 1.2 relating the equilibrium contact angle to interfacial tensions, Helmholtz free energy of interfaces, does not describe the hysteresis of the spreading [6].

During the spreading of liquid on the solid substrate (i.e. the liquid contact line moves on the solid surface), the angle that is formed at the three-phase contact line (i.e. liquid contact line) is called the dynamic contact angle. Spreading dynamics of liquid mixtures (e.g. Newtonian or non-Newtonian) on solid surfaces can be described by instantaneous measurement of the dynamic contact angle at the three-phase contact line of the solid/liquid/vapor interface and then describing the dynamic contact angle dependency to the three-phase contact line velocity. The spreading of liquid on solid surface can be controlled with application of some sort of external force at the three-phase contact line to move in two directions (e.g. forward direction of motion of the liquid contact line and backward direction of motion of the liquid contact line). When the liquid contact line advances on the solid surface then the motion of liquid on the solid surface to wet the solid surface is called the advancing motion. When the liquid contact line recedes on the solid surface to dewet (i.e. unwet) the solid surface, the motion of liquid on the solid surface is called the receding motion. The dynamic contact angle for the advancing motion of the liquid contact line is called the advancing dynamic contact angle (θ_A) and the dynamic contact angle for the receding motion of the liquid contact line is called the receding dynamic contact angle

(θ_R). When the liquid reaches equilibrium state from the advancing motion where the liquid contact line velocity becomes zero, the equilibrium contact angle is called the advancing equilibrium contact angle (θ_{0A}). When the liquid reaches the equilibrium state from the receding motion where the liquid contact line velocity is zero, the equilibrium contact angle is called the receding equilibrium contact angle (θ_{0R}). The advancing equilibrium contact angle and the receding equilibrium contact angle are not necessarily the same. The equilibrium contact angle can be any value between its maximum value (i.e. the advancing equilibrium contact angle) and its minimum value (i.e. the receding equilibrium contact angle) on the solid surface. Figure 1.2 illustrates the definition of the advancing equilibrium contact angle and the receding equilibrium contact angle based on the dependency of dynamic contact angle to the three-phase contact line velocity during the advancing motion and the receding motion.

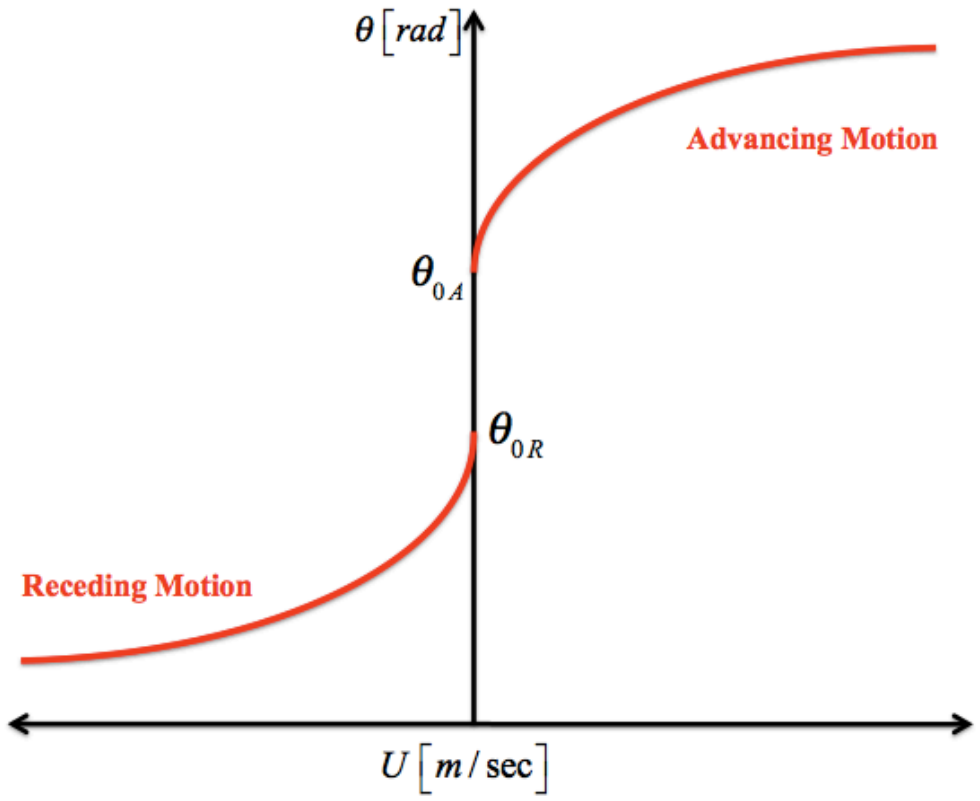

Figure 1.2: Schematic plots of dynamic contact angle versus liquid contact line velocity for the advancing motion and the receding motion of liquid contact line.

The difference between the value of the advancing equilibrium contact angle and the value of the receding equilibrium contact angle is defined as the contact angle hysteresis. Contact angle hysteresis physically signifies the range of values of equilibrium contact angles that liquid droplet can have on a solid surface once achieving to the equilibrium state [7]. The contact angle hysteresis is due to the hysteresis of the solid surface. Contact angle hysteresis can be generally created by chemical heterogeneities and/or physical heterogeneities [8]. Physical causes of contact angle hysteresis can be due to surface roughness, surface heterogeneities, existence of pores and asperities, molecular orientation, or surface strain of the solid substance [8]. The contact angle hysteresis can also be caused by other phenomena like chemical heterogeneities of

the surface, dissolution, adsorption, desorption, or some other non-equilibrium phenomena which fall into chemical causes [7,8]. Contact angle hysteresis is created due to meta-stable states [7]. If contact angle hysteresis does not change based on repeated upward-downward motion of a solid plate into and out of a pool of liquid during contact angle measurement (e.g. advancing and receding using a Tensiometer), it can signify that the contact angle hysteresis is only due to surface roughness or surface heterogeneity [7]. Random vibrations can also effect on the advancing and the receding dynamic contact angle measurements [7] and the contact angle hysteresis. Contact angle hysteresis can be shown in the following forms relating the advancing equilibrium contact angle, θ_{0A}, and the receding equilibrium contact, θ_{0R}, as illustrated by equations 1.3 [9]:

$$\Delta\theta = \theta_{0A} - \theta_{0R} \tag{1.3a}$$

$$\Delta\cos\theta = \cos\theta_{0R} - \cos\theta_{0A} \tag{1.3b}$$

$$H = \frac{\left(\theta_{0A} - \theta_{0R}\right)}{\theta_{0A}} \tag{1.3c}$$

In equation 1.3c, the reduced hysteresis, H, is defined by Kumagai et al. [10].

Kumagai et al. [10] remarked that the contact angle hysteresis is an intrinsic parameter to describe the liquid-solid interactions [9]. They have also concluded that the reduced hysteresis shows the unique value for a solid surface with no dependency to the liquid in contact with the solid [9]. They have also remarked that contact angle hysteresis is mostly dependent to the chemical interactions and the geometric/chemical heterogeneities.

1.2 Mechanisms of Spreading

Spreading mechanisms are generally divided in to two categories, which are spontaneous (i.e. free) spreading and forced spreading. For the spontaneous (free) spreading mechanism, the liquid is spreading on solid surface without any external forces applied on the liquid contact line. In contrast to spontaneous spreading, forced spreading mechanism is performed by forcing the three-phase contact line to move on the solid surface with application of some form of external force(s) which can be hydrodynamics force or mechanical force. In forced spreading, there are two directions of motion of the liquid contact line (i.e. three-phase contact line), which are the advancing motion of the liquid contact line (e.g. wetting the solid surface) and the receding motion of the contact line (e.g. dewetting of the solid surface). Based on the forced spreading, the direction of motion of the liquid contact line and also the speed of motion of the liquid contact line can be controlled hence the wettability can be controlled.

1.3 Types of Wetting Based on the Spreading Parameter, S

There are two types of wetting of liquids on solid surfaces. These two types of wetting can be characterized through determining the value of energy of surface of the solid/liquid/vapor system. The parameter that defines these two types of wetting for the solid/liquid/vapor system is the so-called spreading parameter, S. Spreading parameter signifies the energy difference of the surface when the solid surface is wet compared to the case when the solid surface is dry as shown in equation 1.4 [11].

$$S = \left\{ E_{solid\ surface} \right\}_{dry} - \left\{ E_{solid\ surface} \right\}_{wet} \tag{1.4}$$

Also the spreading parameter can be defined based on the interfacial tensions of solid/liquid, liquid/vapor, and solid/vapor as shown in equation 1.5 [11].

$$S = \sigma_{SV} - \left(\sigma_{SL} + \sigma_{LV}\right) \tag{1.5}$$

1.3.1 Partial Wetting Regime

If the value of the spreading parameter is negative (i.e. $S < 0$), it is called partial wetting. In partial wetting regime, the liquid droplet forms an spherical cap on the solid surface with a finite non-zero equilibrium contact angle [11].

1.3.2 Total Wetting Regime

If the value of the spreading parameter is negative (i.e. $S > 0$), it is called total wetting. In total wetting regime, the liquid droplet completely spreads on the solid surface forming a thin liquid film on the solid surface [11].

1.4 Wettability of Solid Surfaces

Based on the spreading parameter, the solid surfaces are divided into two main categories that are called “High-energy” surfaces and “Low-energy surfaces” [11]. High-energy surfaces such as metals consist of molecules with large-energy chemical bonds (e.g. metallic bonds, ionic bonds, covalent bonds) between them [11]. Hence any types of liquids spread completely on high-energy surfaces. In contrast, low-energy surfaces such as plastics and Teflon plates are composed of molecules with low-energy chemical bonds. Hence liquids spread partially on low-energy surfaces [11].

The characteristic of the solid surfaces can be also described based on their wettability with water. Doing this is by measuring the equilibrium contact angle of water droplet on the solid surface. The solid surfaces can be characterized into three categories based on the equilibrium contact angle of water droplet on them. Solid surfaces, which make an equilibrium contact angle less than 90^o with water droplet, are called hydrophilic surfaces. Solid surfaces, which make an equilibrium contact angle between 90^o and 120^o with water, are called hydrophobic surfaces. Solid surfaces, which make an equilibrium contact angle beyond 120^o with water, are called ultra-hydrophobic surfaces (i.e. super-hydrophobic surfaces). Figure 1.3 illustrates the shapes of water droplet on hydrophilic, hydrophobic, and ultra-hydrophobic surfaces.

(a)

(b)

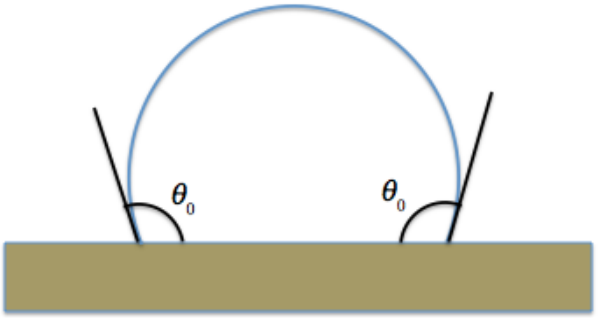

(c)

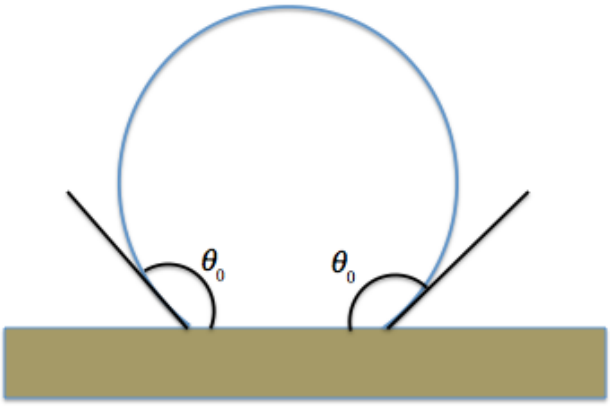

Figure 1.3: Water droplet at equilibrium state on (a) a hydrophilic surface ($\theta_0 < 90^o$), (b) a hydrophobic surface ($90^o < \theta_0 < 110^o$), and (c) an ultra-hydrophobic surface ($\theta_0 > 110^o$).

1.5 Stick-Slip Behavior

In hydrophobic surfaces and ultra-hydrophobic surfaces, sometimes the spreading of a liquid droplet on a solid surface can be observed by a specific behavior of the motion of the three-phase contact line called “Stick-Slip” behavior [8]. In ”Stick-Slip” behavior, a liquid droplet’s radius remains the same for most of the time (e.g. no motion of the three-phase boundary line) during the spreading, and then its radius increases in a very short time (e.g. suddenly motion of the three-phase boundary line in the form of jumping from one position to a new position in a very short time) [8]. This dynamical behavior of the liquid spreading can be seen when a liquid droplet is sliding on an inclined surface, during volume addition or volume reduction of the droplet during its spreading on a horizontal solid surface, and during the evaporation of the liquid droplet during its spreading on a horizontal solid surface. Shanahan [8] has done theoretical investigation on modeling the “Stick-Slip” behavior of the sessile liquid droplet when it is evaporating during its spreading on a solid surface and explained its dynamical behavior in the model. In his model, the liquid droplet height and contact angle decrease while its radius stays the same until the contact angle of liquid droplet reaches to the minimum value. And then the droplet height and droplet contact angle stay the same and the radius of the droplet reduces quickly to the lower value and this cycle repeats again and again [8].

1.6 States of Liquid on an Ultra-hydrophobic Surface

Wenzel [12] has done experimental investigation on describing the state of the liquid droplet on a rough surface to explain the effect of roughness of the solid surface on the wettability of solid surface and he concluded that the physical condition of the solid surface has a prominent

impact on the wettability of the solid surface [12]. Figure 1.4 illustrates the schematic shape of a liquid droplet on a rough surface based on the Wenzel model.

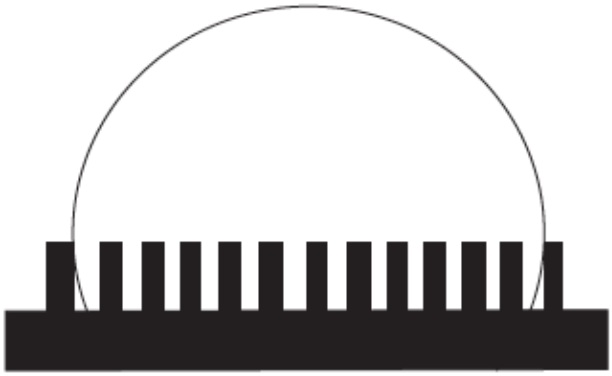

Figure 1.4: Wenzel model for describing the equilibrium state of a water droplet on a micro-textured surface [12].

Wenzel applied the tilting plate method for measuring the apparent contact angle of liquid on the solid surface using the tilting plate apparatus [12]. Based on his research, he concluded that the wetting characteristic of the solid surface is directly proportional to the roughness of the surface of the solid [12]. Wenzel related the apparent contact angle, θ_{app}, and true Young contact angle, θ_{true}, to the roughness ratio, r, which is the ratio the true surface area of the solid surface to the apparent surface area of the solid surface as illustrated in equation 1.6.

$$\cos\theta_{app} = r\cos\theta_{true} \tag{1.6}$$

Cassie and Baxter have done experimental and theoretical investigations to show the effect of porosity and surface heterogeneities on the measurement of apparent contact angle [13,14].

Cassie and Baxter stated a theoretical model for the state of a liquid droplet on a porous surface and explained that air can be remained to be trapped below the liquid droplet, causing ultra-hydrophobic behavior of the surface. Part of the liquid surface is in contact with air, which can cause shear free surfaces and higher contact angle for the droplet on the porous surface [13,14]. Figure 1.5 illustrates the shape of a liquid droplet at equilibrium state on a rough surface using Cassie-Baxter model as vapor phase trapped under the liquid droplet.

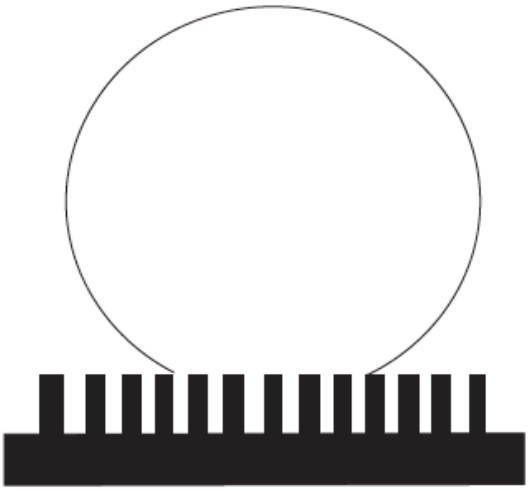

Figure 1.5: Cassie and Baxtor model of the equilibrium state of a water droplet on a micro-textured surface [13,14].

For hydrophobic or very rough surfaces, equation 1.7 shows the relationship between apparent contact angle, θ_{app}, and the Young contact angle, θ_{true}, with effect of the fraction of the solid surface in contact with the liquid, ϕ_s, based on Cassie state of the liquid droplet on ultra-hydrophobic surface [13,14].

$$\theta_{app} = \phi_s \left(1 + \cos\theta_{true}\right) - 1 \tag{1.7}$$

1.7 Methods of Contact Angle Measurement

There have been tremendous attempts to do experimental investigations on measuring dynamic contact angle for forced spreading and spontaneous spreading mechanisms.

Enormous experimental researches have been done using forced spreading methods applying several configurations for measuring dynamic contact angles [7, 15-31]. These configurations of solid/liquid/vapor systems are capillary displacement method [15,16], Wilhelmy plate method in which solid plates immerses/withdraws in the pool of liquid [7], optical method [23,29-31], electro-wetting/electro-dewetting method [26,27], plunge tank configuration method [17,24,28], syringe-needle extrusion coating method [18,25], and rotating cylinders partially immersed in a pool of liquid [19]. In capillary displacement method, the liquid from is forced to move through application of pressure difference between the capillary and pumping the liquid inside the capillary to move in the direction of negative pressure gradient as shown in figure 1.6 [20]. In Wilhelmy plate method (i.e. dip-coating method), the solid substrate is forced to move with specified speed through a pool of liquid as illustrated in figure 1.7 [20-22]. In optical method, the solid substrate such as fiber glass, rod, or solid plate is immersed or withdrawn in the pool of liquid and during these motions, the dynamic contact angles are measured optically using camera focusing on the menisci of the liquid at the three-phase contact line [23]. In electro-wetting/electro-dewetting method, the droplet of liquid is placed through a needle electrode on the solid substrate electrode and then by applying a potential difference between the liquid droplet and the solid substrate, the liquid contact line is forced to move on the solid surface and

then the dynamic contact angle is measured using high-speed camera during the motion of liquid droplet on the solid surface as shown in figure 1.8 [26,27]. In plunge tank configuration, the solid substrate is a continuous plastic film being moved with specified speed through a liquid tank as shown in figure 1.9 [20]. In syringe-needle extrusion coating method, the liquid contact line is forced to move on a solid surface by pumping the liquid through the syringe downward and forcing the liquid droplet formed on the solid surface to get larger and larger as illustrated in figure 1.10 [20]. Figure 1.6 illustrates the schematic pictures of some the methods of dynamic contact angle measurements using forced spreading mechanism.

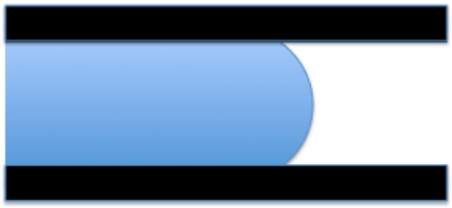

Figure 1.6: Schematic picture of capillary displacement method for forced spreading mechanism [20].

Figure 1.7: Schematic picture of Wilhelmy plate method for forced spreading mechanism [20].

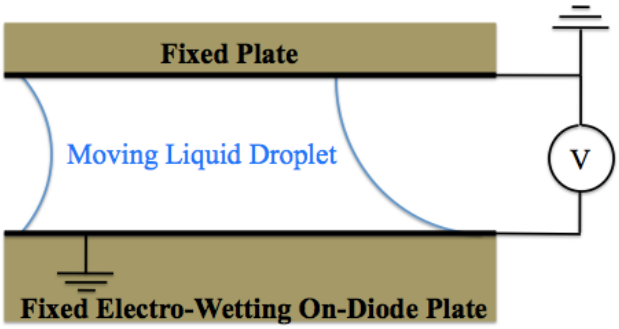

Figure 1.8: Schematic picture of electro-wetting/electro-dewetting method for forced spreading mechanism [20].

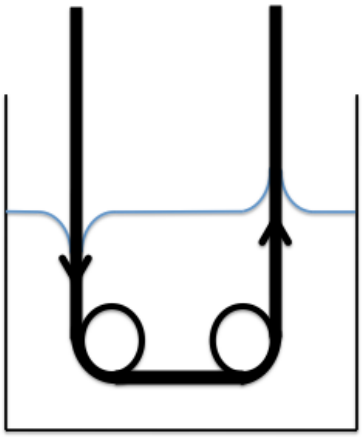

Figure 1.9: Schematic picture of plunge-tank method for forced spreading mechanism [20].

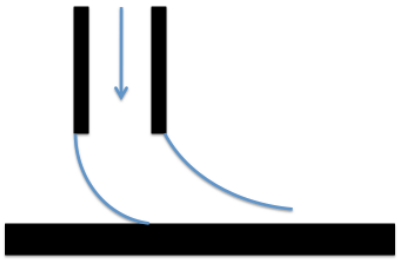

Figure 1.10: Schematic picture of syringe-needle extrusion coating method for forced spreading mechanism [20].

The optical method using goniometric contact angle measurement [25] or drop-shape analyzer (DSA) [32] are common methods to use to investigate on the dynamic contact angle measurement for spontaneous spreading mechanism. Figure 1.11 shows the schematic picture of a typical drop shape analyzer.

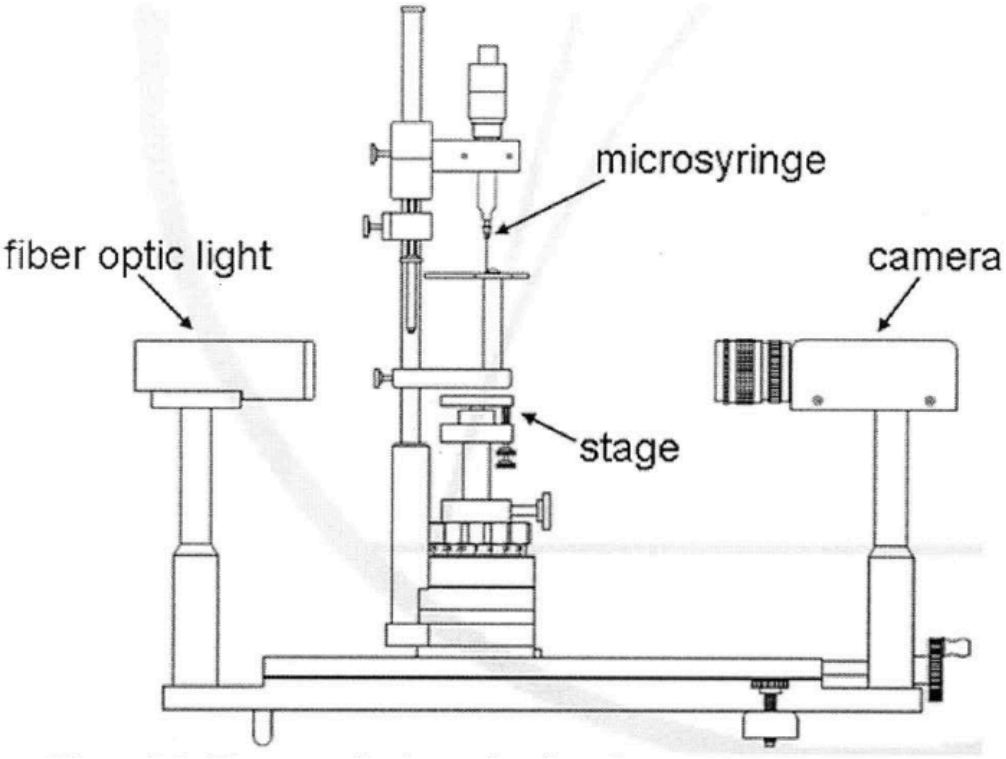

Figure 1.11: Schematic picture of a gomiometer contact angle measurement system [25].

1.8 Spreading Dynamics

The best way to answer to challenges in regards to the wettability of solid surfaces and ability of controlling the wettability can be through research on the dynamics of liquid contact line and study on the dependency of the dynamic contact angle to the liquid contact line velocity [3-152]. Over half a century, there has been a considerable attention on the spreading phenomena both experimentally [7,9-45,47-51,53-57,60,69,76-78,81,84-88,97,98,100,103-111,113-115,117-119,122,124-127,129,132,136,138,140-142,147,152], analytically/theoretically [3-6,8,11,20,22-25,33,45-47,52,53,57-75,77-84,87,88,91,93,96,99,101,107,112,120,121,123,126,128,130,131,133,135,137,139,143,144,146-152], and numerically [11,20,44,77,78,84,89,90,92,94,95,102,116,126,134,135,138,145]. Two fundamental laws have been proposed to describe the dynamics of spreading. First law was based on hydrodynamics theory with focusing on the dynamics of bulk motion of liquid on the solid surface. Based on hydrodynamics theory, for spontaneous spreading of a liquid on a smooth, horizontal, homogeneous solid surface, the radius of the pure liquid droplet has been claimed to vary based on the $1/10^{th}$ power law while spreading on the solid substrate [88]. Equation 1.8 shows the dynamics of liquid contact line motion based on hydrodynamics theory by balancing viscous force with capillary force.

$$R(t) \sim t^{\frac{1}{10}} \tag{1.8}$$

In equation 1.8, R is the instantaneous size of the liquid droplet from the onset of deposition on the solid surface, and t is time.

The dynamic contact angle of the pure liquid droplet spreading on the solid surface follows the Hoffman-Voinov-Tanner (HVT) law [16,70,88], which relates the dynamic contact angle of the droplet to Capillary number during its spreading as shown in equation 1.9.

$$\theta_D^3 \sim Ca = \frac{\mu U}{\sigma} \tag{1.9}$$

In equation 1.9, μ dynamic is viscosity of liquid, σ is surface tension of liquid, and U is velocity of liquid contact line. Equation 1.8 and 1.9 refer to the spreading of liquid on a solid surface where complete wetting occurs (The equilibrium static contact angle goes to zero after complete wetting). Dynamics of spreading for partial wetting regime by considering the effect of non-zero equilibrium contact angle have been also investigated for a long period of time. Universal Hoffmann-Voinov-Tanner (HVT) law [16,70,88] also is applicable to the partial wetting regime by adding the non-zero equilibrium contact angle to the equation 1.9.

Another version of the hydrodynamics theory was proposed by deGennes [73] as it is shown in equation 1.10.

$$\theta_D\left(\theta_D^2 - \theta_0^2\right) = 6\,Ca \ln\left(\frac{L}{L_s}\right) \tag{1.10}$$

In equation 1.10, θ_D is the dynamic contact angle, θ_0 is the equilibrium contact angle, L is the characteristic length, and L_s is the slip length.

Alternative form of the dynamics of spreading was proposed by Cox and Voinov [70,71] as shown in equation 1.11.

$$\theta_D^3 - \theta_0^3 = \pm 9\,Ca \ln\left(\frac{L}{L_s}\right) \tag{1.11}$$

In equation 1.11, the plus sign indicates the advancing motion of the liquid contact line an dthe minus sign indicates the receding motion of the liquid contact line. The details of all these forms of hydrodynamics theory will be explained in chapter 2.

The second fundamental law to describe the dynamics of spreading (i.e. dependency of dynamic contact angle to the velocity of liquid contact line) is called molecular-kinetic theory. Molecular-kinetic theory, which was proposed by Blake and Haynes [67,68], focuses on the molecular attachment/detachment (e.g. molecular hopping) along the liquid contact line region. Molecular-kinetic theory postulates that the total energy dissipation only is due to the friction at the liquid contact line. Molecular-kinetic theory disregards the energy dissipation due to viscous flow of liquid on the solid surface. Molecular-kinetic theory considers solid properties and liquid properties to describe the dynamics of wetting. Equations 1.12a and 1.12b show the dependency of the advancing dynamic contact angle, θ_A , and the receding dynamic contact angle, θ_R , to the velocity of liquid contact line, U , respectively.

$$U = 2K_w \lambda \sinh^{-1}\left(\frac{\sigma \lambda^2 \left(\cos\theta_0 - \cos\theta_A\right)}{2k_B T}\right) \tag{1.12a}$$

$$U = 2K_w \lambda \sinh^{-1}\left(\frac{\sigma \lambda^2 \left(\cos\theta_R - \cos\theta_0\right)}{2k_B T}\right) \tag{1.12b}$$

In equations 1.12a and 1.12b, λ is the average molecular displacement, K_w is the equilibrium frequency of molecular displacement at the liquid contact line, k_B is the Boltzmann constant, σ is the liquid's surface tension, θ_0 is the equilibrium contact angle, and T is the temperature.

The combined molecular-hydrodynamic theory has been proposed by Petrov et al. [60]. The combined molecular-hydrodynamic theory considers the non-hydrodynamic (i.e. molecular-kinetic theory) dependency of equilibrium contact angle to the liquid contact line velocity [60], $\theta_0(U)$, in the equation of spreading dynamics obtained from hydrodynamics theory.

$$\theta_0\left(U\right)=\cos^{-1}\left\{\cos\theta_Y \pm\left(\frac{2k_BT}{\sigma\lambda^2}\right)\sinh^{-1}\left(\frac{U}{2K_w\lambda}\right)\right\} \tag{1.13}$$

In equation 1.13, θ_Y is the Young's static contact angle when the liquid droplet is at stationary condition on the solid surface. The other variables in equation 1.13 have the same definition as they have in equation 1.12. In equation 1.13, the minus sign denotes the advancing motion and the plus sign denotes the receding motion of the liquid contact line.

The combined molecular-hydrodynamic theory can be shown in equation 1.14 [60]:

$$\theta_D^3-\left[\theta_0\left(U\right)\right]^3=\pm 9Ca\ln\left(\frac{L}{L_s}\right) \tag{1.14}$$

In equation 1.14, the plus sign denotes the advancing motion and the minus sign denotes the receding motion of the liquid contact line.

CHAPTER 2

Physical Models for Spreading Dynamics

There are three models that have been applied so far for describing the dynamics of spreading for both spontaneous and forced spreading, which are explained as follows in details. The two fundamental models are molecular-kinetic theory and hydrodynamics theory. The third model is the combination of molecular-kinetic theory and hydrodynamics theory so called “combined theory”. All three models describe the dynamics of spreading by illustrating the dependency of dynamic contact angle to the velocity of liquid contact line. Molecular-kinetic theory is based on the dissipation due to the friction produced by the molecular displacement at the liquid contact line. Hydrodynamics theory is based on the viscous dissipation due to the bulk motion of the liquid. Combined theory considers both dissipation processes for describing the dynamics of spreading. In this chapter the details of these three models will be explained.

2.1 Molecular-Kinetic Theory (MKT)

Molecular-kinetic theory is based on the molecular displacements of the molecules for generally two immisible fluids (e.g. liquid and vapor) on the solid surface due to surface migration or by the contiguous bulk phases [67,68]. On the solid surface, there are n number of adsorption sites where molecules of fluid (e.g. liquid) can attach to or detach from. The distance between centers of two adjacent adsorption sites is defined as λ. The molecular displacements of the molecules of the two fluids (e.g. liquid and vapor) at the vicinity of three-phase contact line are dependent on the amounts of the potential-energy barriers in forward direction of molecular displacement and backward direction of molecular displacement. The frequency of these molecular displacements in forward direction and/or backward direction depend on the magnitudes of energies of these potential-energy barriers. For example, for the forward direction of molecular displacement to be higher than backward direction of molecular displacement, the potential-energy barriers in forward direction of molecular displacement shoud become lowered for the same value of energies of potential-energy barriers in backward directin which should become increased.

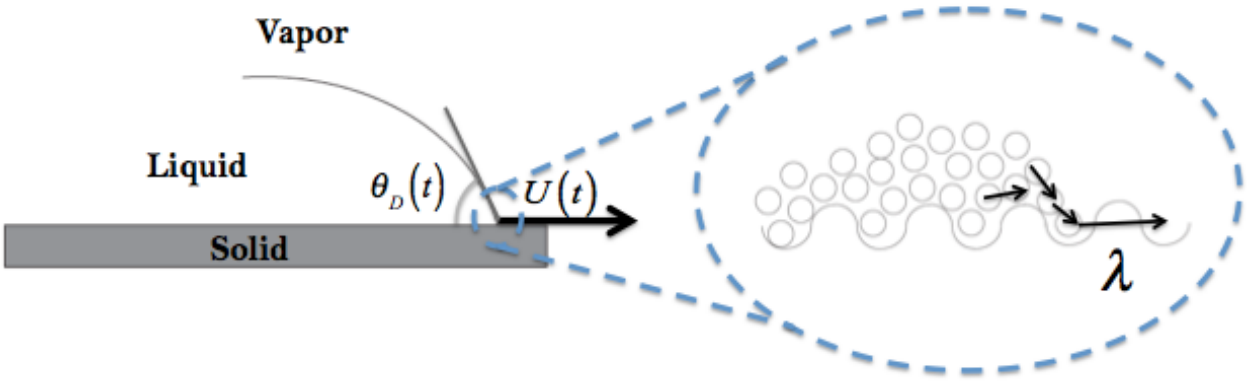

Figure 2.1: Schematic representation of the molecular-kinetic model of spreading dynamics proposed by Blake [68] and Blake and Haynes [67].

Blake [68], and Blake and Haynes [67] have applied the molecular-kinetic theory for describing the spreading dynamics on a solid surface by proposing the idea of the process that explains the adsorption of the molecules of one fluid (e.g. liquid) on adsorption sites of a solid surface and desorption of the molecules of the other fluid (e.g. gas) from the adsorption sites of the solid surface. In their analysis [67,68], they have considered the balance of deriving force due to interfacial tensions and the surface friction force at the three-phase contact zone. Based on the molecular-kinetic theory, the velocity of three-phase contact line, U, can be defined based on the difference in magnitude of frequencies of the molecular displacements of both fluids (e.g. the difference between the net frequency of molecular displacements of liquid and vapor in forward direction for advancing motion and the net frequency of molecular displacements of the liquid and the vapor in backward direction for receding motion by interchanging their positions from one adsorption sites to another adsorption sites) and average molecular displacement, λ [67,68].

$$U = \lambda\left(K_w^+ - K_w^-\right) \tag{2.1}$$

In equation 2.1, K_w^+ is the net time rate of molecular displacements of species (e.g. liquid or gas) in forward direction and K_w^- is the net rate of molecular displacements of species in backward direction.

At equilibrium, the total frequency of molecular displacements in forward direction will be the same as the total frequency of molecular displacements in backward direction.

$$K_w = K_w^+ = K_w^- \tag{2.2}$$

The frequency of molecular displacements, K_w, at equilibrium state of the solid/liquid/vapor system at the three-phase contact line in molecular level has been defined based on the molar activation free energy of wetting by applying the Eyring's theory of absolute reaction rates [75].

$$K_w = \frac{k_B T}{h} \exp\left(- \frac{\Delta G_w}{N_A k_B T} \right) \tag{2.3}$$

In equation 2.3, K_w is the molecular displacement frequency at equilibrium, ΔG_w is molar activation free energy for spreading, k_B is Boltzmann constant and its value is $1.3806488 \times 10^{-23} \left(m^2 \, kg / s^2 \, K \right)$, N_A is Avogadro's number and its value is $6.02214129 \times 10^{23} \left(1 / \, mol \right)$, h is the Planck's constant and its value is $6.62606957 \times 10^{-34} \left(m^2 \, kg / s \right)$, T is the absolute temperature, and σ is the surface tension of the liquid.

For the liquid contact line to move in advancing motion on the solid surface (i.e. spreading process), the shear stress in advancing direction of motion should be applied on the liquid molecules at the liquid contact line which causes decreasing the potential energy barriers to the liquid molecules in the direction of the advancing motion and simultaneously increasing the potential energy barriers to the liquid molecules in the direction of the receding motion. Hence for the liquid contact line to advance on the solid surface, $K_w^+ > K_w^-$.

For the liquid contact line to move in receding motion on the solid surface (i.e. dewetting process), the shear stress in receding direction of motion should be applied on the liquid molecules at the liquid contact line which causes increasing the potential energy barriers to the liquid molecules in the direction of the advancing motion and simultaneously decreasing the potential energy barriers to the liquid molecules in the direction of the receding motion. Hence for the liquid contact line to advance on the solid surface ($K_w^- > K_w^+$). By assuming that potential energy barriers are symmetrical in backward direction and forward direction at equilibrium state [68], then to make liquid contact line to advance, half of potential energy barriers in forward

direction (i.e. advancing direction of motion) is decreased and half of potential energy barriers in backward direction (i.e. receding direction of motion) is increased. Equations 2.4 and 2.5 show the expressions for the total frequency of molecular displacement in advancing motion of the liquid contact line and the total frequency of molecular displacement in receding motion of the liquid contact line.

$$K_w^+ = \left(\frac{k_B T}{h}\right)\exp\left(-\frac{\Delta G_w}{N_A k_B T} + \frac{w}{2 n k_B T}\right) \tag{2.4}$$

$$K_w^- = \left(\frac{k_B T}{h}\right)\exp\left(-\frac{\Delta G_w}{N_A k_B T} - \frac{w}{2 n k_B T}\right) \tag{2.5}$$

In equations 2.4 and 2.5, w is the amount of work done by shear stress applied on the liquid molecules to over come potential energy barriers to drive unit length of the liquid contact line to move for a unit length of displacement.

The net frequency of molecular displacement, $\left(K_w\right)_{net}$, during the motion of the liquid contact line is defined by the difference of the frequency of molecular displacement in advancing motion and the frequency of molecular displacement in receding motion as illustrated in equation 2.6.

$$\left(K_w\right)_{net} = K_w^+ - K_w^- \tag{2.6}$$

By substituting equations 2.4 and 2.5 into equation 2.6, equation 2.7 is obtained.

$$\left(K_w\right)_{net} = K_w \exp\left(\frac{w}{2 n k_B T}\right) - K_w \exp\left(\frac{w}{2 n k_B T}\right) \tag{2.7}$$

So, the net frequency of molecular displacement can be described based on equation 2.8.

$$\left(K_w\right)_{net} = 2 K_w \sinh\left(\frac{w}{2 n k_B T}\right) \tag{2.8}$$

By combining equations 2.1, 2.6, and 2.8, the velocity of the liquid contact line can be defined as follows:

$$U = 2K_w \lambda \sinh\left(\frac{w}{2nk_B T}\right) \tag{2.9}$$

For further simplification of equation 2.9, let's assume that the shear stress required to drive the liquid contact line to move is only due to the out-of-balance interfacial tension forces acting along the liquid contact line. These out-of-balance interfacial tension forces are provided by the change of contact angle from its equilibrium value, θ_0 , to the dynamic contact angle, θ_D as it is shown in equation 2.10.

$$F = \sigma\left(\cos\theta_0 - \cos\theta_D\right) \tag{2.10}$$

In equation 2.10, F is the out-of-balance interfacial tension acting long the liquid contact line. And as it has been noted earlier, dynamic contact angle is a function of the liquid contact line velocity, U. Based on the assumption, the work done by the shear stress, w, on the liquid molecules along unit length of the liquid contact line for unit displacement can be defined by the out-of-balance interfacial tension as shown in equation 2.11.

$$w = F = \sigma\left(\cos\theta_0 - \cos\theta_D\right) \tag{2.11}$$

Equations 2.10 and 2.11 denote the out-of-balance interfacial tension force and the required work done by out-of-balance interfacial tension forces along the liquid contact line for the advancing motion.

By combining equations 2.9 and 2.11, the relationship between dynamic contact angle and the velocity of the liquid contact line can be obtained for the advancing motion can be shown in equation 2.12.

$$U = 2K_w \lambda \sinh\left(\frac{\sigma\left(\cos\theta_0 - \cos\theta_D\right)}{2nk_B T}\right) \tag{2.12}$$

For receding motion of the liquid contact line, the out-of-balance interfacial tension forces along the liquid contact line should be expressed as shown in equation 2.13.

$$F = \sigma\left(\cos\theta_D - \cos\theta_0\right) \tag{2.13}$$

Hence the work done by out-of-balance interfacial tension force is described as shown in equation 2.14.

$$w = F = \sigma\left(\cos\theta_D - \cos\theta_0\right) \tag{2.14}$$

By combining equations 2.9 and 2.14, the relationship between dynamic contact angle and the velocity of the liquid contact line can be obtained for the receding motion can be shown in equation 2.15.

$$U = 2K_w \lambda \sinh\left(\frac{\sigma\left(\cos\theta_D - \cos\theta_0\right)}{2nk_B T}\right) \tag{2.15}$$

As it has been mentioned earlier, n is the number of adsorption sites on the solid surface pre unit surface area of the solid surface and λ is the average distance between two adjacent adsorption sites on the solid surface. By making the assumption of the uniform distribution of the adsorption sites on the solid surface, the following equation 2.16 can be used to relate the number of adsorption sites per unit surface area, n, to the average molecular displacement, λ.

$$n = \frac{1}{\lambda^2} \tag{2.16}$$

By applying equation 2.16 in equations 2.12 and 2.15, the relationship between dynamic contact angle and the liquid contact line velocity for the advancing motion and the receding motion can be obtained based on two molecular-kinetic parameters (i.e. K_w and λ).

Equation 2.17 describes the dynamics of advancing motion of the liquid contact line based on molecular-kinetic theory.

$$U = 2K_w \lambda \sinh\left(\frac{\sigma\lambda^2\left(\cos\theta_0 - \cos\theta_D\right)}{2k_B T}\right) \tag{2.17}$$

Equation 2.18 describes the dynamics of receding motion of the liquid contact line based on molecular-kinetic theory.

$$U = 2K_w \lambda \sinh\left(\frac{\sigma\lambda^2\left(\cos\theta_D - \cos\theta_0\right)}{2k_B T}\right) \tag{2.18}$$

Hence by rearranging equations 2.17 and 2.18, the dependency of the advancing dynamic contact angle, θ_A, and the receding dynamic contact angle, θ_R, to the liquid contact line velocity, U, can be obtained as shown in equations 2.19 and 2.20.

$$\theta_A = \cos^{-1}\left\{\cos\theta_0 - \left(\frac{2k_B T}{\sigma\lambda^2}\right)\sinh^{-1}\left(\frac{U}{2K_w\lambda}\right)\right\} \tag{2.19}$$

$$\theta_R = \cos^{-1}\left\{\cos\theta_0 + \left(\frac{2k_B T}{\sigma\lambda^2}\right)\sinh^{-1}\left(\frac{U}{2K_w\lambda}\right)\right\} \tag{2.20}$$

2.2 Hydrodynamics Theory

Hydrodynamic theory focuses on the bulk flow of the fluid to describe the dynamics of spreading. Hydrodynamics theory applies the lubrication approximation (i.e. creeping flow assumption) on the Navier-Stokes equations. Hydrodynamics theory shows that the dynamics of spreading is a purely competition of the viscous stresses and capillary pressure. Several forms of dynamics of spreading have been proposed through experimental and theoretical studies.

2.2.1 Complete Wetting Liquids

Hoffman [16] has done experimental investigations on forced spreading of silicone oil inside glass capillaries. Hoffman has introduced the following relation between the dynamic contact angle and Capillary number to describe the spreading dynamics of nonvolatile liquids, which completely spread on solid surface.

$$\theta_D = f_{\text{Hoff}}\left(Ca\right) \tag{2.21}$$

In equation 2.21, $f_{\text{Hoff}}\left(Ca\right)$ is an implicit function provided by Hoffman [16] which is illustrated in equation 2.22.

$$\theta_D = f_{\text{Hoff}}\left(Ca\right) = \cos^{-1}\left\{1-2\tanh\left[5.16\left(\frac{Ca}{1+1.31Ca^{0.99}}\right)^{0.706}\right]\right\} \tag{2.22}$$

Hoffman has neglected inertia effects and he assumed the gravitational effect to be very small to drive the spreading dynamics of complete wetting liquids. For very small Capillary number range (i.e. $Ca < O\left(0.1\right)$), equation 2.22 simplifies to the following form:

$$\theta_D = 4.54\,Ca^{0.353} \tag{2.23}$$

In equation 2.23 the dynamic contact angle, θ_D , is in radians. Equation 2.23 is approximately close to the well-known power law relation in hydrodynamics theory, which was derived first by Tanner [88].

$$\theta_D^3 \approx \alpha\, Ca \tag{2.24}$$

In equation 2.24, α is a multiplying factor, which is a function of physical properties of liquid and characteristic length of the flow.

As it has been noted, Tanner was the first person to drive the power law relation between the dynamic contact angle and Capillary number and Tanner verified his power law relation by experimental investigations on the spontaneous spreading of silicon oil droplet on horizontal glass surface. Tanner [88] has applied hydrodynamic theory analysis with application of lubrication assumption, incompressible flow, and quasi-steady state flow assumption to describe the dynamics of spontaneous spreading of liquid droplet on a horizontal solid surface.

Voinov [70] has obtained the same result as Tanner's by doing the theoretical analysis on the spreading dynamics using hydrodynamics theory and excluding the immediate vicinity of the liquid contact line. As a result, equation 2.24 is represented as the *Hoffman-Voinov-Tanner law*. The Hoffman-Voinov-Tanner law applies to the very small Capillary number (i.e. $Ca \le O\left(0.1\right)$) or equivalently in terms of the dynamic contact angle (i.e. $\theta_D \le 135^o$) for spreading of complete wetting liquids.

2.2.2 Partial Wetting Liquids

Hoffman [16] has extended the validity of the universal of law of spreading dynamics (i.e. equation 2.21) for the partial wetting liquids by including the influence of the non-zero static contact angle, θ_0 , in a shift factor $f_{\text{Hoff}}^{-1}\left(\theta_0\right)$ [20].

$$\theta_D = f_{\text{Hoff}}\left(Ca + f_{\text{Hoff}}^{-1}\left(\theta_0\right)\right) \tag{2.25}$$

Hence, Hoffman [16] obtained the universal law of spreading dynamics for both complete wetting liquids and partial wetting liquids in the following form.

$$g_{\text{Hoff}}\left(\theta_D\right) - g_{\text{Hoff}}\left(\theta_0\right) = Ca \tag{2.26}$$

In equation 2.26, $g_{\text{Hoff}}(\theta) = f_{\text{Hoff}}^{-1}(\theta)$, where $f_{\text{Hoff}}^{-1}(\theta)$ is the inverse function of the Hoffman function, $f_{\text{Hoff}}(\theta)$. For the dynamic contact angle range (i.e. $\theta_D \leq 135^o$), $g_{\text{Hoff}}(\theta)$ can be approximated by $\frac{\theta^3}{\mathbb{C}}$ [20] where $\mathbb{C}$ is a constant of proportionality that can be a function of the liquid properties. Equation 2.26 can then be simplified to the following form.

$$\theta_D^3 - \theta_0^3 \cong \mathbb{C}\, Ca \tag{2.27}$$

Equation 2.27 is called the modified *Hoffman-Voinov-Tanner law*.

Huh and Scriven [74] have postulated that no-slip boundary condition at the solid/liquid interface should be relaxed at the liquid contact line unless the shear stress and pressure field will be unbounded at the liquid contact line. Huh and Scriven [74] have done the theoretical analysis on the steady flow of the Newtonian incompressible fluid on a flat smooth solid surface using creeping flow approximation. Huh and Scriven [74] concluded that the shear stress and pressure filed vary as $\frac{1}{r}$ where r is the radial distance from the liquid contact line.

de Gennes [73] has investigated on the spreading dynamics of liquid being pulled out along a smooth vertical solid plate. de Gennes [73] has considered a finite static contact angle at the liquid contact line in his theoretical analysis to investigate on the spreading dynamics of the partial wetting regime. de Gennes [73] has done his theoretical analysis applying the lubrication approximation for small capillary number range for flow away from the immediate vicinity of the liquid contact line and assumed a straight wedge meniscus region with a slop equal to the dynamic contact angle, θ_D . In his theoretical analysis, de Gennes [73] has assumed that the rate of the entropy generation is due to the rate of the total viscous dissipation. The rate of the entropy generation is due to the power produced by the friction force at the liquid contact line.

The contact line friction force, F_Y , is based on the out-of-balance interfacial tension at the liquid contact line due to the difference between the dynamic contact angle and the finite static contact angle as shown in equation 2.28.

$$F_Y = \sigma\left(\cos\theta_D - \cos\theta_0\right) \tag{2.28}$$

Equation 2.29 shows the expression for the power, P, produced by the liquid contact line friction force.

$$P = F_Y U = \sigma\left(\cos\theta_D - \cos\theta_0\right)U \tag{2.29}$$

de Gennes [73] has introduced the spreading dynamics (i.e. equation 2.30) by equating the expression for the power produced by the liquid contact line friction force with the rate of the total viscous dissipation as shown below.

$$\theta_D\left(\theta_0^2 - \theta_D^2\right) = 6\,\frac{\mu U}{\sigma}\,\ln\left(\frac{L_{mac}}{L_{mic}}\right) \tag{2.30}$$

In equation 2.30, L_{mac} is the size of the macroscopic region of the flow, and L_{mic} is the size of the microscopic region of the flow over which the no-slip boundary condition is relaxed. Equation 2.30 is the spreading dynamics obtained by de Gennes, is similar to the *generalized Hoffman-Voinov-Tanner law*.

Cox [71] has performed theoretical analysis for the liquid contact line dynamics. Cox [71] has postulated that the slip condition is necessary at the vicinity of the liquid contact line to remove the stress singularity at the liquid contact line. In order to do that, Cox [71] has concluded that there are three regions near the liquid contact line. These regions are the inner region, the intermediate region, and the outer region. The inner region is the region, where slippage condition happens at the solid/liquid to remove the shear stress singularity. The intermediate region is the region between the outer region and the inner region.

$$g\left(\theta_D,\varepsilon\right)-g\left(\theta_0,\varepsilon\right)=\pm Ca\,\ln\left(\frac{L}{L_s}\right) \tag{2.31}$$

In equation 2.31, L_s is the size of the inner region, which is called the slip length, θ_D is the dynamic contact angle in the intermediate region, and θ_0 is the microscopic static contact angle in the inner region. In equation 2.31, $\varepsilon\equiv\frac{\mu_{vapor\ phase}}{\mu_{liquid}}$, where $\mu_{vapor\ phase}$ is the dynamic viscosity of the vapor phase (e.g. usually air) and μ_{liquid} is the dynamic viscosity of liquid (e.g. usually shown as μ) and $Ca\equiv\frac{\mu U}{\sigma}$.

$$g\left(\theta,\varepsilon\right)\equiv\int_0^{\theta}\frac{d\beta}{f\left(\beta,\varepsilon\right)} \tag{2.32}$$

where

$$f\left(\beta,\varepsilon\right)\equiv\frac{2\sin\beta\left\{\begin{array}{l}\varepsilon^2\left(\beta^2-\sin^2\beta\right)+2\varepsilon\left[\beta\left(\pi-\beta\right)+\sin^2\beta\right]\\ \quad+\left[\left(\pi-\beta\right)^2-\sin^2\beta\right]\end{array}\right\}}{\begin{array}{l}\varepsilon\left(\beta^2-\sin^2\beta\right)\left[\left(\pi-\beta\right)+\sin\beta\,\cos\beta\right]\\ \quad+\left[\left(\pi-\beta\right)^2+\sin^2\beta\right]\left(\beta-\sin\beta\cos\beta\right)\end{array}} \tag{2.33}$$

Voinov [70] has done theoretical analysis for finding the relation between dynamic contact angle and velocity of the liquid contact line by applying the low Reynolds number flow of viscous fluid on a smooth solid surface with assumption of steady state flow. Voinov [70] has obtained the following result (i.e. equation 2.34) based on his theoretical analysis to describe the dynamics of spreading by including the effect of the static contact angle.

$$\frac{1}{2}\int_{\theta_0}^{\theta_D}\frac{\phi-\sin\phi\,\cos\phi}{\sin\phi}d\phi=Ca\ln\left(\frac{L}{L_s}\right) \tag{2.34}$$

Equation 2.34 explains the spreading dynamic of partial wetting liquids by dividing it into two ranges of the dynamic contact angles as shown below

$$\theta_D^3 - \theta_0^3 = 9\,Ca\,\ln\left(\frac{L}{L_s}\right) \qquad \theta_D \le 135^o \tag{2.35a}$$

$$\frac{9\pi}{4}\ln\left(\frac{1-\cos\theta_D}{1+\cos\theta_D}\right) + \left(\pi-\theta_D\right)^3 - \theta_0^3 = 9\,Ca\,\ln\left(\frac{L}{L_s}\right) \qquad \theta_D \ge 135^o \tag{2.35b}$$

Equation 2.31 obtained from Cox [71] can be replaced by equations 2.35a and 2.35b by making the approximation of negligible dynamic viscosity of the vapor phase (i.e. $\mu_{vapor\ phase} = 0$). Hence, equations 2.35a and 2.35b are called "Cox-Voinov" equations to describe the dynamics of spreading for both complete wetting liquids and partial wetting liquids.

2.2.3 Derivation of Hydrodynamics Theory

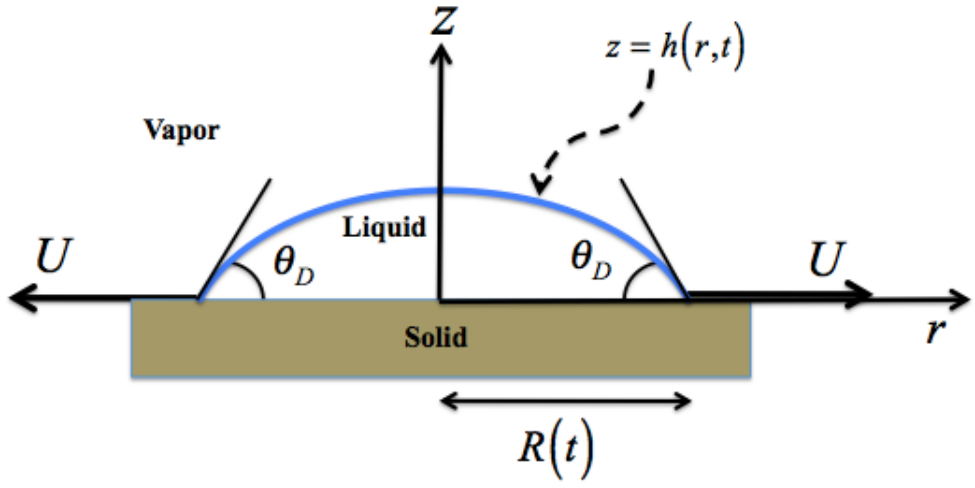

Figure 2.2: Schematic picture of the liquid droplet on a smooth horizontal solid surface.

As it has been mentioned earlier, hydrodynamics theory describes the wetting dynamics by considering the steady state flow of the bulk of the Newtonian incompressible fluid (e.g. liquid) by applying the Navier-Stokes equations and application of low Reynolds number (e.g. creeping flow) [16,70,71,80,88].

Navier-Stokes equations with assumption of constant dynamic viscosity of the liquid:

$$\rho\left(\frac{\partial \underline{u}}{\partial t} + \underline{u}.\nabla\underline{u}\right) = -\nabla p + \rho\underline{g} + \mu\nabla^2\underline{u} \tag{2.36}$$

In equation 2.36, μ is the dynamic viscosity, ρ is the density, $\underline{g}$ is the gravitational acceleration, $\frac{\partial}{\partial t}$ is the time derivative, ∇ is the gradient, p is the pressure field, and $\underline{u}$ is the velocity field.

For the two-dimensional spreading of liquid droplet on a smooth horizontal solid surface as illustrated in figure 2.2 using cylindrical coordinate system, the velocity vector, $\underline{u}$ is defined in equation 2.37.

$$\underline{u} = u\vec{e}_r + w\vec{e}_z \tag{2.37}$$

The profile of the liquid droplet is defined as follows:

$$z = h\left(r,t\right) \tag{2.38}$$

In equation 2.38, z is the height of the liquid dropt, which is a function of time and radial distance from the center of the liquid drop.

Continuity equation is defined as:

$$\nabla.\underline{u} = 0 \tag{2.39}$$

Navier-Stokes equations for very low Reynolds number (i.e. creeping flow equation) by neglecting gravitational effect with assumption of lubrication approximation for Spreading of liquid on a planar horizontal substrate is shown below:

$$\mu \nabla^2 \underline{u} = \nabla p \tag{2.40}$$

The following boundary conditions are applied to solve the equation 2.40.

a) Kinematic boundary condition on the liquid/vapor interface (e.g. no-flow through boundary condition across the interface).

$$\underline{u} . \underline{n} = \frac{\partial h}{\partial t} \tag{2.41}$$

b) Dynamic boundary condition on the liquid/vapor interface are as following:

1) Shear stress-free condition along the liquid/vapor interface:

$$\left(\mu \nabla \underline{u}\right) . \underline{n} . \underline{t}^{j} = 0 \tag{2.42}$$

where $\nabla \underline{u}$ is the rate of shear strain tensor and $\underline{n}$ is the unit normal vector to the interface and $\underline{t}$ is the unit tangent vector on the interface.

2) Balance of normal stress across the liquid/vapor interface by relating pressure inside the liquid, p, to vapor pressure, p_v, with consideration of effect of the curvature, κ, of the liquid/vapor interface and the surface tension of the liquid, σ, and the normal component of the force due to viscous flow.

$$p - p_v - \left(\mu \nabla \underline{u}\right) . \underline{n} . \underline{n} = \sigma \kappa \tag{2.43}$$

Geometric condition of the liquid/vapor interface as following:

$$h\left(R\left(t\right), t\right) = 0 \tag{2.44a}$$

$$\left(\frac{\partial h}{\partial r}\right)_{r=R(t)} = -\tan\theta_D \qquad (2.44b)$$

And finally, the kinematic boundary condition on the liquid/solid interface is as following:

(a) No-flow-through boundary condition:

$$w = 0 \qquad (2.45)$$

(b) Slip condition by introducing the small slip coefficient (i.e. slip length), L_s, to avoid the non-integrable singularity occurred in the rate of shear strain tensor at the three-phase contact line [69,64,66,74,75].

$$u = L_s \frac{\partial u}{\partial z} \qquad (2.46)$$

In equation 2.46, L_s is the so-called slip length, which is the length of the inner region of the liquid over which the no-slip condition is relaxed.

The assumption of preserving the volume of the liquid during the spreading due to the assumption of the negligible evaporation of the liquid during spreading and application of the incompressible assumption:

$$V = 2\pi \int_0^{R(t)} h(r,t)\, r\, dr = \text{constant} \qquad (2.47)$$

The solution of the system of equations (2.39-2.47) is the dynamics of spreading based on the hydrodynamics theory as it is shown below.

$$\theta_D^3 - \theta_0^3 = \pm 9 Ca \ln\left(\frac{L_{mac}}{L_{mic}}\right) \qquad (2.48)$$

In equation 2.48, θ_D is the dynamic contact angle, θ_0 is the static contact angle, $Ca = \frac{\mu U}{\sigma}$, L_{mac} is the macroscopic characteristic length, which is sometimes denoted by the Capillary length (i.e.

$L_{cap} = \sqrt{\frac{\sigma}{\rho g}}$), and L_{mic} is the microscopic characteristic length, which is sometimes denoted by L_s (i.e. the slip length). The plus sign denotes for the advancing motion and the minus sign denotes for the receding motion of the liquid contact line.

2.2.4 Characteristic Length Scales

The dynamics of spreading can be divided into two regions, the microscopic region and the macroscopic region. The microscopic region is the region at the neighborhood of the liquid contact line where the slip condition at the solid/liquid is imposed to be able to remove the existence of the singularity on the viscous shear stress and consequently removing the singularity on the drag force applied on the solid surface [71,74]. The characteristic length for the microscopic region, L_{mic}, has been shown by Eggers and Stone [96] to be a function of the slip length, L_s, and the Capillary number.

$$L_{mic} = f\left(Ca\right) \approx \frac{L_s}{b\ Ca^{1/3}} \tag{2.49}$$

In equation 2.49, $b \approx 1.85$ [96].

And the outer region is the region beyond the microscopic region. The size of the macroscopic region of the fluid is so-called the macroscopic characteristic length, L_{mac}. Some times, the Capillary length, L_{cap}, denotes the macroscopic characteristic length. In general the size of the macroscopic characteristic length should be a lot larger than the size of the microscopic characteristic length ($L_{mac} \gg L_{mic}$). The macroscopic characteristic length, L_{mac}, is the characteristic matching length of the bulk of the liquid where the microscopic profile of the

liquid (i.e. inner region of the liquid) match with the outer profile of the liquid. The macroscopic characteristic length (i.e. also called macroscopic characteristic hydrodynamic length scale) was found to be a function of Capillary number by Eggers and Stone [96].

$$L_{mac} = g\left(Ca\right) = L_{cap}\ Ca^{1/3} \tag{2.50}$$

In equation 2.50, $L_{cap} = \sqrt{\frac{\sigma}{\rho\ g}}$ is the Capillary length.

The most general form of the spreading dynamics based on the hydrodynamics theory by including the effect of the flow on the microscopic characteristic length and macroscopic characteristic length can be obtained by combining equations 2.48, 2.49, and 2.50.

$$\theta_D^3 - \theta_0^3 = \pm 9 Ca \ln\left(\frac{b\ L_{cap}\ Ca^{2/3}}{L_s}\right) \tag{2.51}$$

In equation 2.51, $\frac{b\ L_{cap}}{L_s}$ can be shown as one fitting parameter, α, used in fitting analysis based on the hydrodynamics theory to the experimental data. Hence the spreading dynamics of a Newtonian incompressible liquid on a solid surface can be shown as:

$$\theta_D^3 - \theta_0^3 = \pm 9 Ca \ln\left(\alpha\ Ca^{2/3}\right) \tag{2.52}$$

CHAPTER 3

Hypothesis

There have been a lot of experimental investigations about the spreading dynamics in the spontaneous spreading mechanisms [1-6,11-14,20,32,36-39,41-46,49-54,57-59,65,69,77,80,83,85-89,95-97,104,106,111-116,118,120,121,126-128,130,133,134,136,140] and in the forced spreading mechanisms [7-11,15-31,33-35,37,40,47,48,55,56,60,66,69,72,73,77,87,91,96,102,108,110,119,123,124,126,129,131,132,135]. However, surprisingly there has not been any research in regards to do the comparison between forced spreading and spontaneous spreading for the same solid/liquid/air system. In this research, the experimental research has been performed to compare the results obtained from spontaneous spreading using DSA 100 (see chapter 5 for details) with the results obtained from forced spreading using Tensiometer for the same solid/liquid/air system (see chapter 6 for details). ***Based on the experimental investigations, it has been found out that the experimental results obtained from spontaneous spreading are not the same as the results obtained from forced spreading (see chapter 7 for details). Hence the appropriate dynamics of spreading depends on the mechanism of spreading (i.e. spontaneous or forced). Based on my hypothesis, one should be able to choose the appropriate spreading dynamics (i.e. hydrodynamics theory***

and/or molecular-kinetic theory) for a given spreading mechanism (e.g. spontaneous or forced) for known solid/liquid properties.

In spontaneous spreading, one can experimentally observe the liquid contact line that has higher velocity for the same dynamic contact angle. The schematic of the spontaneous spreading of a liquid droplet on a solid substrate described by the two dynamics of spreading (i.e. hydrodynamics and molecular-kinetic) is shown in figure 3.1. In figure 3.1, the two laws of spreading dynamics describe the same dynamic contact angle, θ, for the two different liquid contact line velocities (i.e. one law with velocity U_1 and the other law with velocity U_2). As it is shown in figure 3.1, the liquid droplet described by the higher liquid contact line velocity (i.e. U_2) is observable.

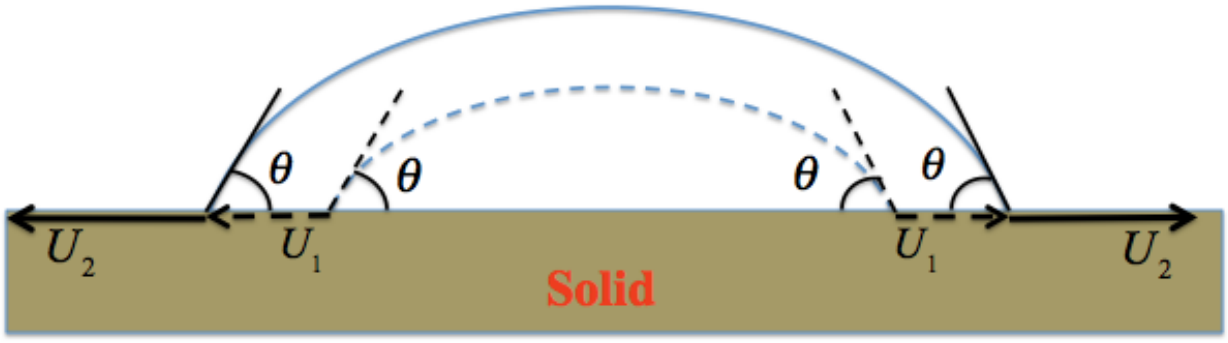

Figure 3.1: Schematics of spontaneous spreading of a liquid droplet on a solid substrate described by the two dynamics of spreading.

Hence the appropriate dynamics of spreading for spontaneous spreading is determined based on the liquid contact line velocity. For a given dynamic contact angle, the dynamics of spreading that shows the higher corresponding liquid contact line velocity is the appropriate spreading

dynamics for spontaneous spreading. Figure 3.2 illustrates the schematic of the hypothesis for choosing the appropriate dynamics of spreading for spontaneous spreading.

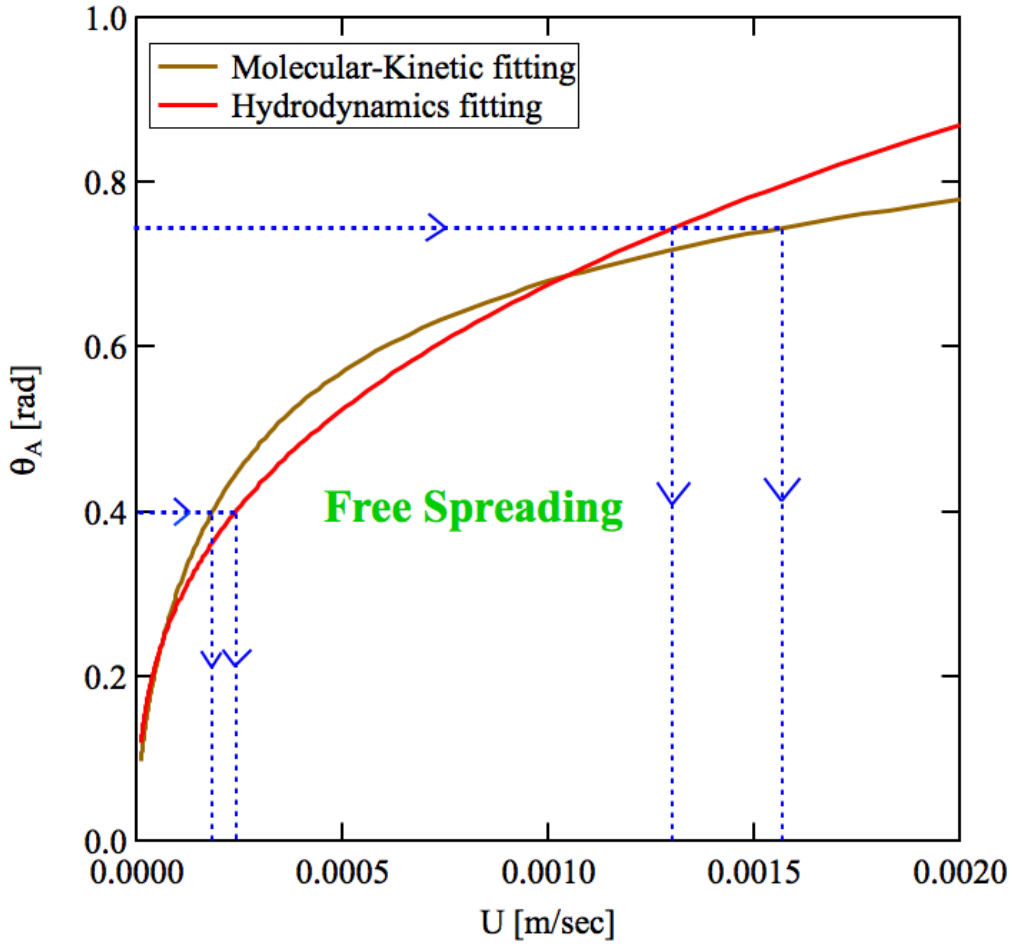

Figure 3.2: Schematics of hypothesis for spontaneous spreading (i.e. free spreading).

As illustrated in figure 3.2, the appropriate spreading dynamics for the region before the crossing point is hydrodynamics theory and after the crossing point is molecular-kinetic theory.

In forced spreading, the liquid contact velocity is controlled by some sort of mechanical force or hydrodynamic force. In forced spreading, one can experimentally observe the liquid contact line that has higher dynamic contact angle for the same liquid contact line velocity. The

schematic of the forced spreading of a liquid on a solid substrate described by the two laws of dynamics of spreading (i.e. hydrodynamics and molecular-kinetic) is shown in figure 3.3. In figure 3.3, the two law of spreading dynamics describe the same liquid contact line velocity, U, for the two different dynamic contact angles (i.e. one with velocity θ_1 and the other with velocity θ_2). As it is shown in figure 3.3, the liquid described by the higher dynamic contact angle (i.e. θ_2) is observable.

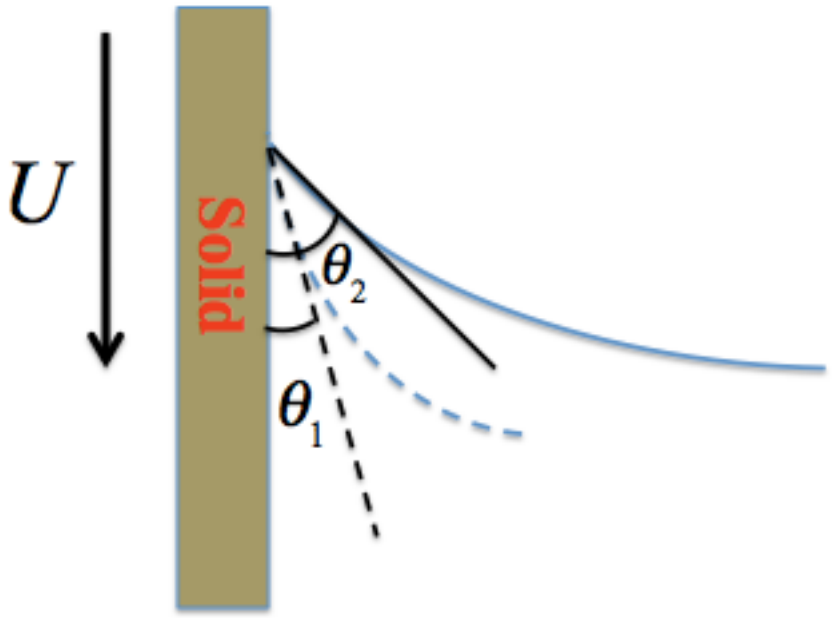

Figure 3.3: Schematics of forced spreading of a liquid on a solid substrate described by the two dynamics of spreading.

Due to this reason, the dynamics of spreading for forced spreading is determined based on the dynamic contact angle at the liquid contact line. For a given liquid contact line velocity, the dynamics of spreading that shows the higher corresponding dynamic contact angle is the

appropriate spreading dynamics for forced spreading. Figure 3.4 illustrates the schematic of the hypothesis for choosing the appropriated spreading dynamics for forced spreading.

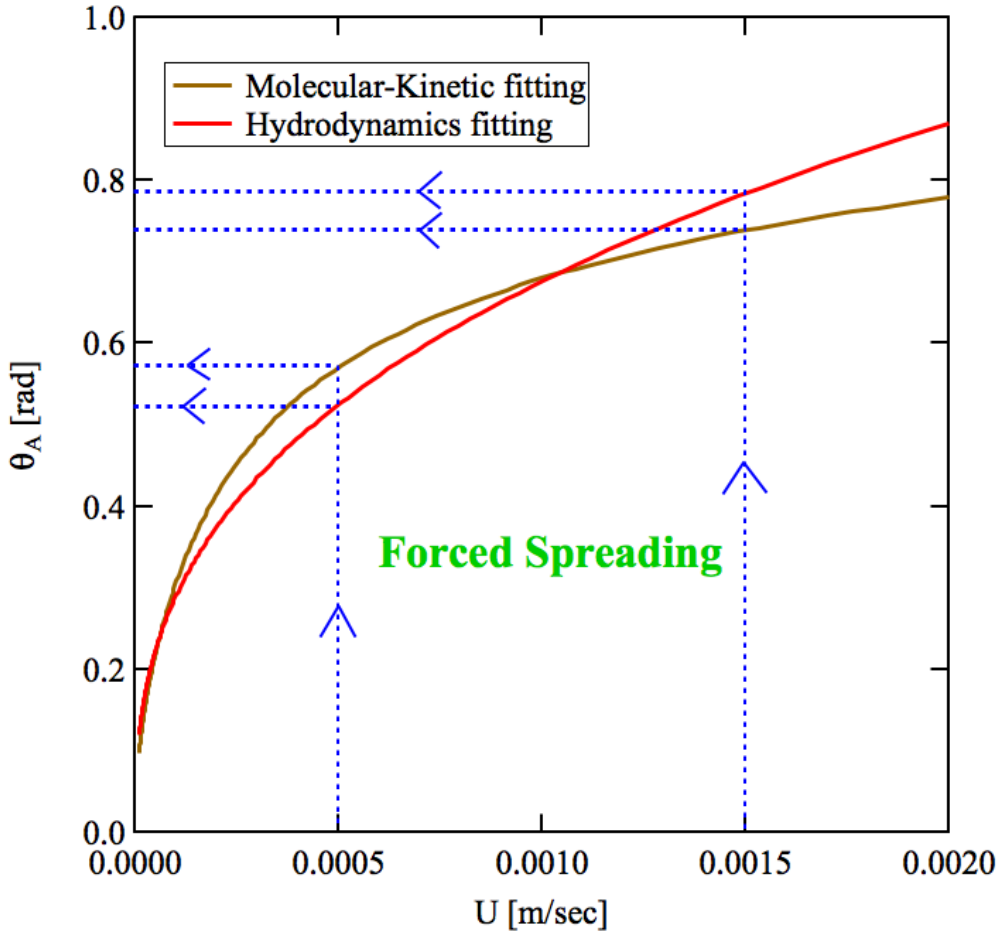

Figure 3.4: Schematics of hypothesis for forced spreading.

As illustrated in figure 3.4, the appropriate spreading dynamics for the region before the crossing point is molecular-kinetic theory and for the region after the crossing point is hydrodynamics theory.

CHAPTER 4

Experimental Techniques

4.1 Forced Spreading Mechanism

Force balance method using the Tensiometer has been applied to perform the experiments for forced spreading mechanism.

Tensiometer measures the advancing dynamic contact angle and the receding dynamic contact angle by moving the sample platform, which is holding the container with pool of liquid, upward and downward. A force sensor measures the forces applied on the plate of the solid substrate and then the Tensiometer software calculates the advancing dynamic contact angle and the receding dynamic contact angle using the theoretical formula that relates the measured force applied on the plate to the advancing dynamic contact angle and the receding dynamic contact angle. The speed of the motion of the sample platform is set to a constant specific speed to maintain a steady motion of the sample platform during measurement. Hence, Tensiometer can control the speed of the liquid contact line during the experiment. Figure 4.1 illustrates the schematic picture and the image of the Tensiometer equipment.

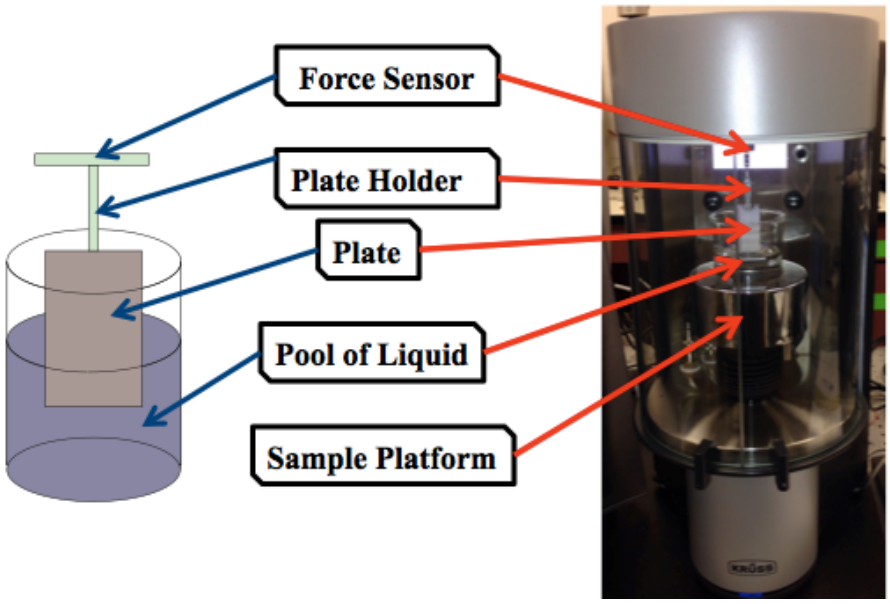

Figure 4.1: Schematic representation and the actual image of the Tensiometer equipment.

Tensiometer is used to investigate on the variation of the dynamic contact angles (e.g. both receding and advancing) versus the speed of the liquid contact line ranging from 0.1 mm/min through 500 mm/min. Tensiometer applies the analytical measurement through force balance method that is applied on the solid plate to do the dynamic contact angle (e.g. both advancing dynamic contact angle and receding dynamic contact angle) measurements. The forces which are considered during the measurement of dynamic contact angles are Capillary force due to surface tension of the liquid and the Buoyancy force applied on the solid plate during its immersion into the pool of the liquid and its emersion from the pool of the liquid.

$$F_{measured} + F_{Capillary} + F_{Bouyancy} + F_{gravity} = 0 \tag{4.1}$$

$$F_{capillary} = F_{\sigma} = 2\sigma\left(w + t\right)\cos\theta \tag{4.2}$$

$$F_{Bouyancy} = F_{B} = \rho g w t x \tag{4.3}$$

$$F_{gravity} = F_g = \rho_{solid}\, g\, w\, t\, l \tag{4.4}$$

In equations (4.2), (4.3), and (4.4) σ is the surface tension of the liquid, w is the width of the plate, t is the thickness of the plate, θ is the dynamic contact angle, l is the length of the plate, ρ is the density of the liquid, ρ_{solid} is the density of the solid plate, g is gravitational acceleration, and x is the immersion depth of the plate in the pool of the liquid.

Figure 4.2 illustrates the schematic of the forced balance method that is used in the Tensiometer software to measure the dynamic contact angle.

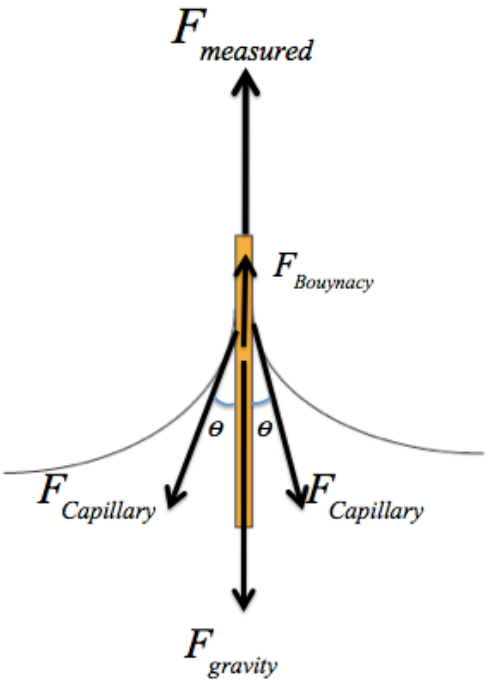

Figure 4.2: The schematic representation of the forces applied on a plate of the solid substrate during the motion of the liquid contact line.

Tensiometer applies dip coating method with the ability of repeating the experiments by performing multiple cycles of advancing and receding motion of the plate inside the pool of the liquid to show the accuracy of the results. Figure 4.3 shows the sample plots of dynamic contact angle (i.e. the advancing and the receding) versus immersion depth and the measured force versus immersion depth.

(a) (b)

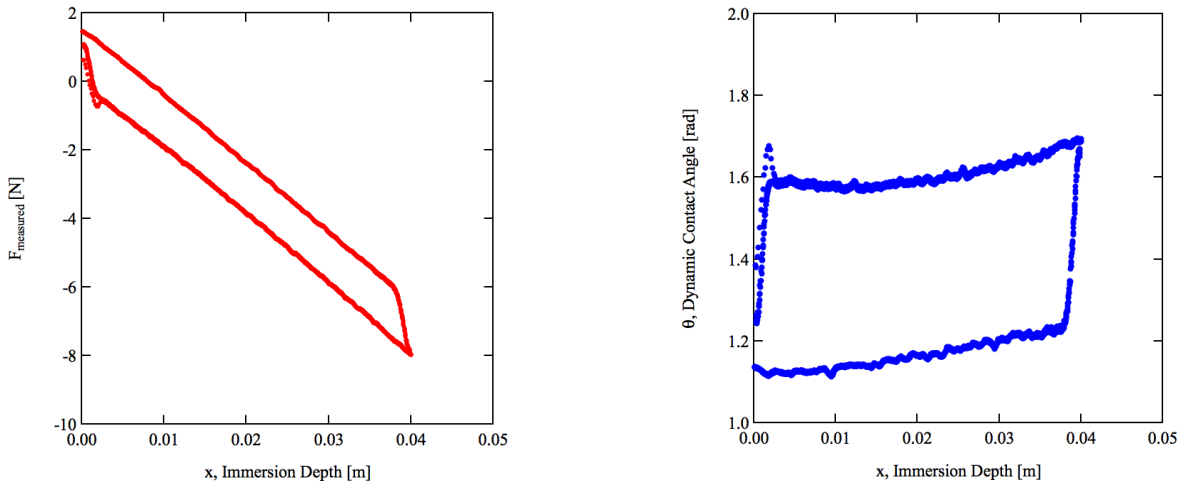

Figure 4.3: Force spreading of pure water on smooth Teflon for the speed of 40 mm/min. (a) Measured force versus immersion depth of the Teflon plate inside the pool of water. (b) Dynamic contact angle versus immersion depth of the Teflon plate inside the pool of water.

To verify the results obtained with Tensiometer, the optical method also was applied simultaneously during the experiment with tensiometer. The optical method was performed using the camera Canon ultrasonic EOS-1 that is a single lens reflex (SLR). The camera was focused at the liquid contact line where the menisci formed during the motion of the solid plate during the immersion and withdrawal of solid substrates into/out of the pool of liquid and the menisci

captured and then the advancing dynamic contact angles and the receding dynamic contact angle were measured using ImageJ. Figure 4.4 illustrates the schematic of the optical method for measuring the dynamic contact angle during the experiment with Tensiometer.

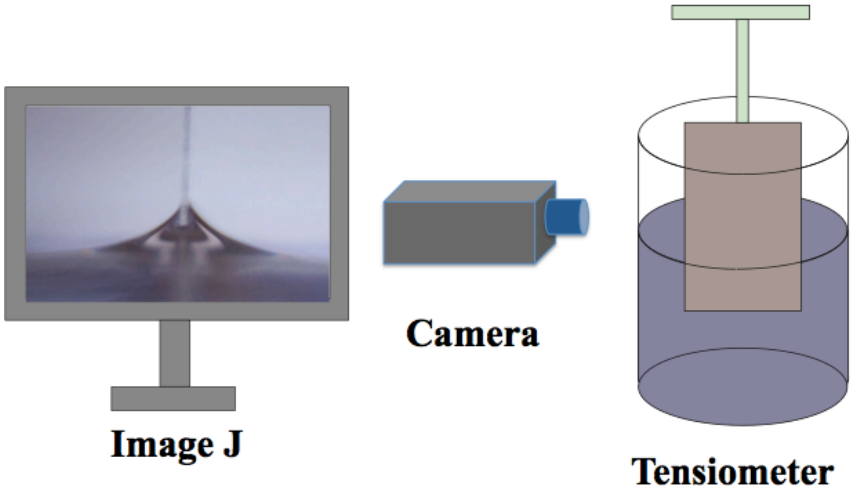

Figure 4.4: Schematic representation of the optical method.

4.2 Spontaneous Spreading Mechanism

Spontaneous spreading experiments were performed using the Drop Shape Analyzer (DSA100) manufactured by Krüss Company. DSA100 measures the dynamic contact angle through observation of the variation of the drop shape profile from side view during spreading of the liquid on the solid surface. Then DSA100 measures the dynamic contact angle formed at the three phase contact points (e.g. left and right contact points), which are formed at the intersection of the base line of the solid surface and the tangent line of the drop shape profile. Spontaneous experiments were done by depositing the liquid droplet with almost zero impact velocity on the solid substrate to be able to neglect the effect of inertia forces during the spontaneous spreading.

Figure 4.5 shows the picture image of the DSA100 equipment and the schematic of the drop shape analysis using the DSA100.

(a)

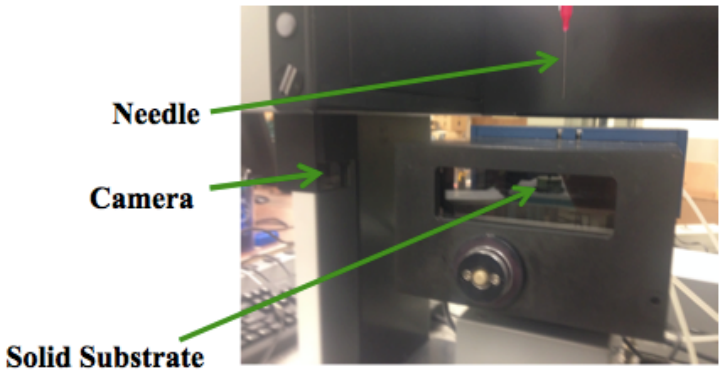

(b)

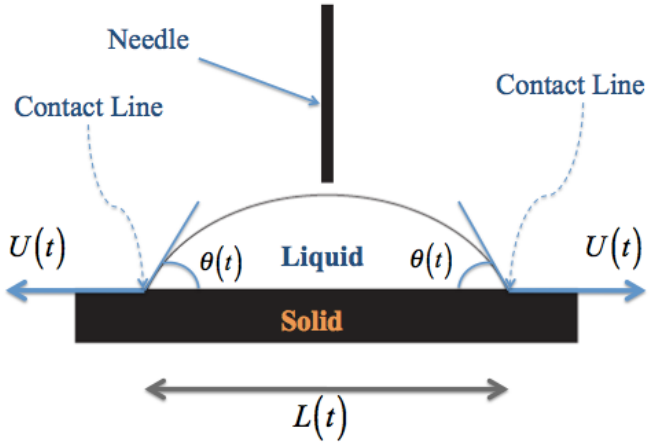

Figure 4.5: (a) The image representation of the Drop Shape Analyzer (DSA 100). (b) The schematic representation of the drop shape analysis during the spreading on the solid surface.

CHAPTER 5

Spontaneous Spreading of Liquids

5.1 Backgrounds and Motivation

Spontaneous spreading dynamics of pure liquids on solid surfaces have been first studied long time ago by Tanner [88]. When a liquid droplet is deposited on a solid surface, the liquid tends to migrate with unsteadily motion on the solid surface to reduce the free surface energy by reducing the solid surface and simultaneously increasing the liquid surface until the thermodynamic equilibrium condition is met where on the other hand sum of all the forces (i.e. interfacial forces applied at the liquid contact line on the liquid) become zero. The type of spreading that happens naturally and no external force is imposed on the liquid to spread on the solid surface until the liquid reaches to the thermodynamic equilibrium condition is called spontaneous spreading. The spontaneous spreading has tremendous applications such as painting technology and adhesives, migration of inks on solid substrates, drag reduction on airplane wings, increasing the efficiency of the pesticides' spreading on the leaves to protect the leaves form harmful pests, etc. Due to the extensive variety of applications of spontaneous spreading in industry, technology, and agriculture, there have been tremendous interests for enhancing the knowledge on spontaneous spreading dynamics. In spit of the enormous investigations in the area of spontaneous spreading

dynamics, many challenges such as the increase in the efficiency such as effect of the pesticides on the leaves, quality and resolution of the ink-jet printing, have not been solved yet.

5.2 Experiment

The spontaneous spreading experiments have been performed for five pure liquids (i.e. glycerin, dodecane, silicone oil 100 cSt, silicone oil 1000 cSt, and silicone oil 10000 cSt) on clean glass surfaces. The experiments for spontaneous spreading have been done using Drop Shape Analyzer (DSA100, KRÜSS). The liquid drops have been deposited on the glass substrates with zero impact velocity and the evolution of the droplets on the glass substrates have been recorded by DSA built-in camera from the side view. Then the dynamic contact angle, and the location of the contact points have been measured to obtain the dependency of the dynamic contact angle to the velocity of the liquid contact point. The equilibrium contact angles of dodecane on glass surface, silicone oil 100 cSt on glass surface, silicone oil 1000 cSt on glass surface, and silicone oil 10000 cSt on glass surface were zero. The equilibrium contact angle of glycerin on glass surface was not zero and it was approximately 0.552 rad, which was due to the impurity of the glycerin. Table 5.1 shows the physical properties of the liquids used in the experiments.

Liquid	Density [kg/m^3]	μ [Pa s]	σ [N/m]
dodecane	746	0.001	0.023
Silicone Oil - 100 cSt	964	0.096	0.020
Silicone Oil - 1000 cSt	969	0.969	0.020
Silicone Oil - 10000 cSt	971	9.710	0.022
Glycerin	1260	1.412	0.064

Table 5.1: Physical properties of the liquids used in the spontaneous spreading experiments.

5.3 Results and Discussion

Figures 5.1, 5.2, 5.3, 5.4, 5.5 show the dependency of the advancing dynamic contact angle to the liquid contact line velocity for the spontaneous spreading experiments performed with DSA of dodecane on glass surface (see figure 5.1), silicone oil 100 cSt on glass surface (see figure 5.2), silicone oil 1000 cSt on glass surface (see figure 5.3), silicone oil 10000 cSt on glass surface (see figure 5.4), and glycerin on glass surface (see figure 5.5).

The dynamic contact angles for the spreading of dodecane on glass substrate have been recorded by using DSA 100 and then their values have been obtained using ImgaeJ due to the fast spreading of dodecane. The velocity range where dodecane spreads spontaneously on the glass surface is approximately ($5\times10^{-4}\ m/s < U < 2\times10^{-3}\ m/s$), as shown in figure 5.1. As illustrated in figure 5.1, the advancing dynamic contact angle increases as the liquid contact line speed increases.

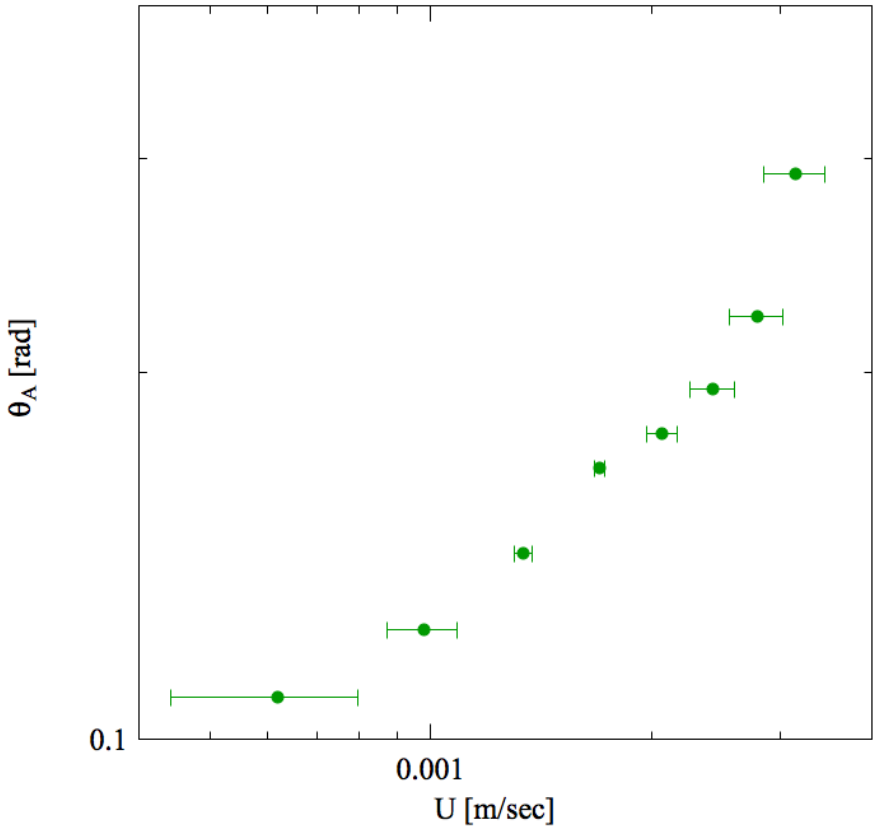

Figure 5.1: The plot of the advancing dynamic contact angle versus the liquid contact line speed for spontaneous spreading of dodecane on a glass surface.

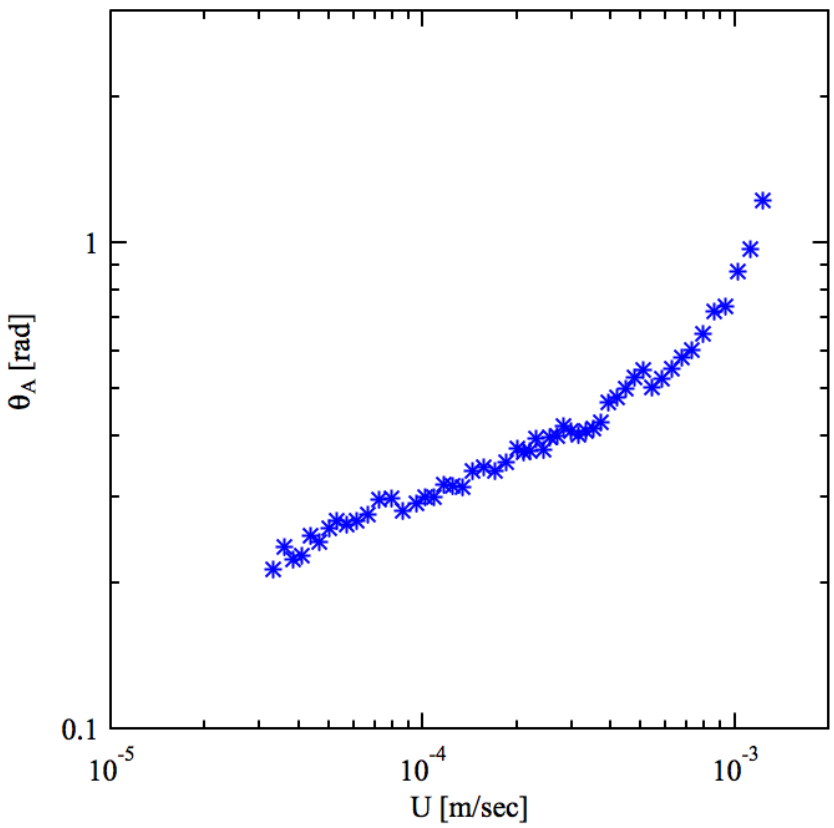

Figure 5.2: The plot of the advancing dynamic contact angle versus the liquid contact line speed for spontaneous spreading of silicone oil 100 cSt on a glass surface.

DSA 100 has recorded the dynamic contact angles for the spreading of silicone oil 100 cSt on glass substrate and then their values have been obtained using ImgaeJ. The velocity range where silicone oil 100 cSt spreads spontaneously on the glass surface is approximately $(3\times10^{-5}\ m/s < U < 10^{-3}\ m/s)$, as shown in figure 5.2. As illustrated in figure 5.2, as the liquid contact line velocity increases, the advancing dynamic contact angle increases.

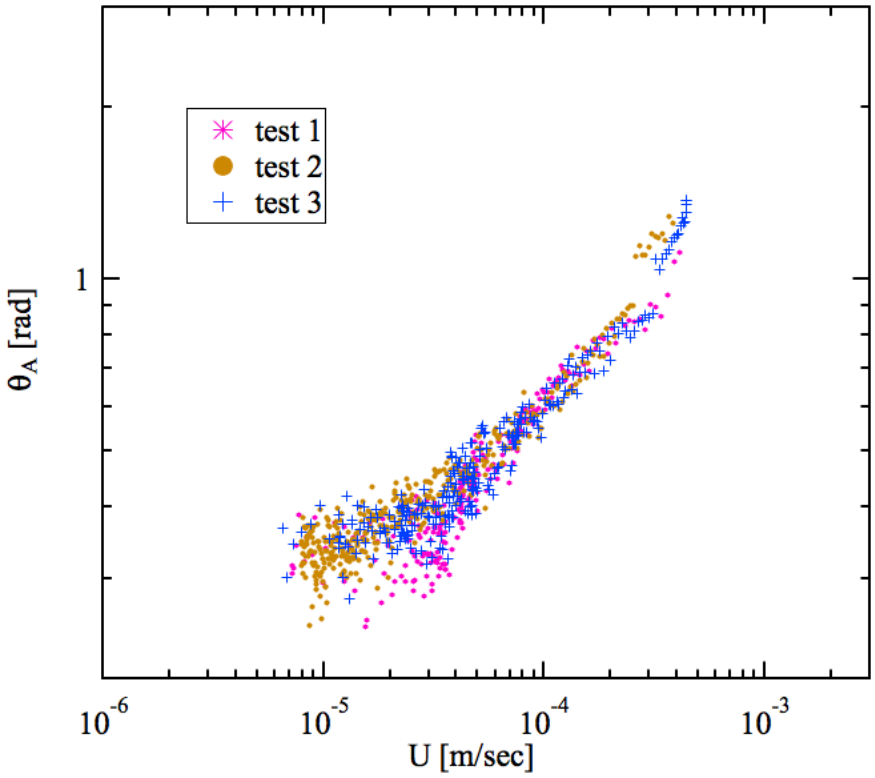

Figure 5.3: The plot of the advancing dynamic contact angle versus the liquid contact line speed for spontaneous spreading of silicone oil 1000 cSt on a glass surface.

The velocity range where silicone oil 1000 cSt spreads spontaneously on the glass surface is approximately ($10^{-5}\ m/s < U < 3\times10^{-4}\ m/s$), as shown in figure 5.3. As illustrated in figure 5.3, as the liquid contact line velocity increases, the advancing dynamic contact angle increases.

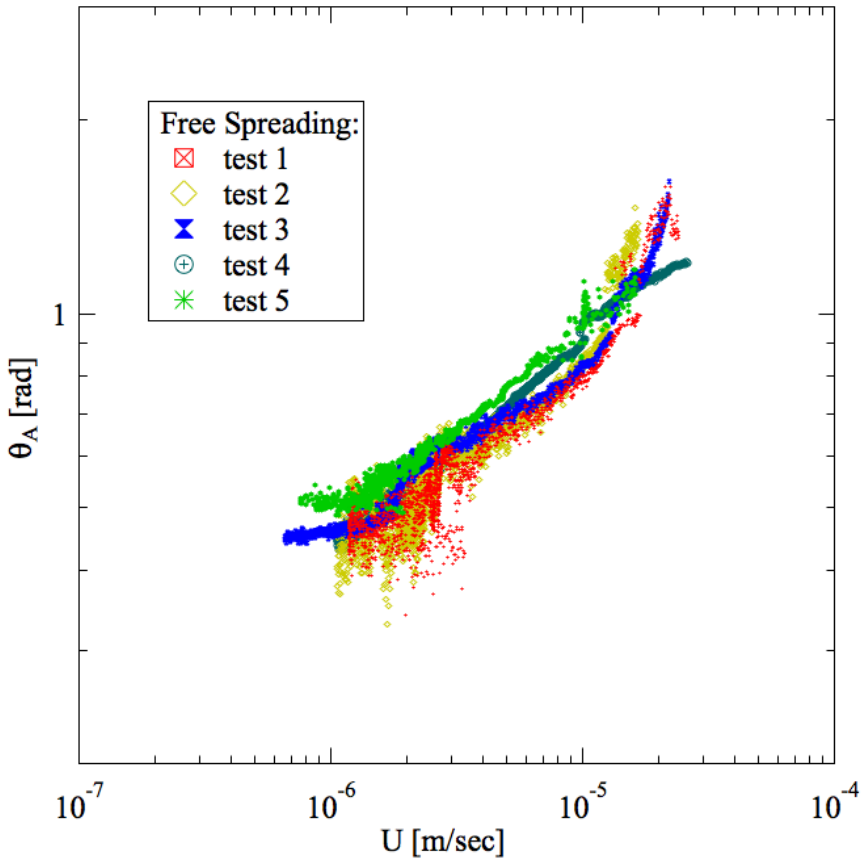

Figure 5.4: The plot of the advancing dynamic contact angle versus the liquid contact line speed for spontaneous spreading of silicone oil 10000 cSt on a glass surface.

The velocity range where silicone oil 10000 cSt spreads spontaneously on the glass surface is approximately ($10^{-6}\ m/s < U < 2\times10^{-5}\ m/s$) as shown in figure 5.4. As illustrated in figure 5.4, as the liquid contact line velocity increases, the advancing dynamic contact angle increases.

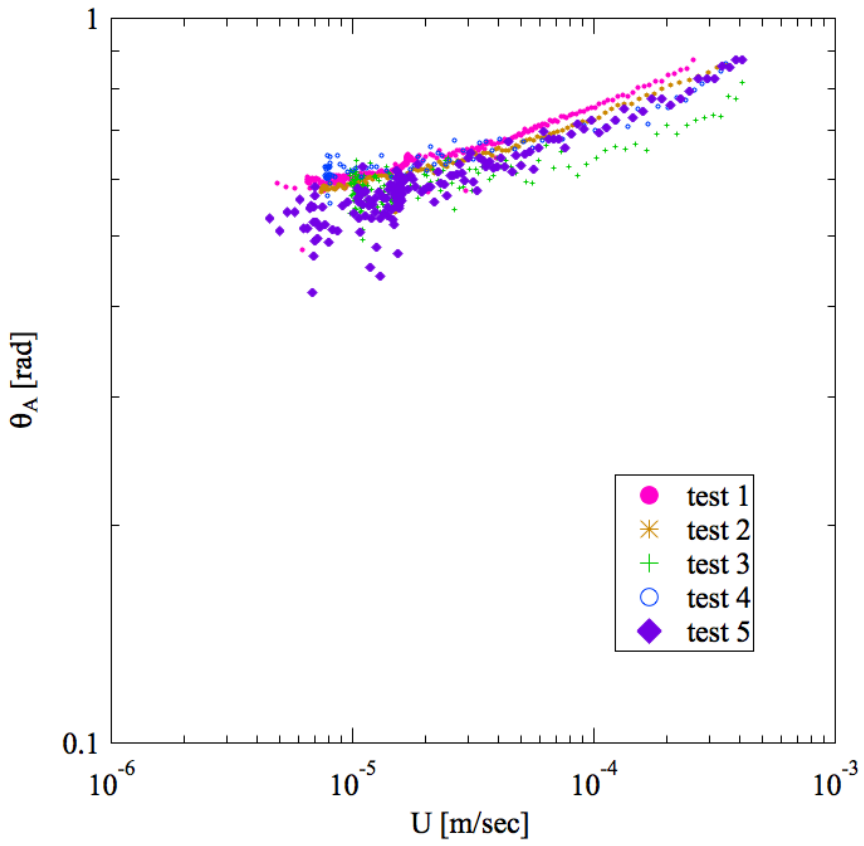

Figure 5.5: The plot of the advancing dynamic contact angle versus the liquid contact line speed for spontaneous spreading of glycerin on a glass surface.

The velocity range where glycerin spreads spontaneously on the glass surface is approximately ($10^{-5}\ m/s < U < 3\times10^{-3}\ m/s$) (Figure 5.5). As illustrated in figure 5.5, as the liquid contact line velocity increases, the advancing dynamic contact angle increases. As viscosity of the liquid increases, the resisting force to the spreading increases, hence the liquid contact line velocity over which the liquid spontaneously spreads decreases.

CHAPTER 6

Forced Spreading of Liquids

6.1 Backgrounds and Motivation

Unlike spontaneous spreading, in forced spreading, an externally imposed force such as a mechanical force or a hydrodynamic force has a prominent effect on the motion of the liquid contact line on the solid surface. Hence in forced spreading, the spreading can also go beyond the condition of thermodynamic equilibrium where the static condition is met. In forced spreading, the speed of the liquid contact line can be controlled. Hence, in forced spreading, both wetting (i.e. advancing motion of the liquid contact line on the solid surface) and de-wetting (e.g. receding motion of the liquid contact line on the solid surface) are possible to happen. Due to the ability of the control on the speed of the liquid contact line, forced spreading has a lot of interests in the coating, micro-fluidics, ink-jet printing, and painting technology. Due to the broad applications of the forced spreading mechanism in industry and technology, there have been tremendous researches in the area of spreading dynamics. In spite of enormous investigations, there are still lots of challenges in the area of spreading dynamics of forced spreading that have not been quite resolved yet such as increasing the efficiency of the coating and painting technology.

6.2 Experiment

The forced spreading experiments have been performed for five pure liquids (i.e. glycerin, dodecane, silicone oil 100 cSt, silicone oil 1000 cSt, and silicone oil 10000 cSt) on clean glass surfaces. The experiments for forced spreading method have been done using Tensiometer. The dependence of the dynamic contact angle on the speed of the liquid contact line has been investigated. For each specified speed of the liquid contact line on the Tensiometer, the experiments have been done for several cycles of advancing-receding motion of the glass substrates in the pool of the liquid to illustrate the level of confidence in the experimental results. The dynamic contact angles have been calculated based on the forced balance method. For liquids with large viscosity (i.e. silicone oil 10000 cSt and glycerin), the menisci of the liquids at the liquid contact line have been observed and recorded with SLR Canon camera during the experiments with Tensiometer and then the dynamic contact angles have been measured using ImageJ software by measuring the angle between the solid surface and the tangent line of the liquid/air interface at the liquid contact line. The images of the menisci of the silicone oil 10000 cSt on the glass substrate and the glycerin on the glass substrate captured by SLR camera during the experiments with Tensiometer are illustrated in figure 6.1 and figure 6.2, respectively.

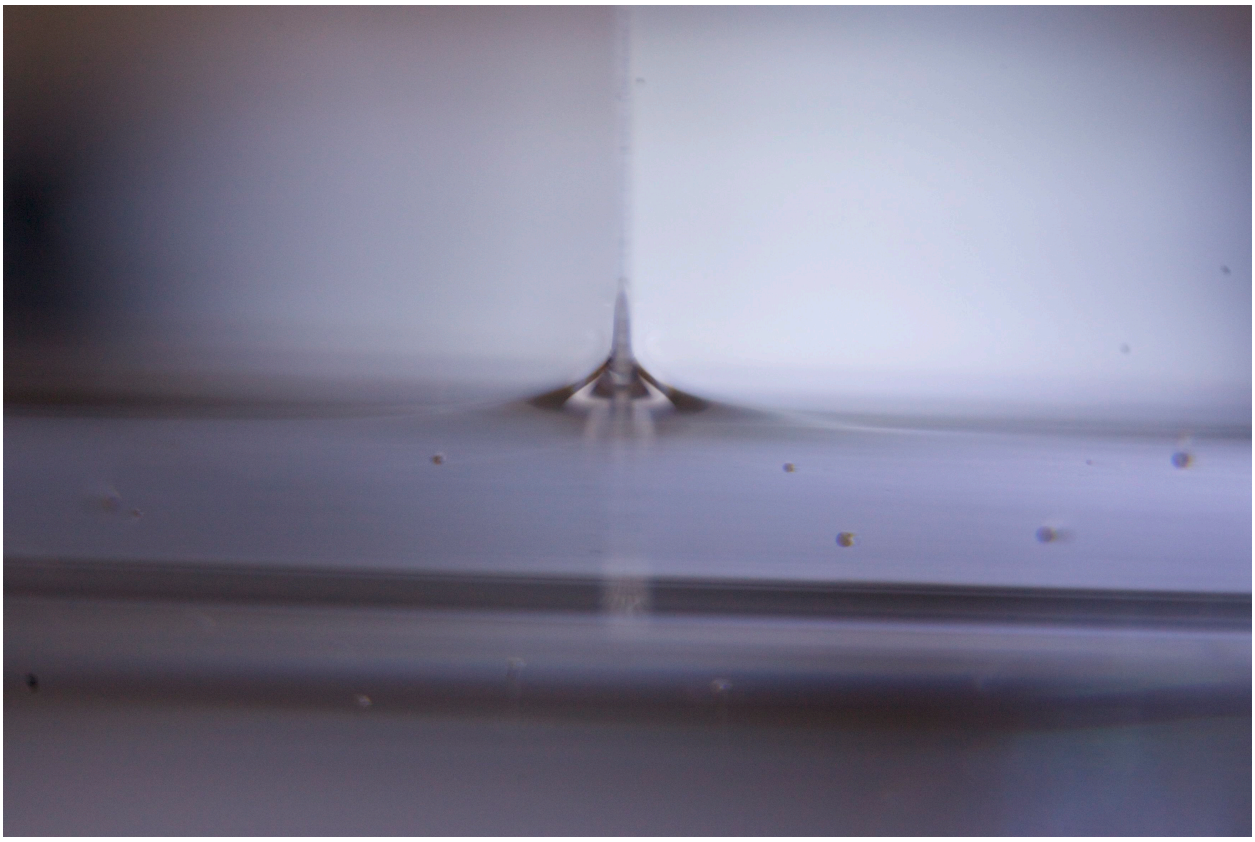

Figure 6.1: The image of the meniscus of the silicone oil 10000 cSt on glass substrate at the 10 mm/min speed of the liquid contact line captured with SLR Canon camera during the experiment with Tesniometer.

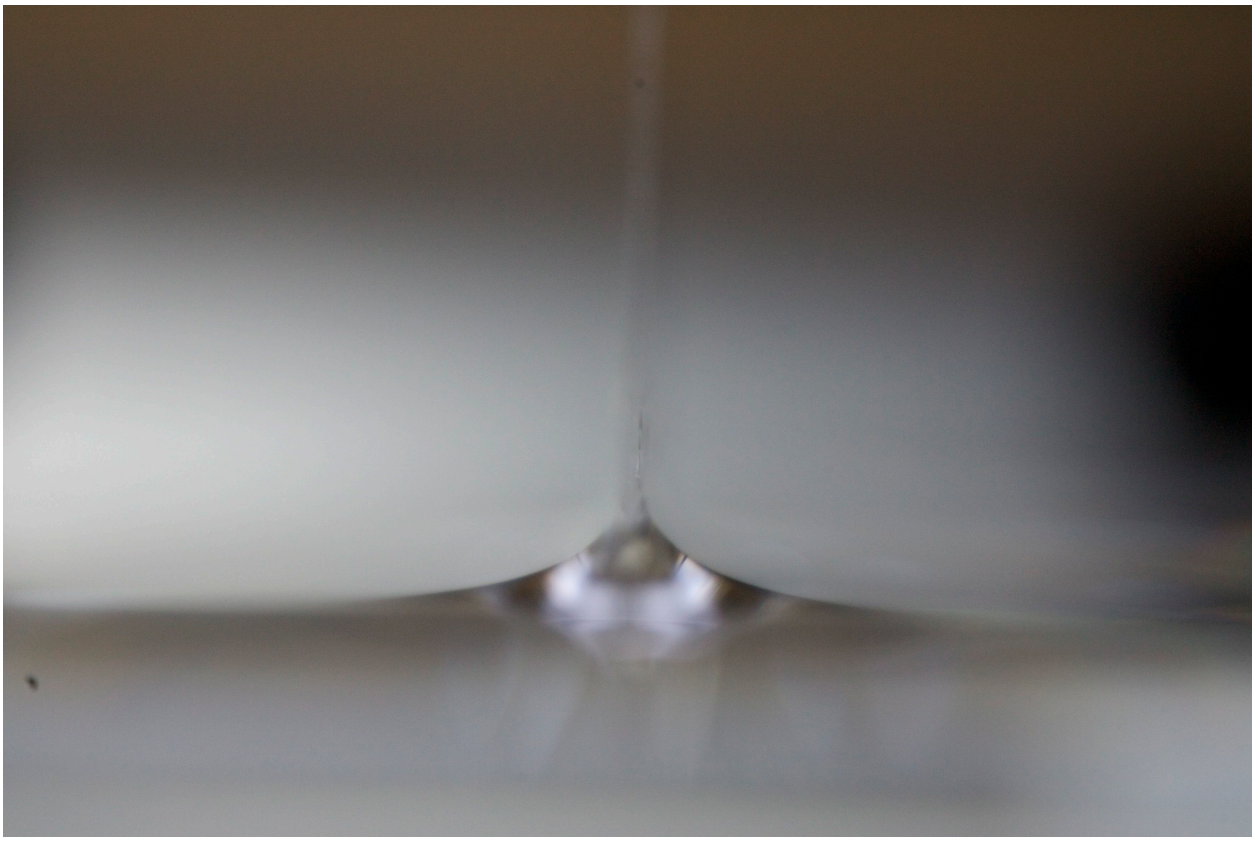

Figure 6.2: The image of the meniscus of the glycerin on glass substrate at the 10-mm/min speed of the liquid contact line captured with SLR Canon camera during the experiment with Tesniometer.

The liquids used in the forced spreading experiments are the same liquids have been used in the spontaneous spreading experiments. Table shows the physical properties of the liquids used in the forced spreading experiments.

Liquid	Density [kg/m^3]	μ [Pa s]	σ [N/m]
dodecane	746	0.001	0.023
Silicone Oil - 100 cSt	964	0.096	0.020
Silicone Oil - 1000 cSt	969	0.969	0.020
Silicone Oil - 10000 cSt	971	9.710	0.022
Glycerin	1260	1.412	0.064

Table 6.1: Physical properties of the liquids used in the forced spreading experiments.

6.3 Results and Discussion

The dependence of the advancing dynamic contact angle to the liquid contact line speed have been investigated for the forced spreading mechanism done with Tensiometer. Figure 6.3 shows the plot of the advancing dynamic contact angle versus the liquid contact line speed for the forced spreading of dodecane on glass substrate. The advancing dynamic contact angle increases as the speed of the liquid contact line increases. The experiments have been done for three cycles of dip coating for each speed of the liquid contact line to show the large level of the confidence on the experimental results. The error bars for each cycle are based on the standard deviations obtained from the dynamic contact angle calculation within the immersion depth interval of 10 mm.

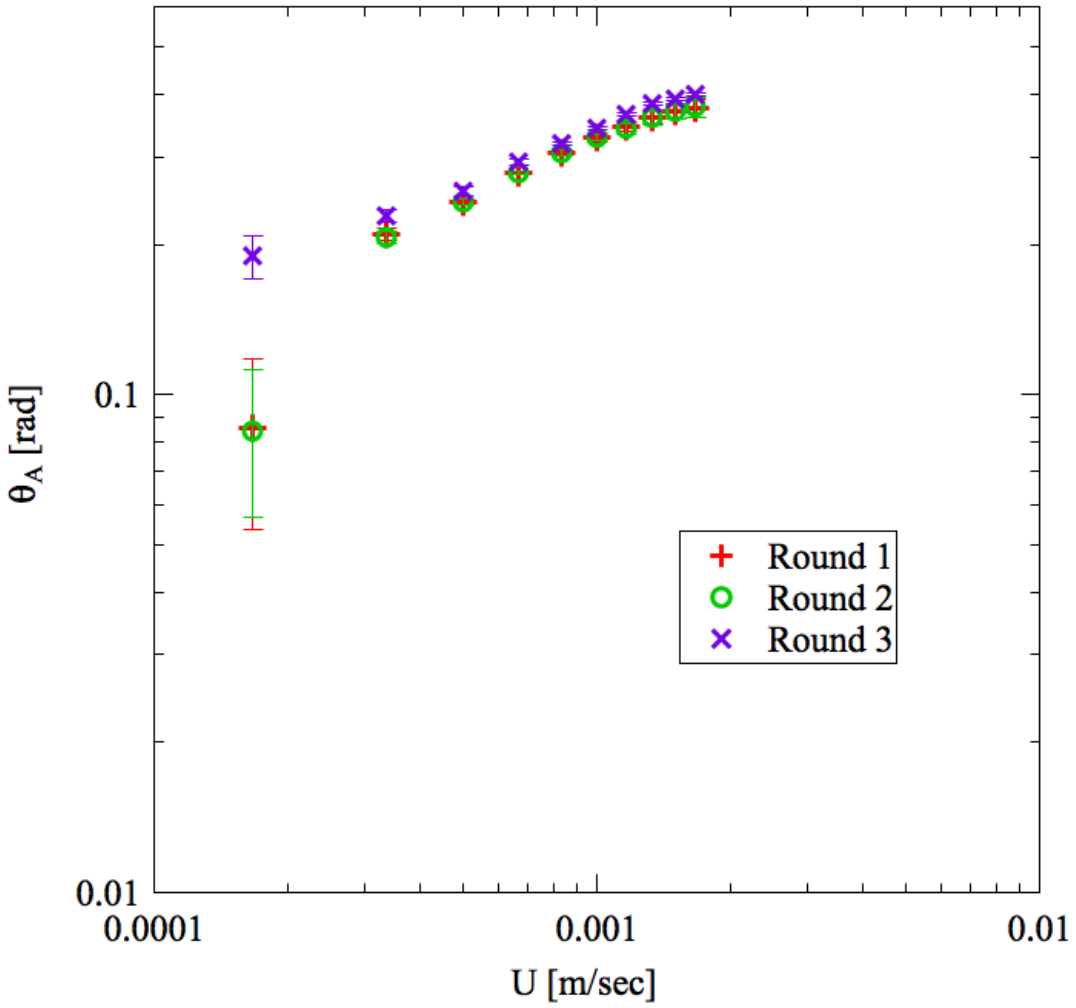

Figure 6.3: The plot of the advancing dynamic contact angle versus the liquid contact line speed for forced spreading of the dodecane on glass substrate.

Figure 6.4 shows the plot of the advancing dynamic contact angle versus the liquid contact line speed for the forced spreading of silicone oil 100 cSt on glass substrate. The advancing dynamic contact angle increases as the speed of the liquid contact line increases. The experiments have been done for three cycles of dip coating for each speed of the liquid contact line to show the large level of the confidence on the experimental results. The experiments have

been repeated two times. The error bars for each cycle are based on the standard deviations obtained from the dynamic contact angle calculation within the immersion depth interval of 10 mm.

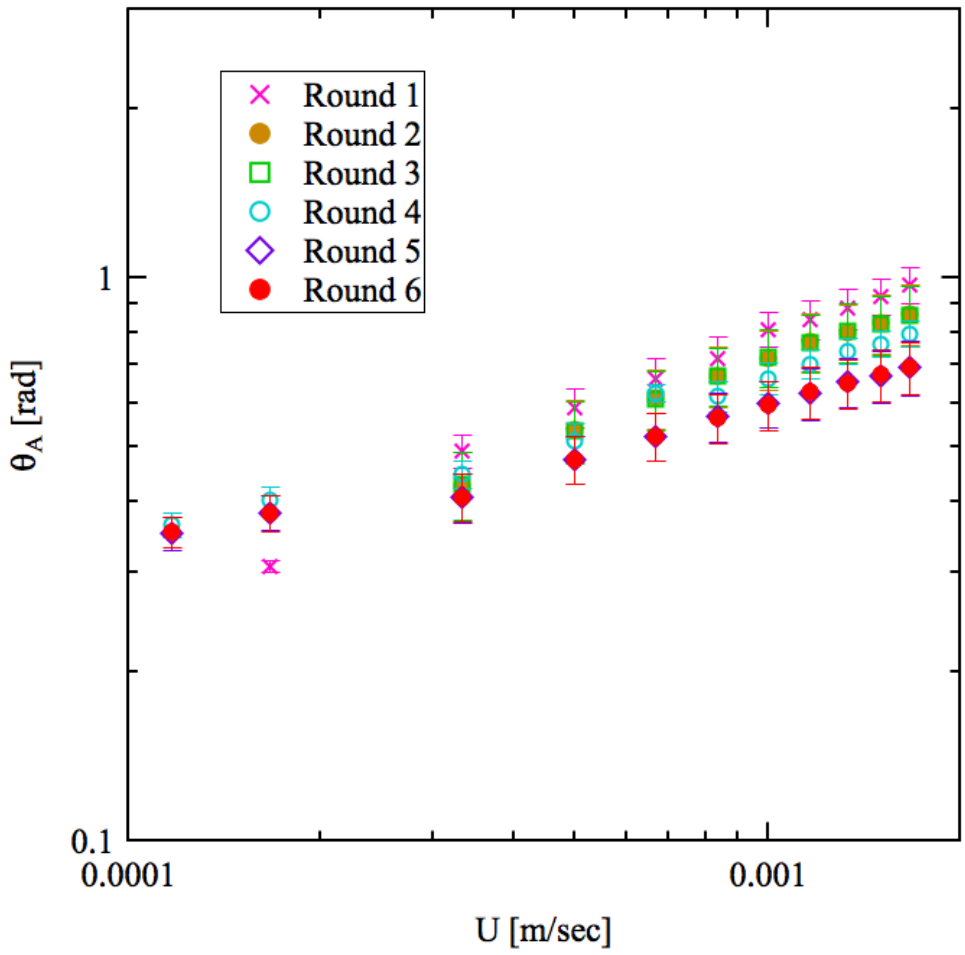

Figure 6.4: The plot of the advancing dynamic contact angle versus the liquid contact line speed for forced spreading of the silicone oil 100 cSt on glass substrate.

Figure 6.5 shows the plot of the advancing dynamic contact angle versus the liquid contact line speed for the forced spreading of silicone oil 1000 cSt on glass substrate. The advancing

dynamic contact angle increases as the speed of the liquid contact line increases. The experiments have been done for three cycles of dip coating for each speed of the liquid contact line to show the large level of the confidence on the experimental results. The error bars for each cycle are based on the standard deviations obtained from the dynamic contact angle calculation within the immersion depth interval of 10 mm.

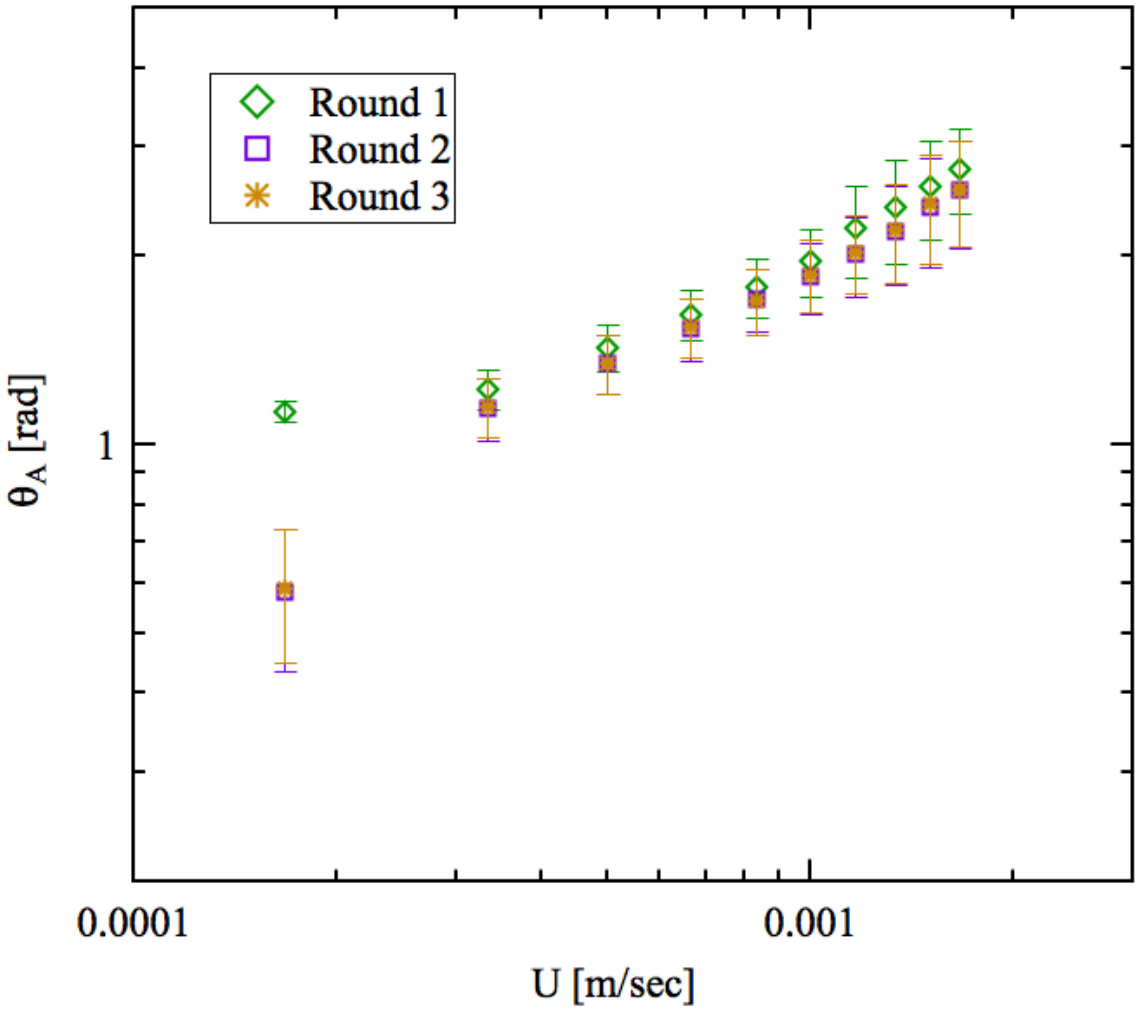

Figure 6.5: The plot of the advancing dynamic contact angle versus the liquid contact line speed for forced spreading of the silicone oil 1000 cSt on glass substrate.

Figure 6.6 shows the plot of the advancing dynamic contact angle versus the liquid contact line speed for the forced spreading of silicone oil 10000 cSt on glass substrate. The advancing dynamic contact angle increases as the speed of the liquid contact line increases. The experiments have been done for 5 rounds of dip coating for each speed of the liquid contact line to show the large level of the confidence on the experimental results.

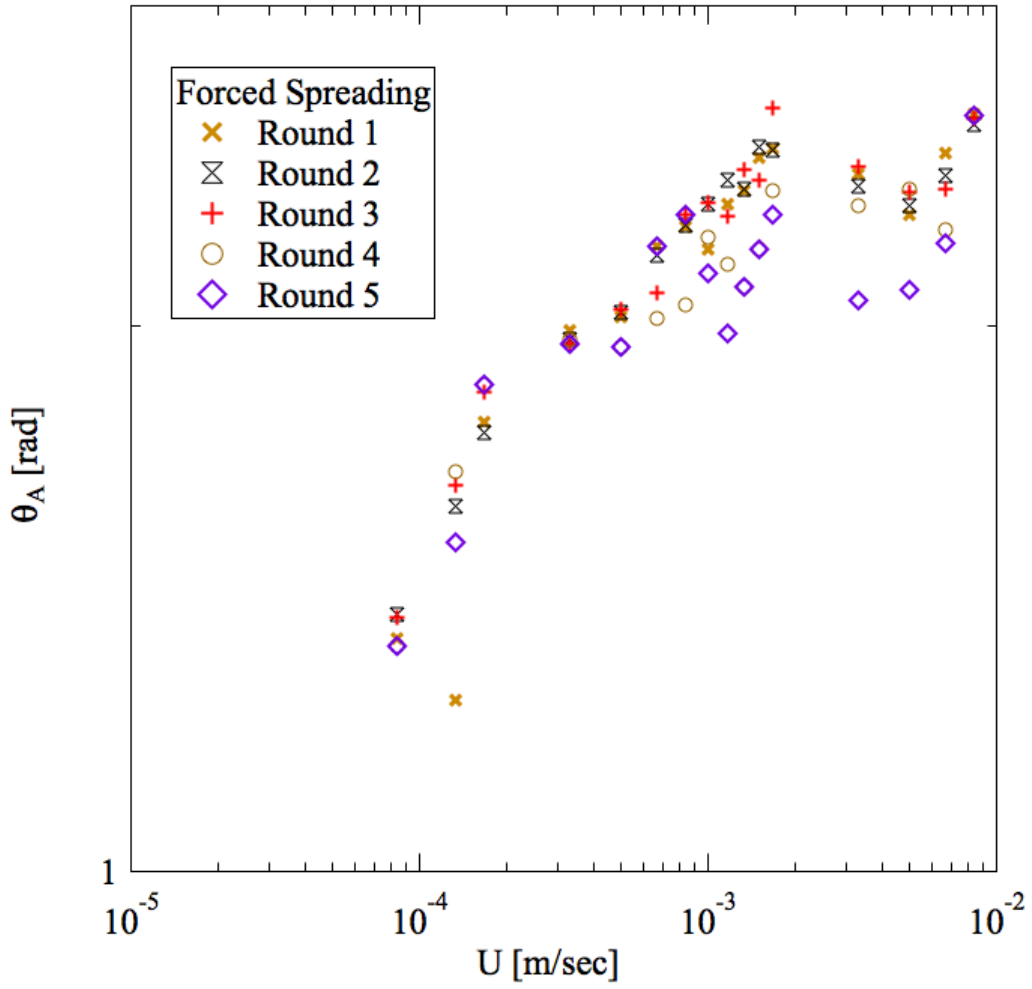

Figure 6.6: The plot of the advancing dynamic contact angle versus the liquid contact line speed for forced spreading of the silicone oil 10000 cSt on glass substrate.

Figure 6.7 shows the plot of the advancing dynamic contact angle versus the liquid contact line speed for the forced spreading of glycerin on glass substrate. The advancing dynamic contact angle increases as the speed of the liquid contact line increases. The experiments have been done for three cycles of dip coating for each speed of the liquid contact line to show the large level of the confidence on the experimental results. The error bars for each cycle are based on the standard deviations obtained from the dynamic contact angle measurements with ImageJ at different locations within the immersion depth interval of 10 mm to show the level of the confidence on the experimental results.

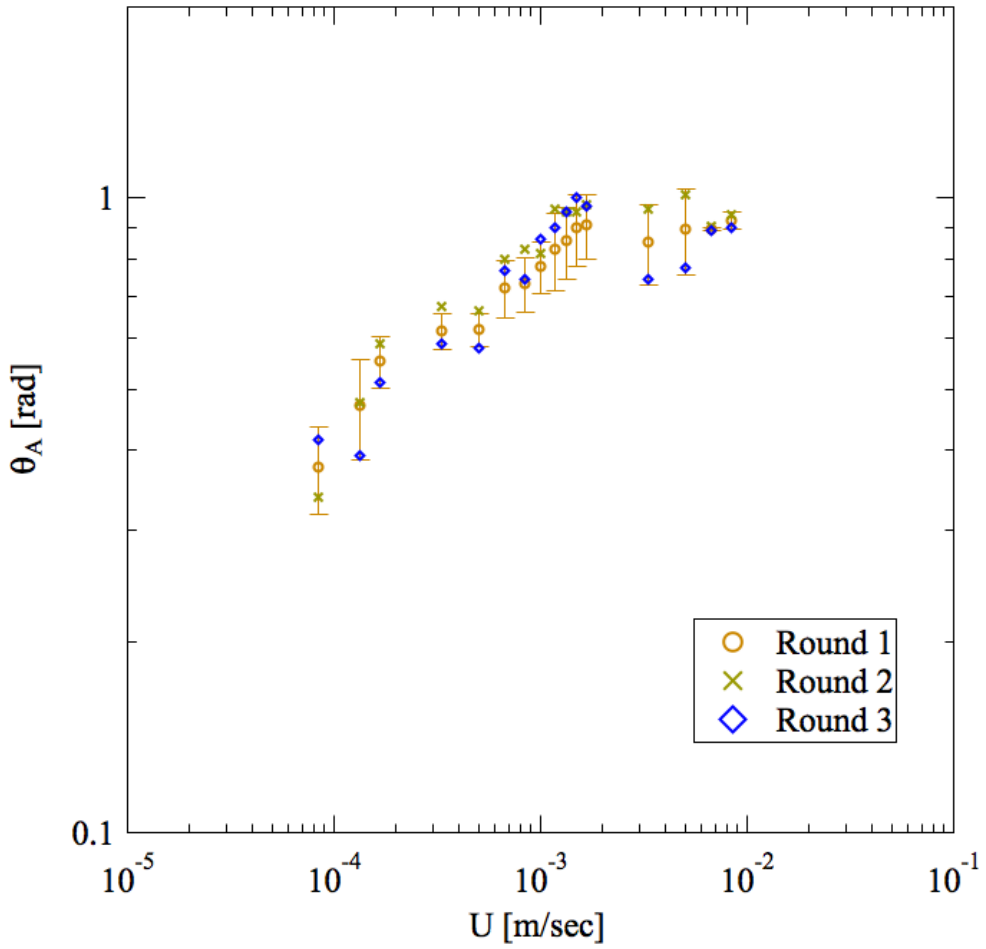

Figure 6.7: The plot of the advancing dynamic contact angle versus the liquid contact line speed for forced spreading of the glycerin on glass substrate.

CHAPTER 7

Forced versus Spontaneous Spreading of Liquids

7.1 Abstract

Over half a century, there have been many experimental/numerical investigations of the moving contact line in forced and free spreading. Surprisingly, there have been no experimental studies comparing these spreading mechanisms for the same solid/liquid/vapor system. In the present research such experiments are performed on identical liquid-solid systems. Experimental results from free (i.e. spontaneous) spreading show different values compared to the experimental results obtained from forced spreading for the same solid-liquid system. For free (i.e. spontaneous) spreading, excellent agreement is found using the hydrodynamics theory, as expected. For forced spreading on the same solid-liquid systems it is shown that does not apply, but instead the molecular-kinetic theory does. The results obtained from our fitting analysis signify that the more appropriate spreading dynamics for experiments on a given solid-liquid system depends on the mechanism of the spreading (i.e. spontaneous or forced). This distinction between free and forced systems has never been noted before. Moreover, this research will

provide a hypothesis for predicting the more appropriate model to describe the contact line dynamics for free and forced spreading mechanisms.

7.2 Introduction

Most of the researchers in the area of spreading have used in several cases a relationship between the dynamic contact angle and velocity of liquid contact line based on hydrodynamics theory (HDT) [1,3,16,20,45-47,50,56,57,61-64,66-68,70-74,79-81,88,96,97], which relates the dynamic contact angle to the speed of the contact line. Different forms of this relationship are known as Tanner's law [88], Hoffman-Voinov-Tanner law [16,70,88], de Gennes model [73], or Cox model [71]. All forms of HDT are derived based on viscous flow.

The general form of hydrodynamics theory to describe the dynamics of spreading can be shown in the following form:

$$\theta^3 - \theta_0^3 = 9Ca \ln\left(\frac{L_{mac}}{L_{mic}}\right) \tag{7.1}$$

where $Ca = \frac{\mu U}{\sigma}$ is the capillary number, μ is the dynamic viscosity of liquid, σ is the surface tension, θ is dynamic contact angle, and θ_0 is equilibrium contact angle. In equation 7.1, plus sign refers to the advancing motion and minus sign refers to the receding motion. In equation 7.1, L_{mac} is the macroscopic length scale in that system and L_{mic} is the microscopic length scale usually related to slip.

Eggers and Stone [96] have shown that L_{mac} / L_{mic} is a velocity dependent parameter. They have obtained the dependence of L_{mac} / L_{mic} to the Capillary number (i.e. $\left(L_{mac} / L_{mic}\right) = \alpha Ca^{2/3}$) for the case of perfectly wetting liquids with consideration of slip boundary condition over small

slip length L_{mic} in the region close to the liquid contact line. Eggers and Stone [96] have assumed a nearly flat interface close to the liquid contact line to apply lubrication assumption for describing the liquid motion and they have considered the pressure variation caused by capillary and van der Waals forces.

Another fundamental law of spreading dynamics is called molecular-kinetic theory (MKT), which has been proposed by Blake [67,68]. MKT ignores bulk liquid flow but focuses on the molecular attachment/detachment at the vicinity of three-phase contact line. Molecular-kinetic theory shows the relationship between dynamic contact angle and contact line speed by applying Eyring's theory [61] giving following:

$$\theta = \cos^{-1}\left\{\cos\theta_0 \pm \frac{2k_B T}{\lambda^2 \sigma} \sinh^{-1}\left(\frac{U}{2K_w \lambda}\right)\right\} \tag{7.2}$$

In equation 7.2, k_B is the Boltzmann constant, T is temperature, K_w is the equilibrium frequency of the random molecular displacements at the contact line and λ is the average distance between adsorption sites on the solid surface on which the random molecular displacements occur. In equation 7.2, plus sign denotes the receding motion and the minus sign denotes the advancing motion.

Both theories describe the dynamics of wetting though, perhaps, in different parameter ranges as it has been investigated in the past for both spontaneous spreading and forced spreading separately. Davis and Davis [80] show that for given material properties, equation 7.1 and equation 7.2 give intersecting plots of θ versus U as depicted in figures 7.1 and 7.2; They argue that the crossing point gives a critical speed below which MKT applies and above which HDT does using free spreading data of silicone oil on glass and high temperature spreading of

liquid metal on molybdenum (Mo). We wish to investigate forced spreading experimentally and determine which theory applies.

Surprisingly, the appropriate spreading dynamics that described the forced spreading mechanism is not usually the same as the spreading dynamics that interpreted the spontaneous spreading mechanism for the same solid-liquid system. The choice of the appropriate spreading dynamics for a solid-liquid system depends also on the mechanism of the spreading.

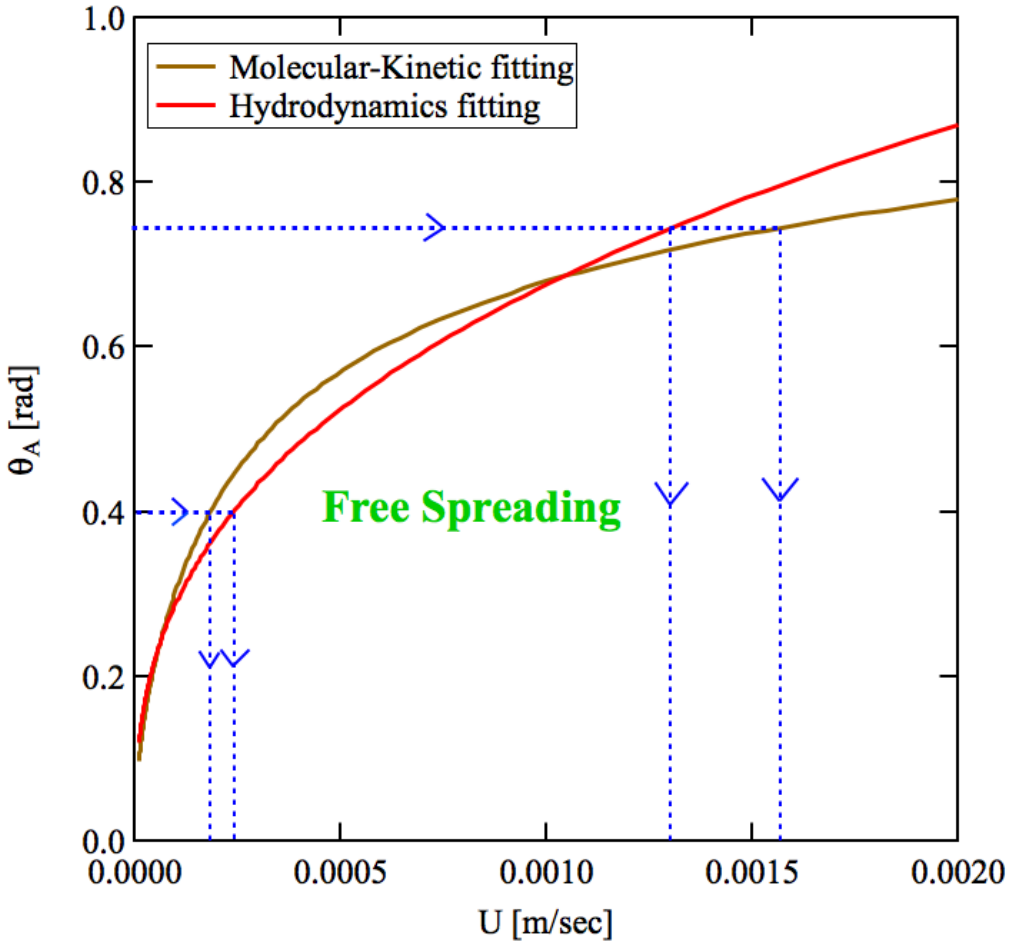

Figure 7.1: Schematic plots explaining our hypothesis for predicting the more appropriate model to describe the contact line dynamics for free (i.e. spontaneous) spreading mechanism. The plots of HDT and MKT shown in the illustrations of hypothesis are obtained from analysis for spreading of silicone oil 100 cSt on glass. Strategy to predict the appropriate spreading dynamics for free spreading: For observed dynamic contact angle, the appropriate spreading dynamics is the one which gives higher contact-line speed for the corresponding observed dynamic contact angle.

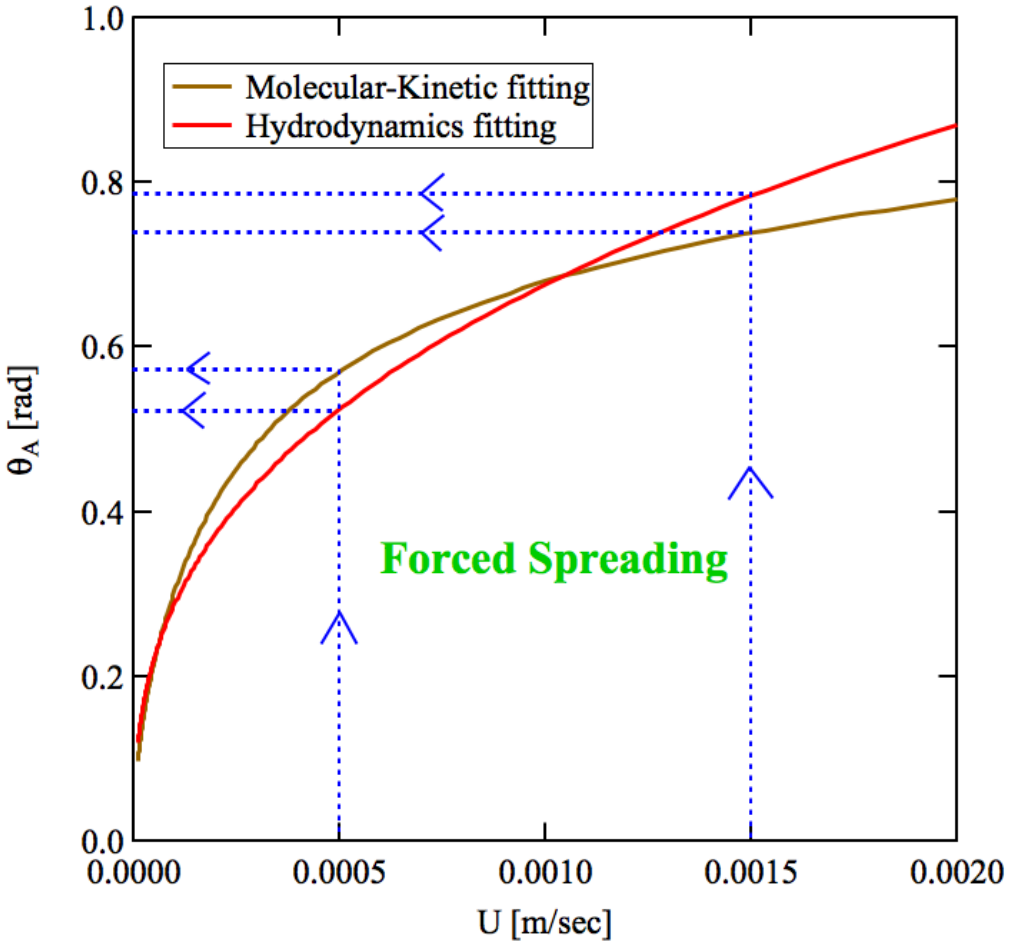

Figure 7.2: Schematic plots explaining our hypothesis for predicting the more appropriate model to describe the contact line dynamics for forced spreading mechanism. The plots of HDT and MKT shown in the illustrations of hypothesis are obtained from analysis for spreading of silicone oil 100 cSt on glass. The strategy to predict the appropriate spreading dynamics for forced spreading: For given fixed contact line speed, the appropriate spreading dynamics is the one which gives higher dynamic contact angle for the corresponding given fixed speed of contact line.

7.3 Experimental Methods and Materials

In the free spreading of a drop on a substrate, figure 7.3, no external force is imposed on the contact line during its motion. In forced spreading, figure 7.4, in which liquid is applied to the substrate that the externally imposed forces such as a mechanical or a hydrodynamic force drives the spreading, and so the speed of the contact line can be controlled.

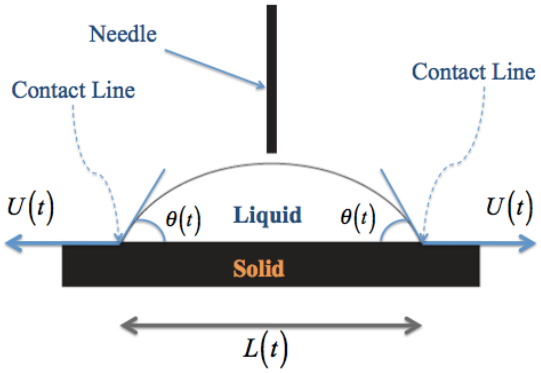

Figure 7.3: Schematic picture of the free spreading experiment.

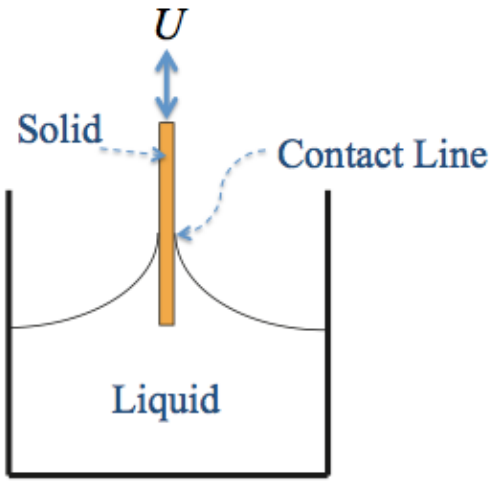

Figure 7.4: Schematic picture of the forced spreading experiment.

In our experimental results obtained from both free and forced spreading, we have used HDT, equation 7.1, and MKT, equation 7.2, for analysis of the experimental results. In equation 7.1, the ratio of macroscopic to microscopic length scales, L_{mac}/L_{mic}, has been replaced by $\left(\alpha Ca^{2/3}\right)$ [96] for the cases where equilibrium contact angle is zero. For the case of partial wetting (i.e. spreading of glycerin on glass), in equation 7.1, the macroscopic length scale was replaced by capillary length, $\sqrt{\sigma/(\rho g)}$, and microscopic length scale was set as a fitting parameter in the hydrodynamics analysis. In our analysis, the physical properties of liquid are set fixed with values shown in table 7.1. For HDT, the multiplicative factor α is used as a free fitting parameter. For MKT, the two solid properties (i.e. λ and K_w) are used as the free parameters.

Here, free spreading experiments are done using Drop Shape Analyzer (DSA100, KRÜSS) with deposition of liquid droplet with zero impact velocity on the solid surface as it is shown. Forced spreading experiments are done using a Tensiometer (K100, KRÜSS) with specified speed of the motion of the contact line. The experiments are performed for several liquids on clean glass substrates where equilibrium contact-angles, θ_0, are zero and for glycerin on glass substrate where the $\theta_0 \approx 0.552$ rad. Table 7.1 shows the experimentally measured physical properties of pure liquids that have been used in the experimental investigations.

Liquid	Density [kg/m^3]	μ [Pa s]	σ [N/m]
dodecane	746	0.001	0.023
Silicone Oil - 100 cSt	964	0.096	0.020
Silicone Oil - 1000 cSt	969	0.969	0.020
Silicone Oil - 10000 cSt	971	9.710	0.022
Glycerin	1260	1.412	0.064

Table 7.1: Physical properties of pure liquids used in the experiments.

In our experimental results obtained from both free and forced spreading, we have used HDT (equation 7.1) and MKT (equation 7.2) for analysis of the experimental results. In equation 7.1, the ratio of macroscopic to microscopic length scales, L_{mac} / L_{mic} , has been replaced by $\alpha Ca^{2/3}$ [96]. In our analysis, the physical properties of liquid are set fixed with values shown in table 7.1. For HDT, the multiplicative factor α is used as a free fitting parameter. For MKT, the two solid properties (i.e. λ and K_w) are used as the free parameters.

7.4 Results and Discussion

The experimentally measured dynamic contact angles for free and forced spreading are drastically different for all cases of liquids as shown in figures 7.5, 7.6, 7.7, 7.8, 7.9, 7.10, and 7.11. θ_A is the advancing dynamic contact angle and U is the velocity of the liquid contact line. The free spreading of dodecane on glass and silicone oil 100 cSt on glass are consistent only with HDT, as expected; The free spreading of silicone oil 1000 cSt on glass may be approximately consistent with HDT as shown in figure 7.7.

In contrast, the forced spreading of dodecane on glass and silicone oil 1000 cSt on glass are consistent only with MKT as shown in figures 7.5 and 7.7. Forced spreading of silicone oil 100 cSt on glass surface could be described by both theories as shown in figure 7.6 because the experimental data corresponding to silicon oil 100 cSt are within the narrow region about the crossing point of the two theories.

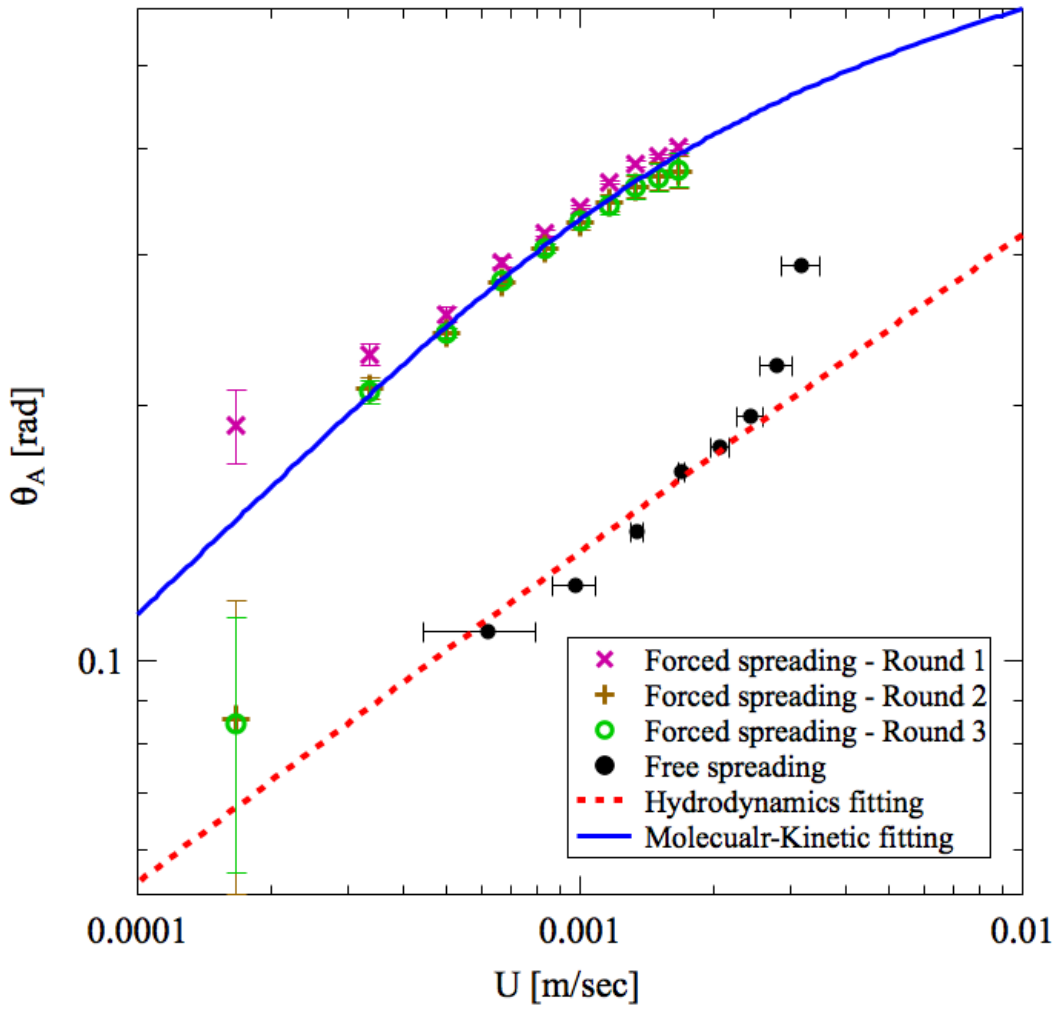

Figure 7.5: Experimental comparison between free and forced spreading for spreading of dodecane on glass surface: $\alpha = 86751 \pm 3.54\times10^{4}$, $\lambda = 2.6421\times10^{-9} \pm 1.86\times10^{-10}\left[\mathrm{m}\right]$, $K_{w} = 1.5019\times10^{5} \pm 3.92\times10^{4}\left[\mathrm{Hz}\right]$.

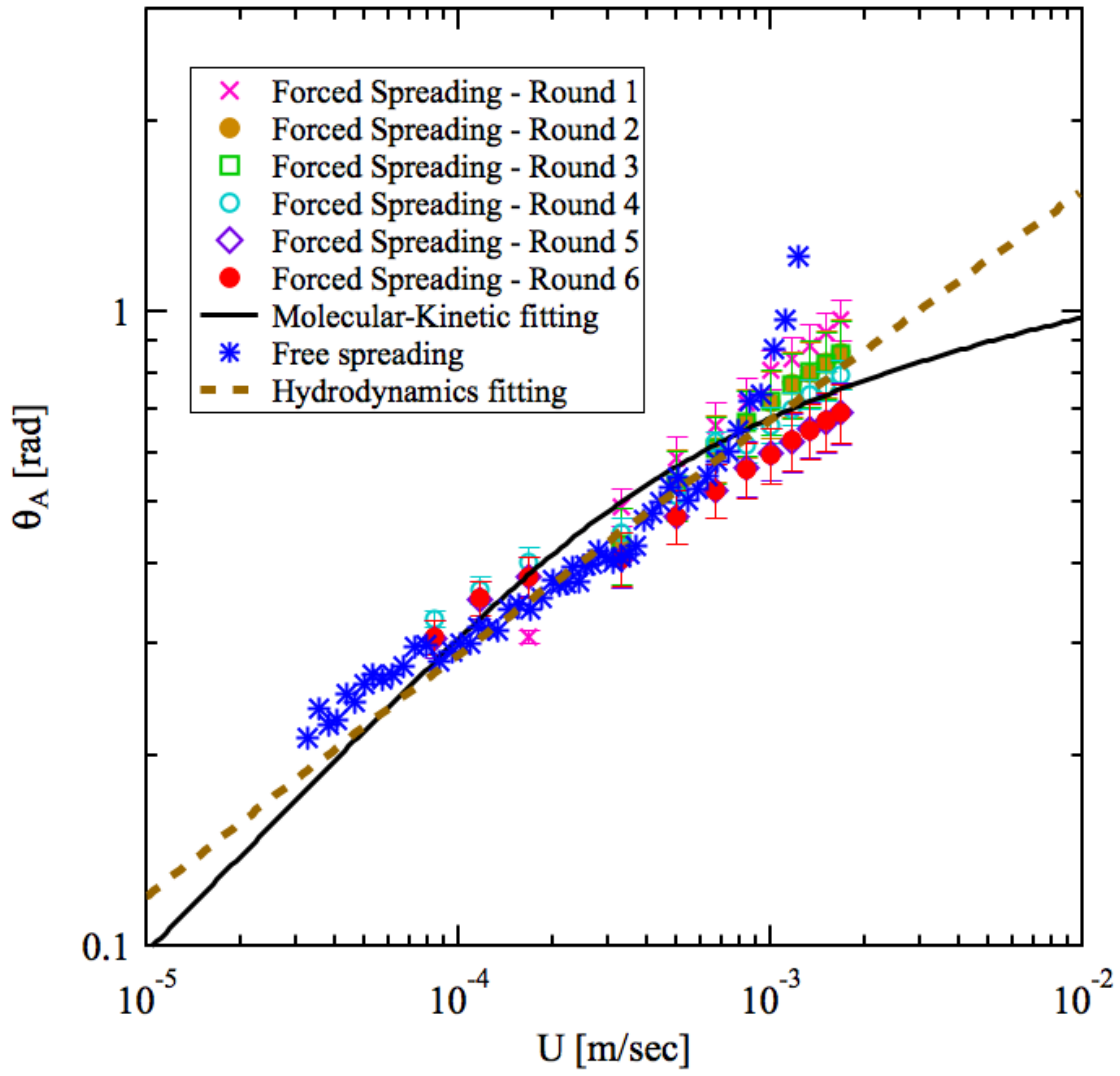

Figure 7.6: Experimental comparison between free and forced spreading for spreading of Silicone Oil 100 cSt on glass surface: $\alpha = 37183 \pm 5.96\times10^{3}$, $\lambda = 2.0762\times10^{-9} \pm 1.23\times10^{-10}\left[\mathrm{m}\right]$, $K_w = 48172 \pm 1.44\times10^{4}\left[\mathrm{Hz}\right]$.

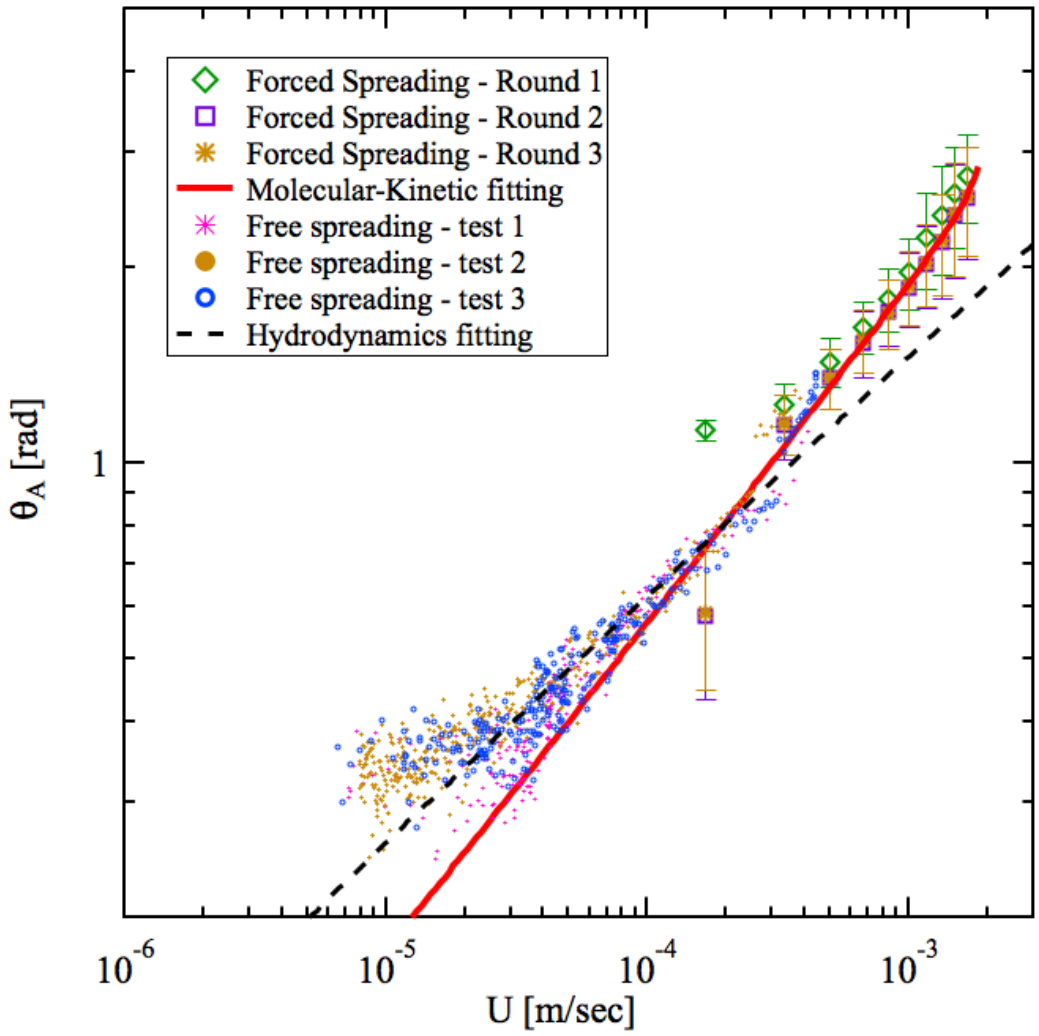

Figure 7.7: Experimental comparison between free and forced spreading for spreading of Silicone Oil 1000 cSt on glass surface: $\alpha = 9767.5 \pm 1.37\times10^{3}$, $\lambda = 5.7932\times10^{-10} \pm 2.95\times10^{-11}\left[\mathrm{m}\right]$, $K_{w} = 6.6252\times10^{5} \pm 1.36\times10^{5}\left[\mathrm{Hz}\right]$.

For the free spreading of dodecane on glass, HDT only applies up to approximately speed of contact line equal to 2.0491×10^{-3} m/sec, which corresponds, to the capillary number, $Ca \approx 1.37\times10^{-4}$. This is due to the fact that beyond this speed, the assumption of quasi-steady-

state is not valid since evaporation of the dodecane starts to happen which is an unsteady effect. For spreading of dodecane on glass, MKT (forced spreading dynamics) and HDT (free spreading dynamics) cross at two points, which are at equilibrium and at the contact line speed of 0.10353 [m/sec] corresponding to the advancing dynamic contact angle of 0.792 rad.

For free spreading of silicone oil 100 cSt on glass, HDT does not apply beyond contact-line speed of 7.89×10^{-4} m/sec corresponding to capillary number, $Ca\approx3.8\times10^{-2}$, which is not small and HDT only works for very small capillary number. For spreading of silicone oil 100 cSt on glass, the results of forced and free spreading were very close until the contact-line speed of 7.89×10^{-4} m/sec.

Free spreading of silicone oil 1000 cSt on glass does not follow HDT beyond contact-line speed of 2.48×10^{-4} m/sec corresponding to capillary number, $Ca\approx1.2\times10^{-2}$. The crossing point of MKT and HDT for spreading of silicone oil 1000 cSt on glass occurs at contact line speed of 1.95×10^{-4} m/sec corresponding to 0.8 rad which is very close to the point beyond where HDT could not be applied on the free spreading of silicone oil 1000 cSt on glass due to large capillary number as mentioned earlier here and as shown in figure 7.7 the free spreading of silicone oil 1000 cSt on glass follows MKT beyond the crossing point with the same trend of results of forced spreading for silicone oil 1000 cSt on glass.

For free spreading of silicone oil 10000 cSt on glass, HDT applies up to contact line speed of 1.28×10^{-5} m/sec corresponding to capillary number, $Ca\approx5.8\times10^{-3}$. For spreading of silicone oil 10000 cSt on glass, the crossing point of MKT and HDT obtained from the experiments, which are at contact-line speed of 9.9×10^{-11} m/sec corresponding to 0.0145 rad match with the crossing point of MKT and HDT predicted from analysis of Davis and Davis [80] which are found to be the contact-line speed of 9.0067×10^{-11} m/sec corresponding to 0.0139 rad. Another

crossing of MKT and HDT for spreading of silicone oil 10000 cSt on glass occurs at contact-line speed of 5.5×10^{-5} m/sec corresponding to 1.66 rad.

The trend of dependency of contact angle, θ, versus speed, U, for free and forced spreading of silicone oil 10000 cSt on glass substrate are very different as shown in figure 7.8.

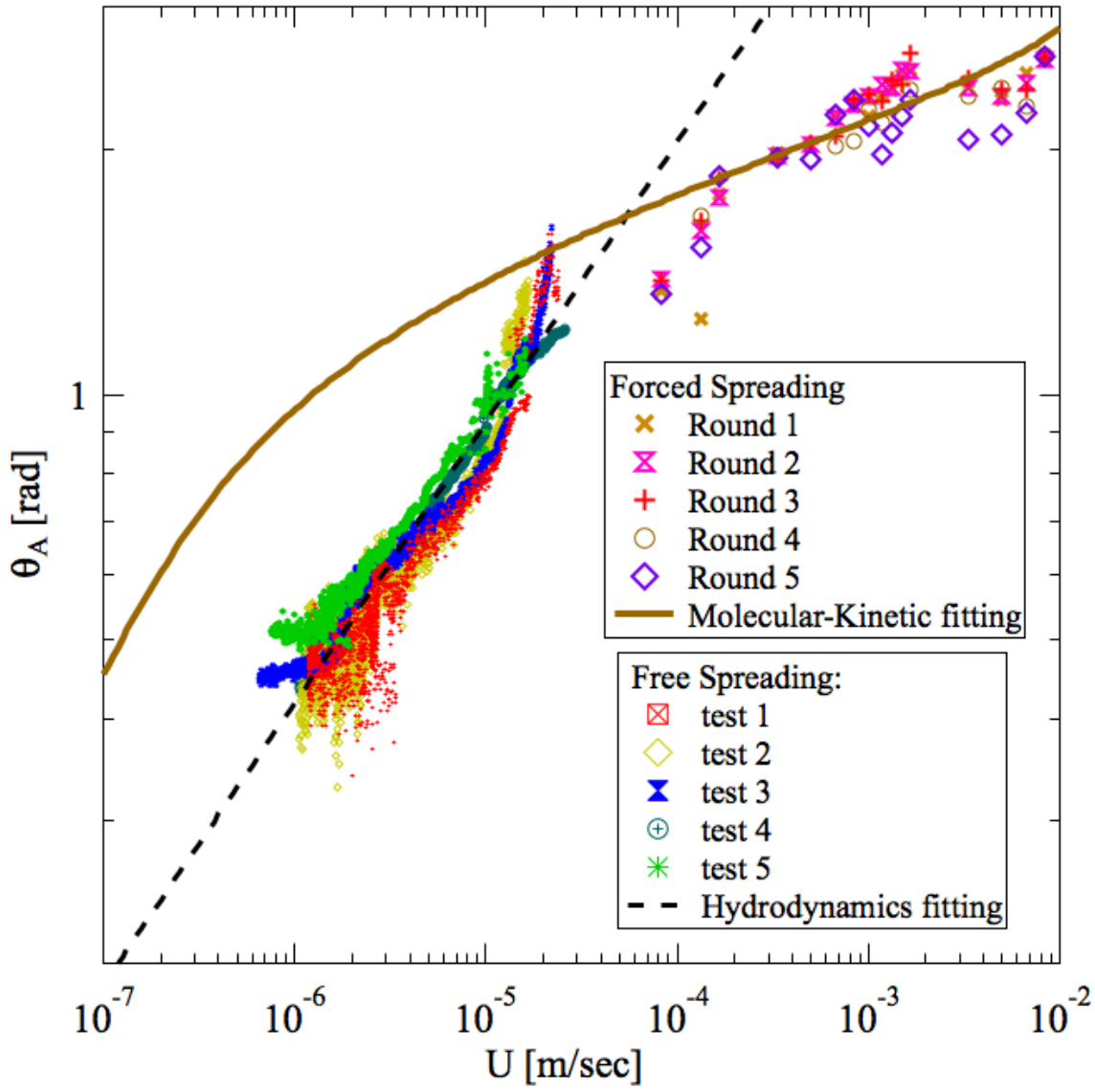

Figure 7.8: Experimental comparison between free and forced spreading for spreading of Silicone Oil 10000 cSt on glass surface: $\alpha = 1.0716\times10^{10} \pm 9.74\times10^{7}$,

$\lambda = 1.5194\times10^{-9} \pm 1.17\times10^{-10}\left[\mathrm{m}\right]$, $K_w = 50.962 \pm 84.1\left[\mathrm{Hz}\right]$.

The dynamics of free spreading of silicone oil 10000 cSt on glass is consistent with HDT where as that of forced spreading of silicone oil 10000 cSt on glass substrate is consistent with MKT. Note that the free-spreading experiments could not reach to the range of speeds of the

contact line that are seen in the forced spreading. Hence, we cannot compare the two spreading mechanisms for the same contact-line speed.

Free spreading of glycerin on glass follows HDT up to contact line speed of 4.1×10^{-4} m/sec corresponding to capillary number, $Ca \approx 9.0\times10^{-3}$. Crossing of MKT and HDT for spreading of glycerin on glass happens at very high speed of contact line (i.e. 0.0106 m/sec) corresponding to 2.7634 rad obtained from analysis of Davis and Davis [80] which is consistent with the experiments which shows the crossing may happen at very high speeds of the contact-line, a value almost impossible to obtain for free spreading. The trends of contact angle, θ, versus speed, U, for free (HDT) and forced (MKT) spreading of glycerin on glass substrate are completely different as shown in figures 7.9, 7.10, and 7.11.

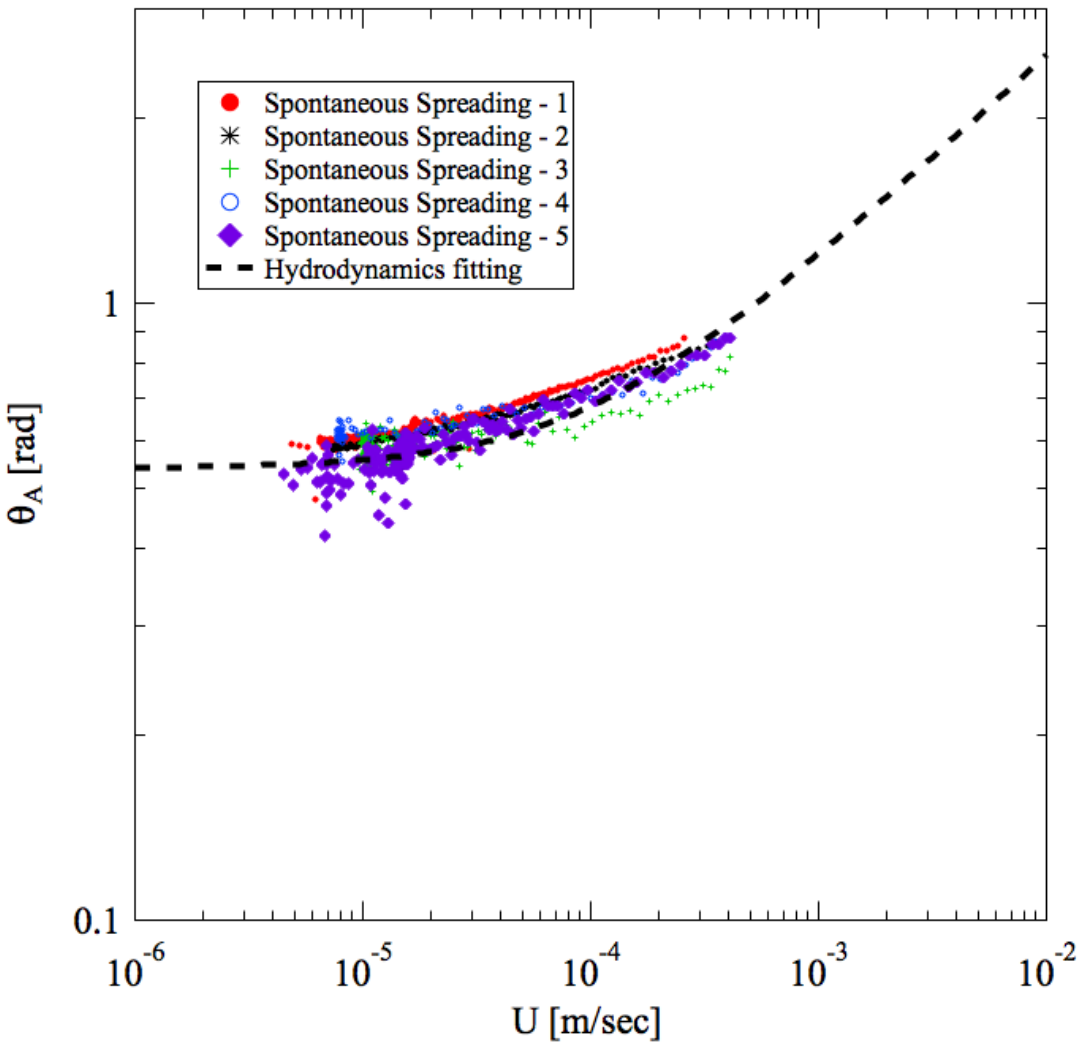

Figure 7.9: Free spreading of glycerin on glass substrate:

$\theta_{0A} = 0.5397 \pm 0.00387 \left[\text{rad}\right],\ \mu = 1.412 \left[\text{Pa.sec}\right],\ \sigma = 0.064 \left[\text{N/m}\right],\ \rho = 1260 \left[\text{kg/m}^3\right],$

$L_s = 7.7421 \times 10^{-7} \pm 2.75 \times 10^{-7} \left[\text{m}\right].$

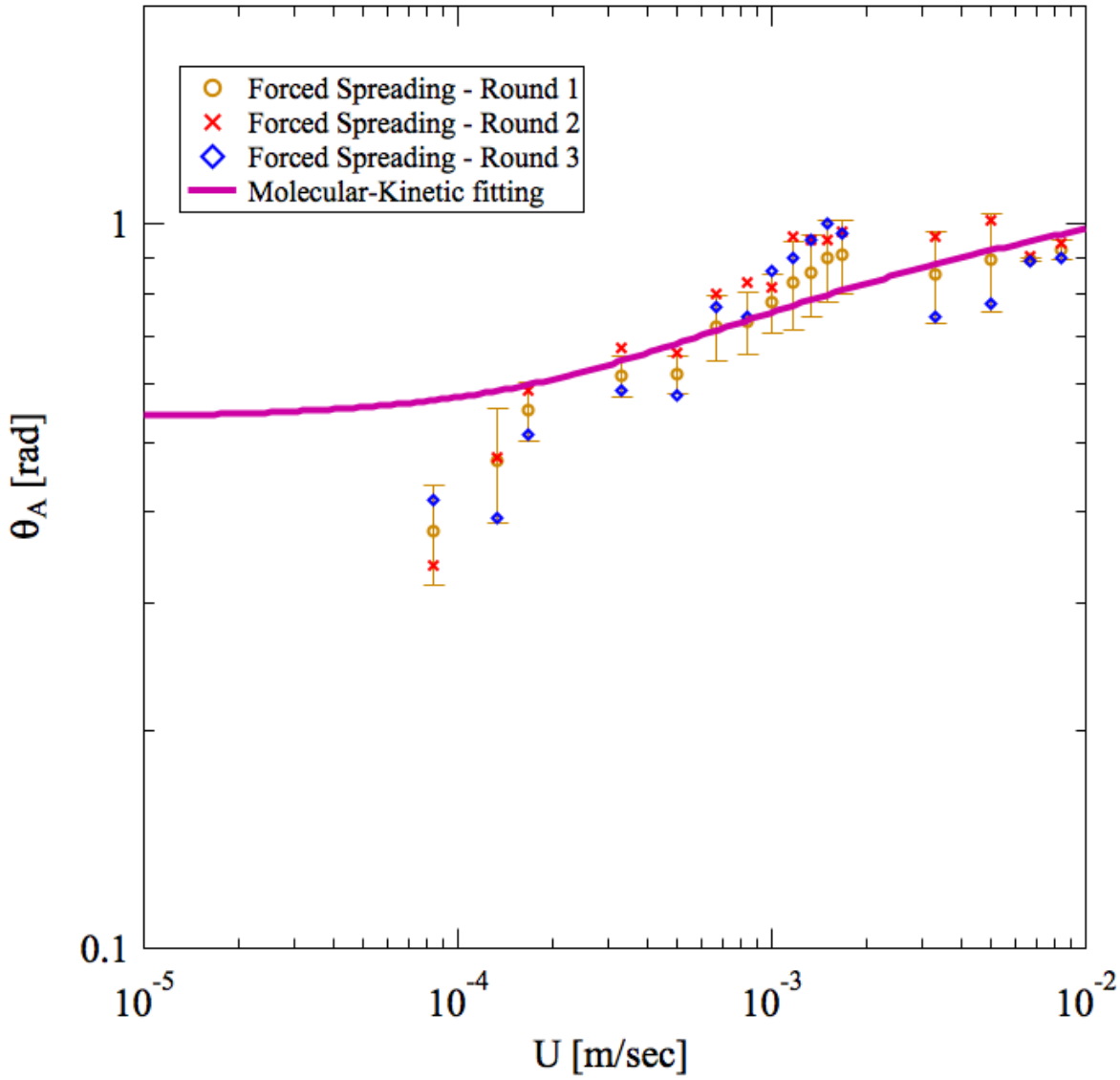

Figure 7.10: Forced spreading of glycerin on glass substrate: $\theta_{0A} = 0.5397\left[\text{rad}\right]$,

$\lambda = 1.2894\times10^{-9} \pm 1.8\times10^{-10}\left[\text{m}\right]$, $K_w = 1.4984\times10^{5} \pm 1.17\times10^{5}\left[\text{Hz}\right]$.

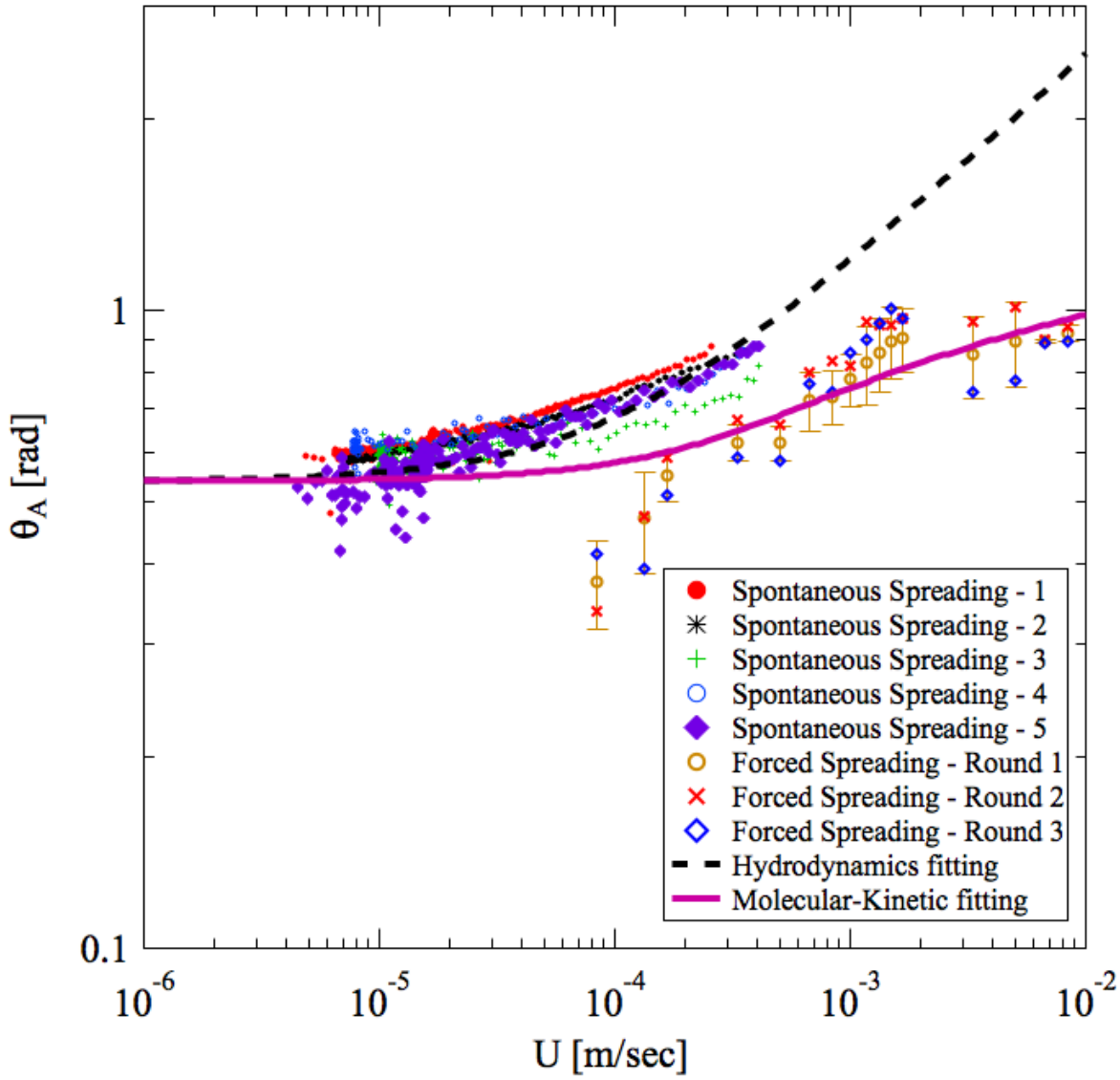

Figure 7.11: Comparison between free and forced spreading of glycerin on glass substrate.

The free spreading of glycerin on glass substrate is only consistent with HDT. The dynamic contact angle from free spreading are larger than that of forced spreading possibly due to the presence of impurities in the glycerin.

7.5 Conclusions

Clearly, the experimental results obtained from free and forced spreading mechanisms are distinct for the same solid/liquid/vapor. This is due to the fact that the physics, which controls the dynamics of liquid contact line for free and forced mechanism of spreading are different. As a result of this, the appropriate dynamics of spreading for each mechanism of spreading (i.e. free and forced) may not be the same. We have obtained a hypothesis that explains the reason of these differences between free and forced spreading. Our hypothesis also helps to choose the more appropriate spreading dynamics (i.e. between HDT and MKT) for each spreading mechanism (i.e. free and forced).

As illustrated in figure 7.1, we have claimed that for the free spreading mechanism, the model of spreading dynamics, which shows a higher contact line speed for the given dynamic contact angle, is the more appropriate model to describe the dynamics of free spreading. For results obtained from free spreading in our experimental investigations, HDT applies more appropriately compared to MKT for the solid-liquid systems, which have been investigated. And this is associated with the higher contact-line speed obtained for a given dynamic contact angle from HDT compared to the contact-line speed obtained for the same given dynamic contact angle from MKT (see figure 7.1). The conclusion of theoretical investigations by Davis and Davis [80] on previous experimental findings for free spreading also validates our hypothesis.

For forced spreading in which the speed is controlled, MKT applies more appropriately and that is associated with the higher dynamic contact angle obtained for a given contact line speed from MKT model compared to the dynamic contact angle obtained for the same given contact line speed from analysis with HDT model. For the first time, the physical reason that explains why the dynamics of forced spreading has been shown to be describable by different dynamics

of wetting (e.g. MKT) compared to the wetting dynamics used to describe the spontaneous spreading has been illustrated. It is worth to be noted that Blake et. al. have done the numerical analysis to do the comparison between spontaneous spreading and forced spreading in the same solid/liquid system applying the molecular-dynamics simulations. Blake et. al. [163] have also found out the difference between the dynamic contact angle obtained from spontaneous spreading for a given liquid contact line speed compared to the dynamic contact angle obtained from forced spreading for the same liquid contact line speed in the same solid/liquid system. These results are compatible with selection of the higher contact angle, θ, (see figure 7.2) between the two curves. Further studies should reveal the sources of the selection.

CHAPTER 8

Dynamics of Spreading on Ultra-hydrophobic Surfaces

This chapter was taken with slight modification from the article "Dynamics of spreading on ultra-hydrophobic surfaces", published in Journal of Coatings Technology and Research [161].

8.1 Abstract

Despite the extensive variety of applications for ultra-hydrophobic surfaces in industry, technology, and biology, due to their wetting characteristics, there has not been considerable attention in the area of dynamics of wetting on ultra-hydrophobic surfaces. In this research, the experimental investigations have been done by applying forced spreading of several Polyethylene-glycol/water mixtures in different weight ratios on Teflon plates and ultra-hydrophobic sprayed glass substrates. Hydrodynamics theory and molecular-kinetic theory have been applied to investigate the dynamics of wetting on these substrates. It has been found out that the dynamics of receding motion of liquid contact line on ultra-hydrophobic surfaces could be described perfectly with molecular-kinetic theory. In the case of advancing motion on ultra-hydrophobic surface, dynamic contact angle is independent of liquid contact line velocity. The

advancing and receding motion of liquid contact line on smooth Teflon plates followed molecular-kinetic theory.

Key words: wetting dynamics, ultra-hydrophobic surface, hydrodynamics, molecular-kinetic theory, dynamic contact angle

8.2 Introduction

Low-energy surfaces are surfaces on which water does not spread completely and instead it forms a droplet on the surfaces with large contact angles in the range of 40 degrees and 140 degrees (e.g. hydrophobic) and equilibrium contact angles larger than 140 degrees (e.g. ultra-hydrophobic surfaces). Ultra-hydrophobic surfaces can be sufficiently described with extreme water repellency characteristics. Controlling the surface wettability of hydrophobic and super hydrophobic surfaces have extensive industrial applications ranging from coating, painting and printing technology, satellite communications technology, self-cleaning characteristics due to the large water repellency of ultra-hydrophobic surfaces, and waterproof clothing to efficiency increase in power and water plants. The high demand needed of ultra-hydrophobic surfaces in every aspect of daily life requires enhancing the knowledge of their dynamics of wetting and having an adequate understanding of the underlying physics of liquid contact line motion on such surfaces. There has been considerable attention on the spreading phenomena both experimental investigations [7,9,10,12-14,16,22,23,25,28-30,32,36-40,42,45,49,50,53-55,57,58,60,88,97] and theoretical investigations [3,8,20,52,59,64,66-74,79,88,91,96] for hydrophilic (high energy surfaces) and hydrophobic surfaces (low energy surfaces) for a long period of time. It has been claimed that spreading dynamics on such surfaces follow either hydrodynamics [3,16,70,71,88]

(e.g. due to viscous dissipation in the bulk motion of liquid) or molecular-kinetic theory [67,68] (e.g. dissipation due to friction from molecular attachment/detachment at the vicinity of liquid contact line on solid surface). Hydrodynamics theory [3,16,70,71,88] focuses on the bulk motion of liquids by applying the assumption of lubrication approximation and describes the dynamics of wetting based on the following dynamic contact angle dependency to Capillary number.

Hydrodynamics theory for advancing motion as shown in equation 8.1:

$$\theta_A^3 - \theta_{0A}^3 = \alpha Ca \tag{8.1}$$

Hydrodynamics theory for receding motion as shown in equation 8.2:

$$\theta_{0R}^3 - \theta_R^3 = \alpha Ca \tag{8.2}$$

Where θ_A is advancing dynamic contact angle; θ_R is receding dynamic contact angle; θ_{0A} is equilibrium advancing contact angle; θ_{0R} is equilibrium receding contact angle; Capillary number, $Ca = \frac{\mu U}{\sigma}$, which shows the relative importance of viscous force to capillary force; μ is dynamic viscosity of liquid; U is liquid contact line velocity; and σ is surface tension of liquid mixture. Front factor α is a constant that depends on the physical properties of the liquid mixture (e.g. dynamic viscosity and surface tension) and velocity of liquid contact line.

Molecular-kinetic theory [67,68] focuses on the molecular attachment/detachment at the liquid contact line and considers both solid properties and liquid properties to describe the dependency of dynamic contact angles to the contact line velocity. Blake [67,68] used the activated reaction rate theory by Glasstone, Laidler, and Eyring [75] to describe the molecular adsorption/desorption of the adsorption sites on the solid surface at the vicinity of liquid contact line based on the following model indicated in equation 8.3:

$$\theta = \cos^{-1}\left\{\cos\theta_0 \pm \frac{2k_B T}{\sigma\lambda^2}\sinh^{-1}\left(\frac{U}{2K_w\lambda}\right)\right\} \tag{8.3}$$

In equation 8.3, the minus sign refers to the advancing motion of the liquid contact line and the plus sign refers to the receding motion of the liquid contact line. θ is dynamic contact angle, θ_0 is equilibrium contact angle, k_B is Boltzmann constant, T is temperature, K_w is equilibrium frequency of molecular adsorption/desorption at the liquid contact line, and λ is the average distance between centers of adjacent adsorption sites on the solid surface where liquid molecules attach/detach. K_w and λ are two fitting parameters in addition to physical properties of liquid mixture that are used to investigate the validity of the molecular-kinetic model on describing the dynamics of wetting of motion of liquid contact line.

Surprisingly, there has not been any research on modeling the dynamics of wetting on ultra-hydrophobic surfaces despite their extensive variety of applications in several areas of daily life, technology and science, etc. In this research, we have done experimental investigations on the forced spreading dynamics on ultra-hydrophobic surfaces by applying hydrodynamics theory and molecular-kinetic theory. The analytical results obtained from the investigation on dynamics of wetting on ultra-hydrophobic surfaces have been compared with the analytical results obtained from the investigation of the dynamics of wetting on hydrophobic surfaces.

8.3 Experimental Methods and Materials

8.3.1 Sample Preparation

We have performed the experiments on three different mixtures of Polyethylene glycol (PEG) mixed with pure water in different weight ratios, with almost the same surface tension but with

different dynamic viscosity of liquid mixtures, to see the effect of the dynamic viscosity of the liquid mixtures on the dynamics of wetting of ultra-hydrophobic surfaces. The dynamic viscosities of all three PEG/water mixtures have been measured using a stress-controlled Rheometer. All three PEG/water mixtures exhibited Newtonian behavior as shown in figure 8.1.

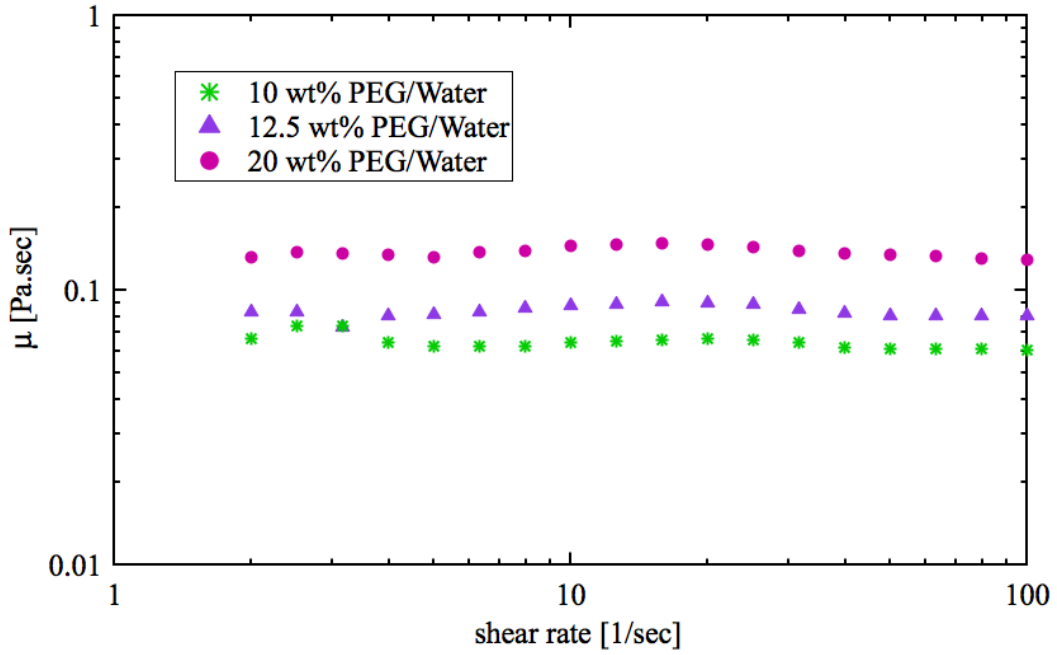

Figure 8.1: The dynamic viscosity of PEG/water mixtures versus shear rate of strain measured using a Rheometer.

The densities of all PEG/water mixtures have been also measured using the Tensiometer. The surface tension of all PEG/water mixtures have been measured using both the Tensiometer, applying the ring-tear off method, and the Wilhelmy plate method. Table 8.1 shows the physical properties of PEG/water mixtures used in the experiments.

PEG/Water Liquid Sample [wt%]	Density [kg/m^3]	Dynamic Viscosity [Pa sec]	Surface Tension [N/m]
10	1012	0.0607	0.054
12.5	1018	0.081	0.048
20	1031	0.1295	0.052

Table 8.1: The measured physical properties of the PEG/Water mixtures used in forced spreading experiments with a Tensiometer.

The solid substrates that have been used to do the experimental investigation of wetting dynamics were smooth Teflon plates and ultra-hydrophobic sprayed glass (e.g. glass has been sprayed uniformly on both sides using WX2100 paint). WX2100 paint is manufactured by Cytonix Corporation. WX2100 is an aerosol paint spray which is composed of mineral spirits and fluoropolymers that are driven by a mixture of Propane and Butane. A glass substrate with dimensions of $50 \times 24 \times 0.15$ mm^3 (VWR microcover glass) was used to be coated with WX2100 paint. Before coating the glass substrate, the can of the WX2100 was shaken for 30 seconds. Then the can was held vertically approximately 30 cm away from the glass substrate during spraying the WX2100 paint spray on the surface of the glass. The spraying has been done evenly on the glass surface to cover all part of the glass surface. After coating one side of the glass substrate with WX2100 paint, then the coated surface was allowed to be dried for at least 2 hours. Then the same procedure has been done on the other side of the glass. The glass substrate

coated with WX2100 becomes ultra-hydrophobic.

8.3.2 Experimental Technique

Force balance method (e.g. Wilhemy plate method) using the Tensiometer was applied to do the experiments for forced spreading mechanism. A Tensiometer, which was manufactured by KRÜSS GMBH, conducted measurement of the advancing dynamic contact angle and receding dynamic contact angle by moving the sample platform, which was holding the pool of liquid, upward and downward as shown in figure 8.2. A force sensor measured the Measured Force applied on the plate of solid substrate from the solid plate holder, which was connected to the force sensor from the top and it held the solid plate from the bottom, and then the Tensiometer software calculated the advancing dynamic contact angle and receding dynamic contact angle using the theoretical formula relating the Measured Force applied on the plate to the advancing and receding dynamic contact angles. The Tensiometer applied the analytical method through force balance method (i.e. Wilhelmy plate method) on the forces applied on the solid plate during the experiment to do the dynamic contact angle measurements (i.e. both advancing dynamic contact angle and receding dynamic contact angle). There were four forces which were considered to be applied on the solid plate during its immersion into the pool of the liquid and its emersion from the pool of the liquid. These forces were Capillary Force, $F_{Capillary}$, (i.e. due to surface tension of the liquid), the Buoyancy, $F_{Bouyancy}$, due to difference in density of solid plate and density of liquid, Measured Force, $F_{measured}$, (i.e. tension force from the solid holder which is being measured by Tensiometer force sensor) and the Gravity, $F_{gravity}$, (i.e. due to the weight of the solid plate). The Gravity was calibrated at the onset of touch of the edge of the solid plate

with the liquid-air interface hence the Gravity was not considered during the force measurement and dynamic contact angle measurement. As a result, the equation 8.4 has been applied in the Tensiometer software to measure the advancing and receding dynamic contact angle during the experiment.

$$F_{measured} + F_{Capillary} + F_{Bouyancy} = 0 \tag{8.4}$$

The Capillary force and Buoyancy force have been evaluated using the equation 8.5a and 5b which are shown as follows:

$$F_{capillary} = 2\sigma\left(w + t\right)\cos\theta \tag{8.5a}$$

$$F_{Bouyancy} = \rho g w t x \tag{8.5b}$$

In equations 8.5a and 8.5b, w is the width of the solid plate, t is the thickness of the solid plate, σ is the surface tension of the liquid, ρ is the density of the liquid, g is the gravitational acceleration, θ is the dynamic contact angle (i.e. advancing or receding dynamic contact angle), and x is the immersion depth at each instant of the experiment. The speed of the motion of the sample platform was set to a constant specific speed for each experiment to have a steady motion of the sample platform during measurement and to control the speed of the three-phase contact line. All experiments have been performed at room temperature.

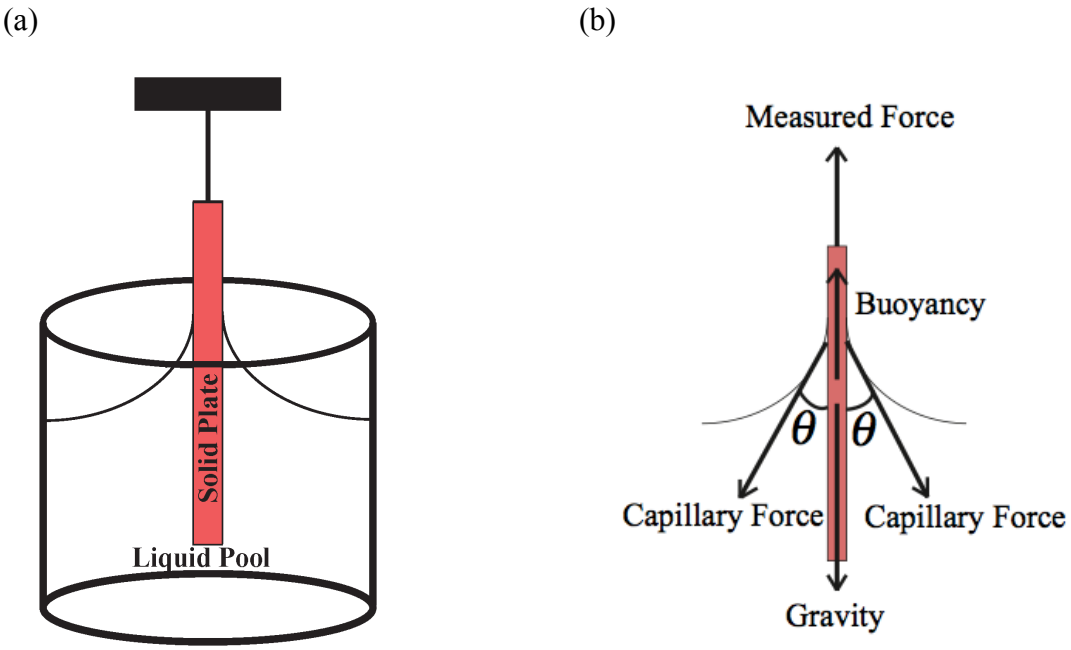

Figure 8.2: (a) The schematic picture of forced spreading using Tensiometer. (b) The force balance diagram used in Tensiometer equipment to measure the dynamic contact angle during advancing/receding motion of solid plate in the pool of liquid.

8.4 Results and Discussion

The spreading dynamics on hydrophobic surfaces follow the molecular-kinetic theory for both advancing and receding motion as shown in figure 8.3. Figure 8.3 shows the dependency of the dynamic contact angle to the contact line velocity for the forced spreading experiments done for two different weight ratios of mixtures of PEG/Water on smooth Teflon plates using Tensiometer equipment applying the Wilhelmy plate method. The general form of hydrodynamics theory has also been applied to investigate the dynamics of wetting on a hydrophobic surface (e.g. smooth Teflon plate) and we found that the hydrodynamics theory is

not an appropriate model to describe the dynamics of wetting on smooth Teflon plates on complete range of contact line velocity.

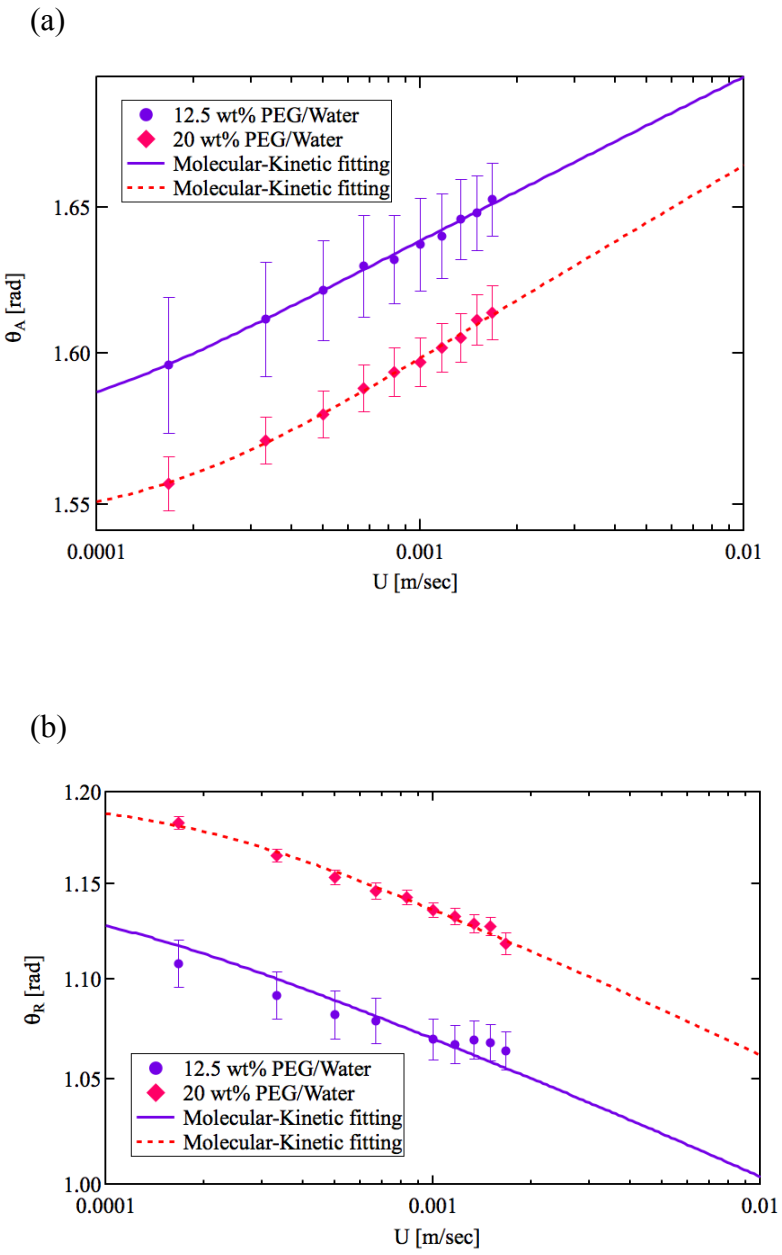

Figure 8.3: The forced spreading of Polyethylene Glycol/Water mixtures on smooth Teflon plate performed by Tensiometer. (a) Advancing motion of PEG/Water on smooth Teflon plate. (b)

Receding motion of PEG/Water on smooth Teflon plate. Molecular-Kinetic fitting parameters in both advancing and receding motion;

12.5 wt% PEG/Water: $\theta_{0A} = \left(1.5679 \pm 0.0138\right)\left[rad\right]$, $\theta_{0R} = \left(1.1487 \pm 0.00243\right)\left[rad\right]$,

$T = 298\left[K\right]$, $\sigma = 0.048\left[N/m\right]$, $\lambda = \left(2.6244 \times 10^{-9} \pm 7.25 \times 10^{-11}\right)\left[m\right]$,

$K_w = \left(22549 \pm 1.63 \times 10^{4}\right)\left[Hz\right]$.

20 wt% PEG/Water: $\theta_{0A} = \left(1.5404 \pm 0.0033\right)\left[rad\right]$, $\theta_{0R} = \left(1.1992 \pm 0.000691\right)\left[rad\right]$,

$T = 298\left[K\right]$, $\sigma = 0.052\left[N/m\right]$, $\lambda = \left(2.3403 \times 10^{-9} \pm 5.7 \times 10^{-11}\right)\left[m\right]$,

$K_w = \left(58267 \pm 1.35 \times 10^{4}\right)\left[Hz\right]$.

For the case of ultra-hydrophobic surfaces, the dynamics of wetting showed a completely different behavior. The dynamics of wetting (e.g. dynamic contact angle variation versus contact line velocity) for receding motion is not the same as the dynamics of wetting for advancing motion for the same system of solid/liquid/vapor in the same experiment as obtained from Tensiometer measurements. The advancing dynamic contact angle is almost independent of the capillary number and it is almost a constant value for the whole range of contact line velocity especially for a large contact line velocity range. As it is shown in figure 8.4, only for a very low contact line velocity range, the dynamic contact angle decreases as the contact line velocity increases with a very small slope due to the effect of stick-slip behavior which most likely occurred for the ultra-hydrophobic surfaces and beyond that low contact line velocity, the

advancing dynamic contact angle is independent of the liquid contact line velocity for the rest of velocity range.

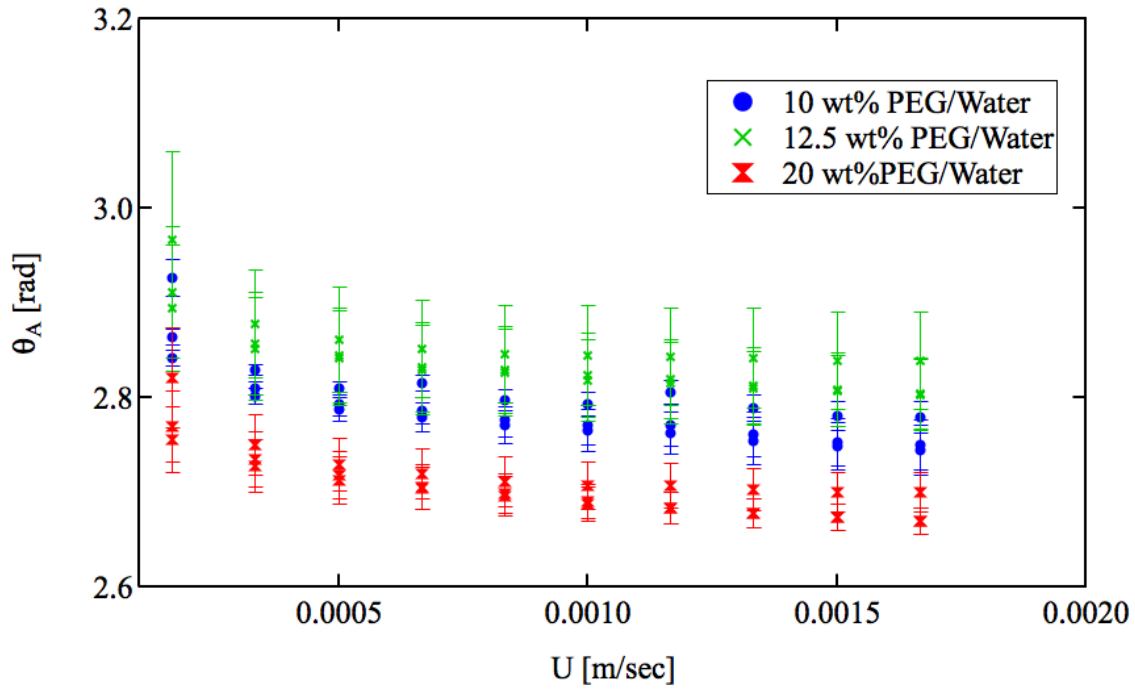

Figure 8.4: The advancing dynamic contact angle versus contact line velocity for PEG/Water liquid mixtures on ultra-hydrophobic sprayed glass.

For the case of the receding motion of the liquid contact line on ultra-hydrophobic surfaces, hydrodynamic theory could not be applied to describe the dynamics of wetting. The molecular-kinetic theory, which focuses on the molecular attachment/detachment at the vicinity of the liquid contact line, has been found to be the best model to describe the dynamics of wetting on ultra-hydrophobic surfaces. Figure 8.5 shows the details of the fitting of molecular-kinetic theory on the experimental results obtained for receding motion of ultra-hydrophobic surface in the pool of PEG/water liquid mixture. This is due to the fact that the molecular-kinetic theory focuses on

both solid and liquid properties to describe the dependency of dynamic contact angles to the liquid contact line velocity.

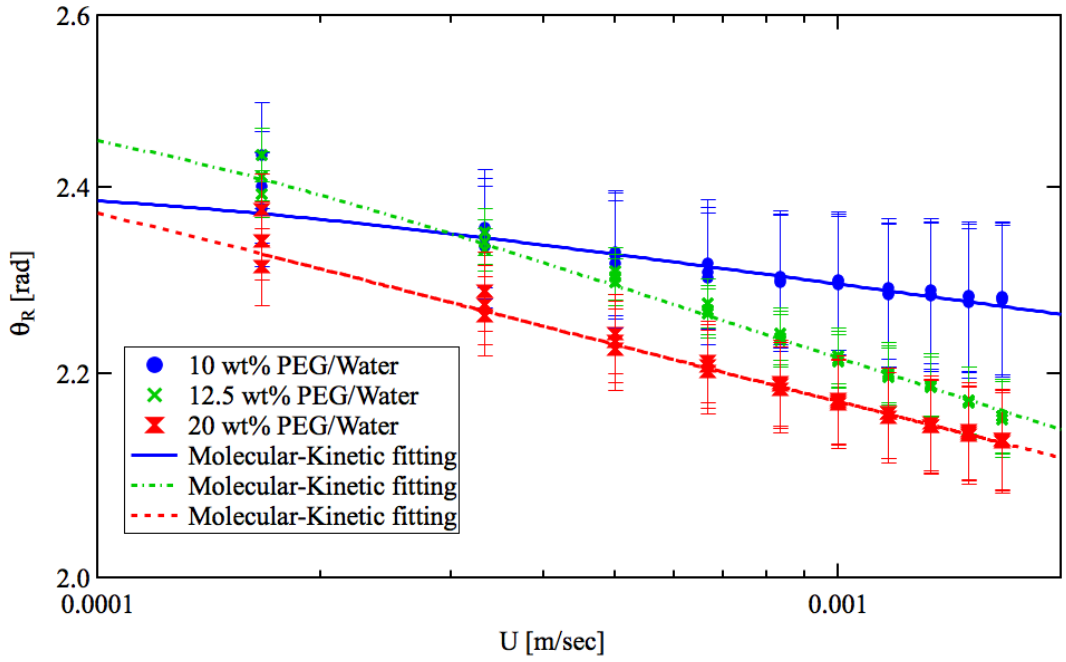

Figure 8.5: The theoretical analysis on the dynamics of wetting of different PEG//water mixtures on ultra-hydrophobic sprayed glass by applying the molecular-kinetic theory.

10 wt% PEG/Water: $\theta_{0R} = 2.41\left[rad\right]$, $T = 298\left[K\right]$, $\sigma = 0.054\left[N/m\right]$,

$\lambda = 2.07\times10^{-9} \pm 1.02\times10^{-10}\left[m\right]$, $K_w = 48300 \pm 1.32\times10^{4}\left[Hz\right]$.

12.5 wt% PEG/Water: $\theta_{0R} = 2.54\left[rad\right]$, $T = 298\left[K\right]$, $\sigma = 0.048\left[N/m\right]$,

$\lambda = 1.3968\times10^{-9} \pm 2.25\times10^{-11}\left[m\right]$, $K_w = 55557 \pm 5.25\times10^{3}\left[Hz\right]$.

20 wt% PEG/Water: $\theta_{0R} = 2.51\left[rad\right]$, $T = 298\left[K\right]$, $\sigma = 0.052\left[N/m\right]$,

$\lambda = 1.5227\times10^{-9} \pm 1.67\times10^{-11}\left[m\right]$, $K_w = 19042 \pm 1.59\times10^{3}\left[Hz\right]$.

8.5 Conclusions

The molecular-kientic theory was the appropriate dynamical model to describe the dynamics of wetting on hydrophobic surfaces for both advancing and receding motion as have been shown for the forced spreading experiments on smooth Teflon plate into/out of the pool of PEG/Water mixtures. The equilibrium advancing contact angles of the PEG/water liquid mixtures on ultra-hydrophobic surfaces are above 140 degrees and there is a small window of variation for the advancing dynamic contact angle to change by increasing the liquid contact line velocity on ultra-hydrophobic surfaces. Due to this fact, the advancing dynamic contact angle of the PEG/water mixtures on ultra-hydrophobic surfaces is independent of the contact line velocity. The molecular-kinetic theory was best model to describe the dynamics of wetting on ultra-hydrophobic surfaces for receding motion since the molecular-kinetic theory focuses on the liquid molecular displacement at the vicinity of the liquid contact line by considering both properties, solid substrate and liquid properties. Hydrodynamics theory is not an appropriate model to describe the dynamics of wetting on ultra-hydrophobic surfaces since the liquid contact line on the ultra-hydrophobic surface is most likely moving on the liquid/air interface where shear stress is negligible and the lubrication approximation is not valid to be used to describe the dynamics of wetting.

CHAPTER 9

Partial Wetting on Rough Surfaces

9.1 Abstract

Due to the extensive variety of application of rough surfaces in industry and technology, experimental investigations have been done on the dynamics of spreading (i.e. dependency of the dynamic contact angle to the three-phase contact line velocity) of Poly Ethylene Glycol (PEG) mixed with pure water in different weight ratios on the rough Teflon plates roughened with three different mesh sizes applying Wilhelmy plate method using Tensiometer. The advancing dynamic contact angle has been found to be independent of the three- phase contact line speed. The receding dynamic contact angle decreases with increase of the three-phase contact line velocity. The degree of roughness on the rough Teflon surfaces has important effect on the dynamic contact angles. The dynamics of receding motion of all PEG/water mixtures on all rough Teflon plates followed the molecular-kinetic theory. A relation between the receding dynamic contact angles to a non-dimensional parameter, which shows the relative significance of the macroscopic scale of flow to the microscopic scale of the flow, has been obtained and follows a power law with power of 1/2.

9.2 Introduction

Majority of practical solid surfaces have roughness to some degree. In a vast range of industrial and aeronautical applications, the degree of roughness on solid surfaces is a crucial factor. Increasing the roughness on hydrophobic surfaces increases their hydrophobicity and increasing the roughness on hydrophilic surfaces increases their hydrophilicity. There have been tremendous investigations in the area of spontaneous spreading of liquid droplets on rough surfaces, which produce equilibrium contact angle in the hydrophilic region [157-160] where equilibrium contact angle is less than 90 degrees. There has been a considerable attention to rough hydrophobic surfaces due to their large water-repellency characteristic in science, industry and technology [98-111,117,122,125,127,129,137-151, 155, 156]. Controlling the wettability of rough hydrophobic surfaces is important in industry and technology such as coating, painting, ink-jet printing, waterproof clothing, increasing efficiency in power plants, drag reduction on air-plane wings, drag reduction in micro-channels, and increasing the efficiency of satellite communication devices during heavy snow or heavy rain conditions to receive more accurate and reliable signals, etc [101-103, 105-107, 137-139, 144, 147, 149-150, 155-156].

This broad variety of applications of rough hydrophobic surfaces requires enhancing the knowledge in the area of dynamics of spreading on rough hydrophobic surfaces. There are two important factors to control the wettability of these surfaces [137]. These two factors are the chemical composition of the surface and the degree of surface roughness on the surface [137]. By increasing the degree of roughness on the surface area of the hydrophobic surface, the hydrophobicity of hydrophobic surface increases. Due to this fact, having the control on increase of the degree of roughness on the hydrophobic surfaces can be very crucial in industry and technology. One typical way to control on increase the degree of roughness on the hydrophobic

surface (e.g. Teflon surface) is by producing uniform patterns on smooth hydrophobic surfaces. The degree of roughness on hydrophobic surfaces can produce higher surface hydorphobicity with either creating the Cassie-Baxter equilibrium state or the Wenzel equilibrium state of the contact angle.

Recently, there has been an experimental research on the dynamics of spreading of liquids on rough hydrophobic surfaces with extremely large equilibrium contact angle in the ultra-hydrophobic region with Cassie-Baxter state of the equilibrium contact angle which has been done by Rothstein and his co-workers [153] and the study on the effect of sizes of micro-textured posts on the spreading dynamics on rough surfaces in the ultra-hydrophobic region [154]. Rothstein and his co-workers [153] have done experimental investigation on the dynamic contact angle (i.e. both advancing and receding) measurements on ultra-hydrophobic surfaces applying optical method with modified Wilhelmy plate method. They have prepared the systematically patterned ultra-hydrophobic surfaces by hot pressing a pattern of micro-posts on the smooth Teflon surface [153]. So far, there has not been any study on the dynamics of forced spreading on rough hydrophobic surfaces with the Wenzel state of the equilibrium contact angle.

In order to do further study in the area of spreading dynamics on the rough hydrophobic surfaces in the Wenzel state, we have fabricated three different degrees of roughness by producing the patterns on smooth Teflon plates by following the same procedure of micro-post preparation as Rothstein and his co-workers have done [153]. Then, the experimental investigation has been done on the dynamics of the forced spreading of Newtonian liquid mixtures on such prepared controlled-rough surfaces. The test liquid mixtures were Poly Ethylene Glycol (PEG) mixed with water for two different weight ratios. In our experimental investigations, the controlled-rough hydrophobic Teflon surfaces are in the Wenzel state of the

equilibrium contact angle with the PEG/water mixtures used in the experiments producing the equilibrium contact angle ranging from 100 deg to 120 deg. We have also investigated the effect of degree of roughness of Teflon plates on the forced spreading dynamics on these surfaces.

The best way to investigate the dynamics of spreading of liquid on a solid surface is by looking into the dependency of the dynamic contact angle (i.e. the angle between solid/liquid and liquid/air at the three-phase contact line where solid, liquid, and air coexist) to the velocity of the three-phase contact line [3,16,23,29,30,40,45,50,52,57,59,64,66-74,79,88,91].

Up to now, there have been only two fundamental laws that describe the dependency of the dynamic contact angle to the speed of the three-phase contact line. These laws are called the hydrodynamics theory and the molecular-kinetic theory. Hydrodynamics theory determines the relation between the dynamic contact angle and the velocity of the three-phase contact line by focusing on the bulk motion of liquid on the solid surface.

Hydrodynamic theory describes the dynamics of spreading by focusing on the viscous dissipation due to the flow of liquid on the solid substrate. Through application of the lubrication assumption (e.g. low-Reynolds number flow) on the Navier-Stokes equations and applying kinematic boundary conditions, dynamic boundary conditions, and geometric boundary conditions applied at the three-phase contact line, hydrodynamics theory describes the dependency of the dynamic contact angle to the three-phase contact line velocity [3,66,69-71,73,74,88]. The kinematic boundary conditions consist of the no-flow through boundary condition across the liquid/vapor interface and across the solid/liquid interface. Another kinematic boundary condition is the slip condition across the solid/liquid interface at the proximity of the three-phase contact line by introducing a slip length parameter, L_s, to avoid the non-integrable singularity in the shear-rate-of-strain tensor at the three-phase contact line

[64,66,69,75]. The dynamic boundary conditions are shear-free across the liquid/vapor interface and balance of normal stress across the liquid/vapor interface. The constant-liquid-volume-assumption due to the assumption of negligible evaporation of liquid during spreading and application of the incompressible assumption were also applied in the analysis of hydrodynamics theory. As a result, (9.1) shows the dependency of the dynamic contact angle to the three-phase contact line velocity obtained using hydrodynamics theory.

$$\theta^3 - \theta_0^3 = \pm 9 \frac{\mu U}{\sigma} \ln\left(\frac{L}{L_s}\right). \tag{9.1}$$

In (9.1), the minus sign is for the receding motion of the three-phase contact line and the plus sign is for the advancing motion of the three-phase contact line. In (9.1), θ is the dynamic contact angle at the three-phase contact line, θ_0 is the equilibrium contact angle, μ is the dynamic viscosity of liquid, σ is the surface tension, U is the three-phase contact line velocity, L is the characteristic length of flow of liquid, and L_s is the slip length over which the slip condition happens on the solid/liquid interface.

Molecular-kinetic theory describes the dependency of the dynamic contact angle to the velocity at the three phase contact line based on the molecular displacements of liquid molecules on the solid surface at the three-phase contact line by considering both solid properties and liquid properties [67,68]. Blake [67,68] applied the absolute activated reaction rate theory proposed by Glasstone, Laidler, and Eyring [75] to describe the dynamics of spreading of liquid on solid surface by focusing on the molecular attachment/detachment of liquid moleculars on adsorption sites of the solid surface at the vicinity of the three-phase contact line. Molecular-kinetic theory was based on the dissipation due to friction created at the vicinity of the three-phase contact line caused by the molecular attachment/detachment of liquid molecules on solid surface. The

following equation shows the relation between the dynamic conact angle and the three-phase contact line velocity based on the molecular-kinetic theory:

$$\theta = \cos^{-1}\left\{\cos\theta_0 \pm \frac{2k_B T}{\sigma\lambda^2}\sinh^{-1}\left(\frac{U}{2K_w\lambda}\right)\right\} \tag{9.2}$$

In (9.2), the minus sign refers to the advancing motion of the three-phase contact line on the solid surface and the plus sign refers to the receding motion of the three-phase contact line on the solid surface. In (9.2), θ is the dynamic contact angle, θ_0 is the equilibrium contact angle, k_B is the Boltzmann constant and its value is 1.3806488×10^{-23} (m^2kg/s^2K), T is the temperature, σ is the surface tension, U is the three-phase contact line speed. In (9.2), λ is the molecular distance between two adjacent adsorption sites (i.e. sites where liquid molecules attach on the solid surface and/or detach from the solid surface) on the solid surface and K_w is the frequency of molecular attachment/detachment at equilibrium state.

9.3 Experimental Set-up and Materials

9.3.1 Sample Preparation

The solid substrates that were used to do the experimental investigation on spreading dynamics were rough Teflon plates. The rough Teflon plates were prepared by placing the Teflon plates in between the two plates of the corrosion-resistant-stainless-steel-wire-cloth with the same mesh size of interest. This prepared Teflon plate sandwiched between the two corrosion-resistant-stainless-steel-wire-cloth plates was put in between two aluminum plates, and then the whole system (e.g. Teflon plates sandwiched with two wire-cloth plates sandwiched together between two aluminum plates) was placed inside a manual presser. Then the sandwiched Teflon with

wire-cloth plates was pressed manually with high compressive force applied with the presser. Then the compressed sandwiched Teflon plate in between wire-cloth plates on its both sides with the presser was placed inside an oven. The oven was set to heat up the sandwiched Teflon plate to temperature of 300^{o}F. The oven continued to heat the sandwiched Teflon plate with wire-cloth plates for 2-2.5 hours while the sandwiched Teflon plate with wire-cloth plates was being compressed. Then the oven was turned off, and we waited for the oven to cool off for almost a day. This way, the uniform roughness was patterned evenly on both surfaces of the Teflon plate. After that, the experiments were performed on the uniform rough Teflon plates. This was done for three rough Teflon plates with three different degrees of roughness.

The geometric specifications of the corrosion-resistant stainless steel woven wire cloths with three mesh sizes (i.e. 40×40 mesh size, 200×200 mesh size, and 400×400 mesh size) are shown in table 9.1.

Mesh size	Opening Size, micro-post width, a [m]	Open Area [%]	Wire Diameter, micro-post distance, b [m]
40×40	30.48×10^{-5}	21	34.29×10^{-5}
200×200	8.636×10^{-5}	46	4.064×10^{-5}
400×400	3.81×10^{-5}	36	2.54×10^{-5}

Table 9.1: The geometric specifications of corrosion-resistant type 304 stainless steel woven wire cloth for three different mesh sizes.

Figures 9.1, 9.2, 9.3 show the side-view pictures of the uniform-roughened Teflon surfaces taken by Drop Shape Analysis (DSA). In figures 9.1, 9.2, and 9.3, the PEG/water is at equilibrium state on the micro-textured Teflon surfaces.

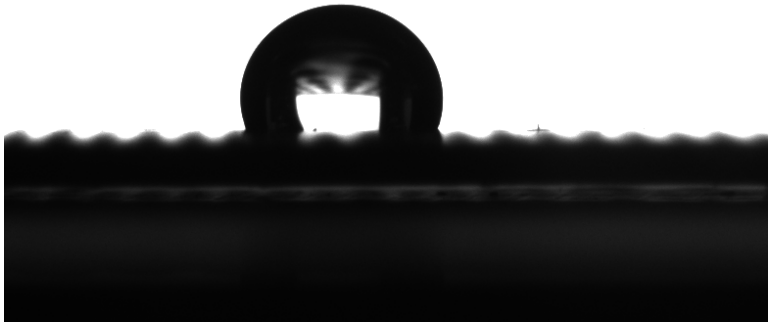

Figure 9.1: The side view picture of PEG/water droplet at equilibrium state on the micro-textured (i.e. rough) Teflon surface with mesh size 40 × 40.

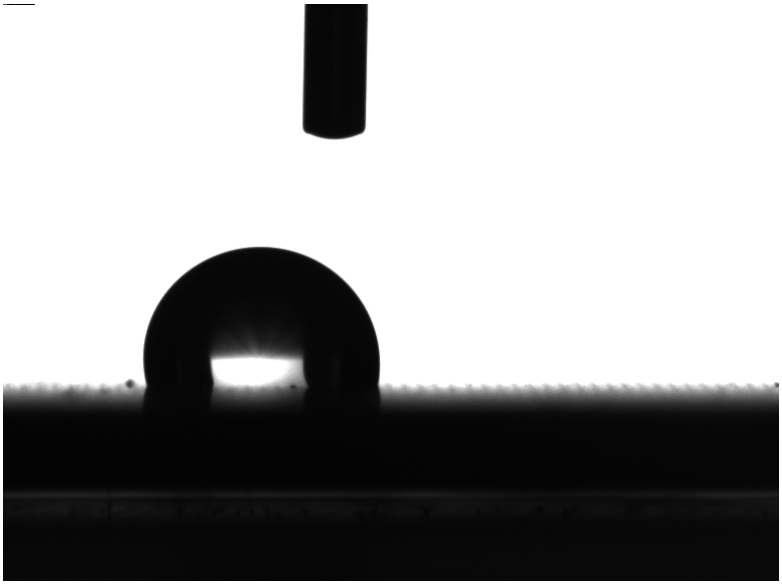

Figure 9.2: The side view picture of PEG/water droplet at equilibrium state on the micro-textured (i.e. rough) Teflon surface with mesh size 200 × 200.

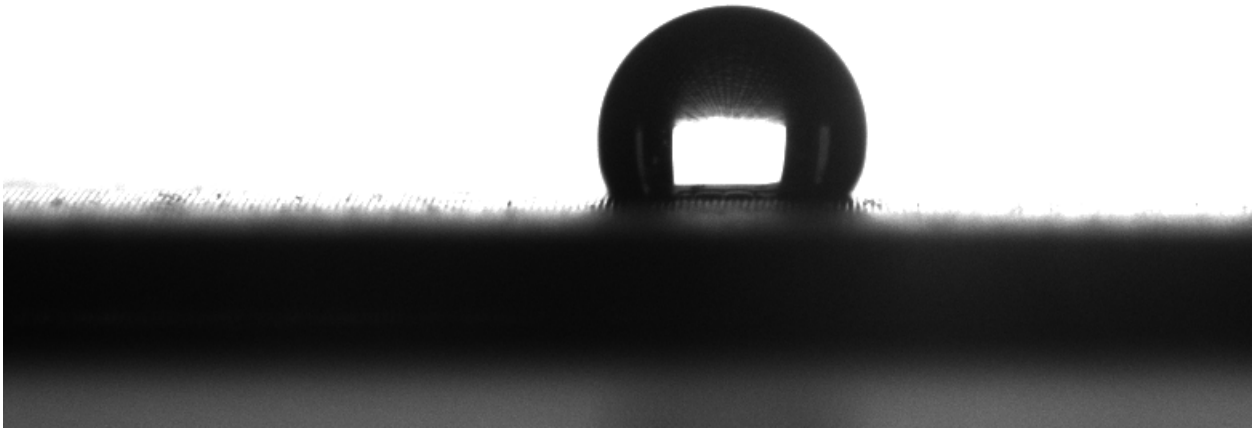

Figure 9.3: The side view picture of PEG/water droplet at equilibrium state on the micro-textured (i.e. rough) Teflon surface with mesh size 400 × 400.

Figure 9.4 shows the top view picture of the micro-textured (i.e. rough) Teflon surface with mesh size 40 × 40 to illustrate the uniform pattern of the micro-posts on the Teflon surface.

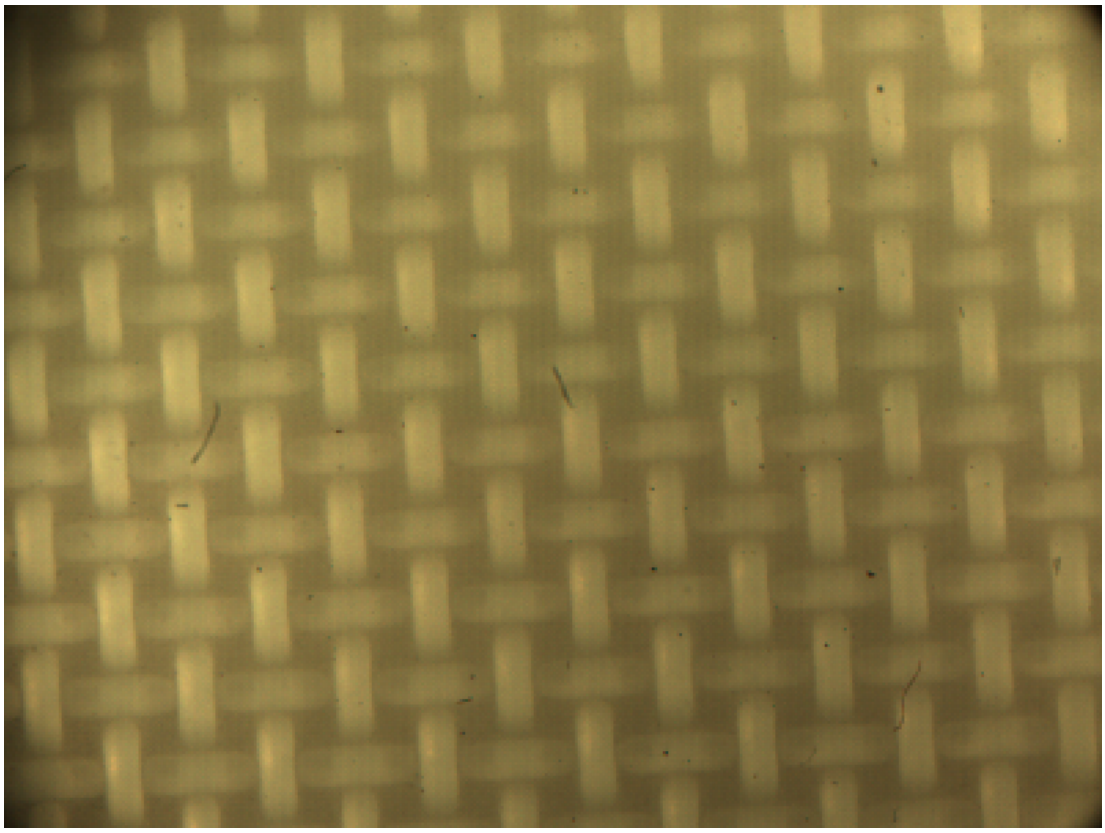

Figure 9.4: The top view picture of micro-textured (i.e. rough) Teflon surface patterned with mesh size 40 × 40.

We have done the experiments on two different liquid mixtures of Poly Ethylene Glycol (PEG) mixed with pure water in different weight ratios. Both PEG/Water mixtures have almost the same surface tension but with different dynamic viscosities. The dynamic viscosities of both PEG/water mixtures were measured using a stress-controlled Rheometer. Both PEG/water mixtures have exhibited the Newtonian behavior (e.g. the dynamic viscosity of each PEG/water mixture was constant and independent of the shear rate of strain) as shown in figure 9.5. The surface tensions of both PEG/Water mixtures were measured using the ring tear-off method with

Tensiometer (K100 Krüss). The densities of both PEG/water mixtures were also measured experimentally using the Tensiometer (K100 Krüss). The physical properties (i.e. the densities, the dynamic viscosities, and the surface tensions) for both PEG/water mixtures are given in table 9.2.

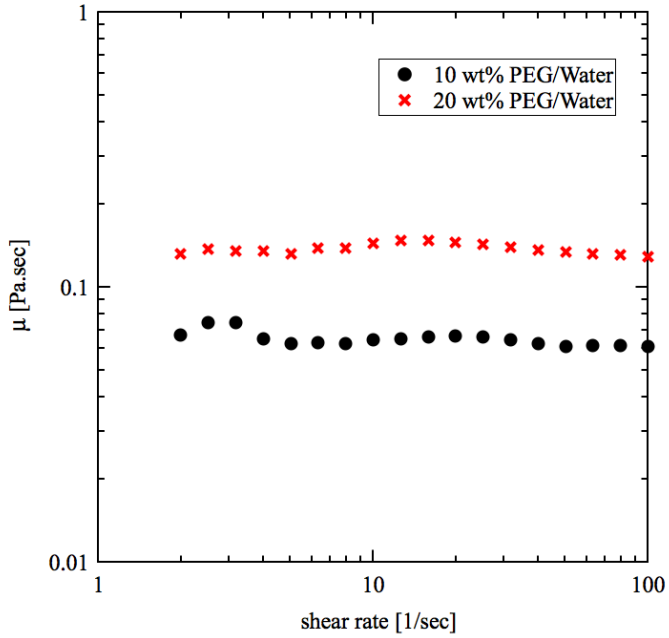

Figure 9.5: The dynamic viscosity of PEG/water mixtures versus shear rate of strain measured using a Rheometer.

PEG/Water Mixture [wt%]	ρ, Density [kg/m^3]	μ, Dynamic Viscosity [Pa sec]	σ, Surface Tension [N/m]
10	1012	0.0607	0.0533
20	1031	0.1295	0.0512

Table 9.2: The measured physical properties of the PEG/Water mixtures used in forced spreading experiments with tensiometer.

9.3.2 Experimental Set-up

The Tensiometer (K100 Krüss) was used to perform the experiments for forced spreading of PEG/water mixtures on micro-textured Teflon plates. Figure 9.6(a) shows the schematic picture of a Tensiometer during the motion of plate in PEG/water. The Tensiometer applies the force balance method (i.e. Wilhelmy plate method) to measure the advancing dynamic contact angle and the receding dynamic contact angle at the three-phase contact line during the advancing motion of the micro-textured Teflon plate in the pool of PEG/water mixture (the upward motion of sample platform holding the container with pool of PEG/water) and the receding motion of micro-textured Teflon plate in the pool of PEG/water mixture (the downward motion of sample platform holding the container with pool of PEG/water), respectively. The measurements of the dynamic contact angles were done for three cycles of motion for each set of experiment. A force sensor measured the force applied on the plate of solid substrate and then the Tensiometer software calculated the advancing dynamic contact angle and receding dynamic contact angle using the equation of balance of forces applied on the plate based on the free-body diagram shown in figure 9.6(b) during the advancing and the receding motion for each cycle. The velocity of motion of the sample platform, which holds the container with PEG/water, is set to a specific constant value to maintain a steady-state motion of the three-phase contact line during the advancing and the receding motion of plate in the pool of PEG/water.

The forces that are applied on the plate during the advancing motion and the receding motion are Gravitational force, F_g, due to the weight of the plate, force from the plate holder on the

plate being measured by the force sensor, F, Capillary force, F_σ, due to the surface tension of the PEG/water, and the Buoyancy force, F_B, due to the difference between the density of plate, ρ_{plate}, and the density of PEG/water, ρ.

$$F_\sigma = 2\sigma\left(w+t\right)\cos\theta \tag{9.3a}$$

$$F_B = \rho g w t x \tag{9.3b}$$

$$F_g = \rho_{plate} g w t L \tag{9.3c}$$

In (9.3), L is the length of the solid plate, w is the width of the plate, t is the thickness of the plate; σ is the surface tension of the liquid, ρ is the density of the fluid, ρ_{plate} is the density of the plate, g is gravitational acceleration, θ is the dynamic contact angle, and x is the immersion depth. As a result, (9.4) shows the force balance for the steady-state motion of the plate in the pool of liquid as follows:

$$F + F_\sigma + F_B + F_g = 0 \tag{9.4}$$

The gravitational force is calibrated at the first moment of contact of the solid plate with the PEG/water. Hence, (9.5) expresses the balance of forces applied on the plate for maintaining constant velocity motion of the three-phase contact line during the advancing and the receding motion by excluding the effect of the gravitational force during the experiment for each cycle.

$$F + F_\sigma + F_B = 0 \tag{9.5}$$

(a) (b)

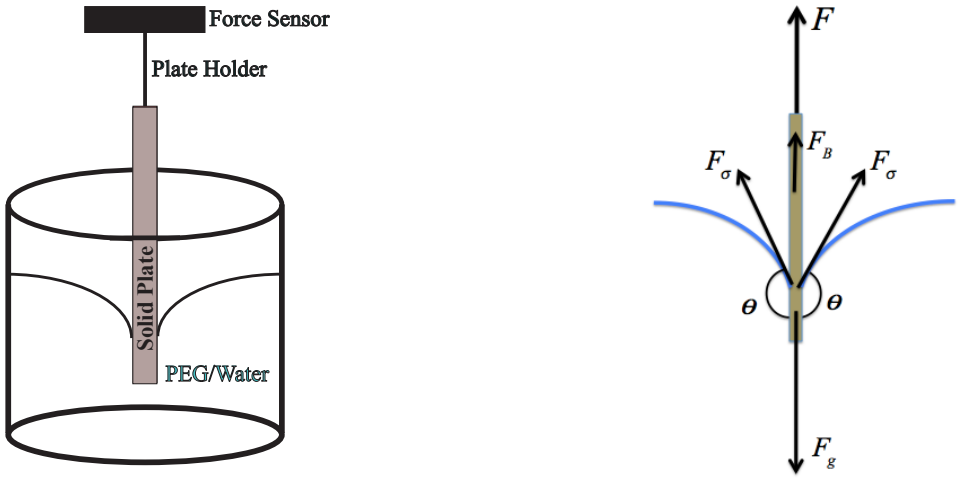

Figure 9.6: (a) Schematic picture of Tensiometer. (b) The schematic representation of the Free-Body diagram of forces applied on a plate during its motion in a pool of liquid.

9.4 Results and Discussion

Forced spreading has been done for two PEG/water mixtures on the rough Teflon plates with three different mesh sizes of roughness. Forced spreading was performed with Tensiometer with three cycles of the advancing and the receding motions. Figure 9.7(a) shows the advancing dynamic contact angle versus the liquid contact line velocity (e.g. the three-phase contact line velocity) for 10 wt% PEG/water mixture on the rough Teflon plates with three roughness densities (i.e. 40 × 40, 200 × 200, and 400 × 400). Figure 9.7(b) shows the advancing dynamic contact angle versus the liquid contact line velocity for 20 wt% PEG/water mixture on rough Teflon plates with the three roughness densities (i.e. 40 × 40, 200 × 200, and 400 × 400). The advancing motion of both PEG/water mixtures on all three rough Teflon plates show no dependence of the dynamic contact angle on the three-phase contact line velocity as it is shown

in figure 9.7 unlike the spreading on smooth Teflon surface where the advancing dynamic contact angle increases as contact line velocity increases. This no dependence relation between the advancing dynamic contact angle and the contact line velocity for spreading on rough surfaces has also been observed from optical method for rough hydrophobic surfaces in the Cassie-Baxter state done by Rothstein and his co-workers [153]. This fact signifies that the presence of the roughness on smooth hydrophobic surfaces makes the advancing contact angle independent of the contact line velocity with no dependency on the type of the state of the equilibrium on rough surfaces (e.g. either the Cassie-Baxter state or the Wenzel state). The physical reason of independency of the advancing dynamic contact angle to the liquid contact line velocity can be due to the pinning effect happening along the roughness on the rough surfaces. It has to be noted that as the roughness density increases on the rough Teflon plate (i.e. both the roughness size, a, and the distance between roughness, b, decrease on the rough Teflon plate), the constant advancing dynamic contact angle increases to the higher value for the same PEG/water mixture on the same given contact line velocity as it is shown in figures 9.7(a) and 9.7(b). This is due to the fact that as the density of the roughness increases, the effect of stick-slip and pinning effect that happen more frequently as the liquid contact line tries to move on the rough surface with a given constant velocity specified on the Tensiometer hence causing the advancing dynamic contact angle to increase to a higher value for each corresponding contact line velocity.

(a) (b)

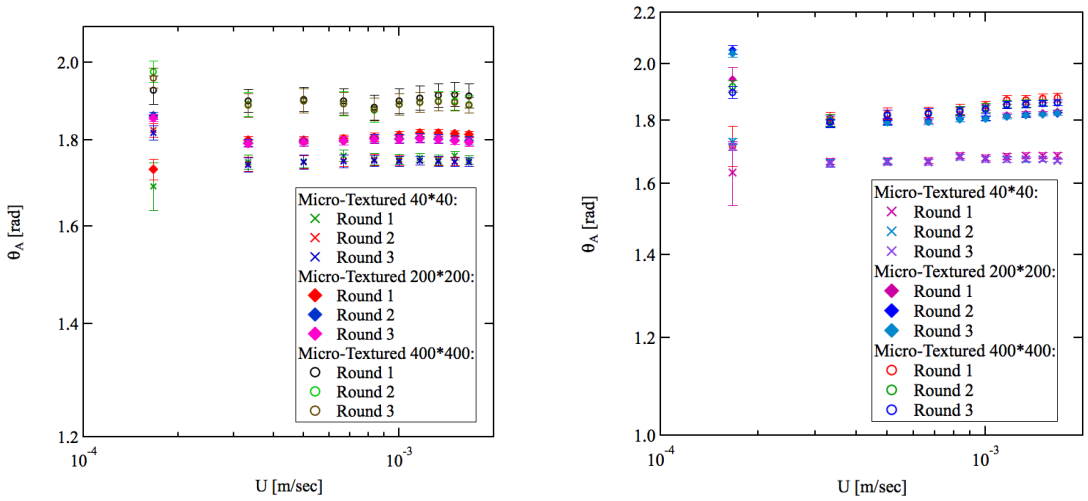

Figure 9.7: (a) Advancing motion of 10 wt% PEG/water on micro-textured (i.e. rough) Teflon plates. (b) Advancing motion of 20 wt% PEG/water on micro-textured (i.e. rough) Teflon plates.

Figure 9.8(a) illustrates the receding dynamic contact angle versus the liquid contact line velocity for 10 wt% PEG/water mixture on the rough Teflon plates, in the Wenzel state of the equilibrium contact angle, with three roughness densities (i.e. 40 × 40, 200 × 200, and 400 × 400). Figure 9.8(b) shows the receding dynamic contact angle versus the liquid contact line velocity for 20 wt% PEG/water mixture on the rough Teflon plates, in the Wenzel state of the equilibrium contact angle, with the three roughness densities (i.e. 40 × 40, 200 × 200, and 400 × 400). The receding motions of both PEG/water mixtures on all three rough Teflon plates show significant dependence of the dynamic contact angle on the three-phase contact line velocity, as it is shown in figure 9.8, like the case on smooth Teflon surface. The receding dynamic contact angle decreases as the liquid contact line velocity increases for all experiments. Unlike the advancing motion, as the roughness density increases on the rough Teflon plate, the receding dynamic contact angle decreases to a lower value for the same PEG/water mixture on the same

given liquid contact line velocity as it is shown in figures 9.8(a) and 9.8(b). This is due to the same physical reason that as the density of the roughness increases, the effect of the stick-slip and pinning force happen more frequently as the liquid contact line tries to move on the rough hydorophobic surface with a given constant velocity specified on the Tensiometer causing the receding dynamic contact angle to lower value for the same PEG/water mixture.

(a) (b)

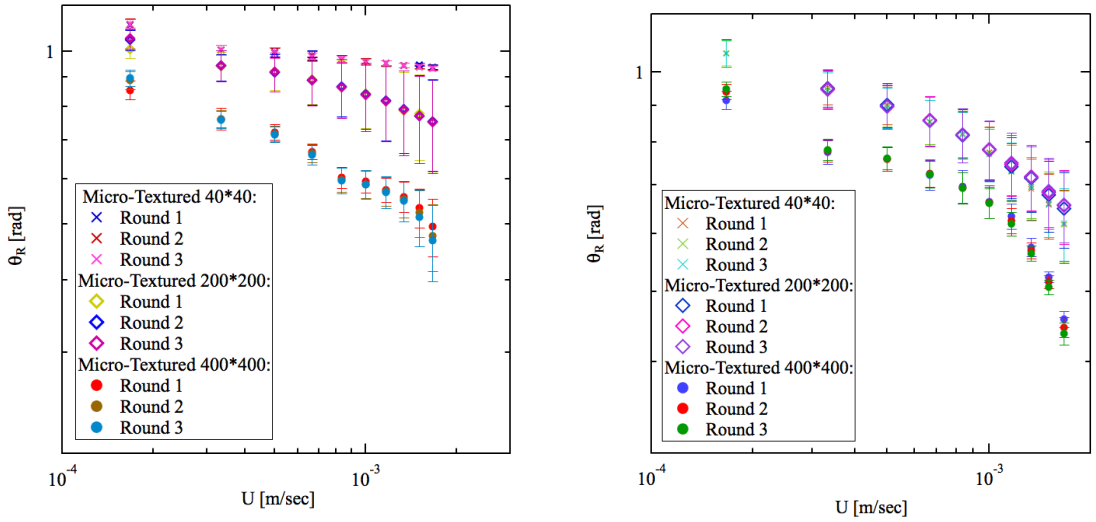

Figure 9.8: (a) Receding motion of 10 wt% PEG/water on micro-textured (i.e. rough) Teflon plates. (b) Receding motion of 20 wt% PEG/water on micro-textured (i.e. rough) Teflon plates.

Figure 9.9(a) shows the contact angle hysteresis (i.e. difference between the advancing contact angle and the receding contact angle) versus the liquid contact line velocity for forced spreading of 10 wt% PEG/water mixture on the rough Teflon plates with the Wenzel state of the equilibrium contact angle. Figure 9.9(b) shows the contact angle hysteresis versus the liquid contact line velocity for forced spreading of 20 wt% PEG/water on the rough Teflon plates with

the Wenzel state of the equilibrium contact angle. As the velocity of liquid contact line increases, the contact angle hysteresis increases for all experiments as shown in figures 9.9(a) and 9.9(b). For forced spreading of 10 wt% PEG/water on the rough Teflon plates, as the density of the roughness increases, the contact angle hysteresis increases for each liquid contact line velocity. Likewise, for forced spreading of 20 wt% PEG/water on the rough Teflon plates, as the density of the roughness increases, the contact angle hysteresis increases for each liquid contact line velocity. The slope of variation of the contact angle hysteresis versus the liquid contact line velocity is the same for all of the rough Teflon plates on the same PEG/water mixture (i.e. the density of the roughness on the rough surfaces has no influence on the slope of the variation of the contact angle hysteresis versus the liquid contact line velocity). However, the slope of variation of the contact angle hysteresis versus the liquid contact line velocity increases as the dynamic viscosity of liquid increase as it is illustrated with figures of 9.9(a) and 9.9(b). This can be due to the fact that higher dynamic viscosity, resulting the higher resisting force for both directions of the liquid motion hence causing the higher difference between the advancing and receding dynamic contact angle for each contact line velocity.

(a) (b)

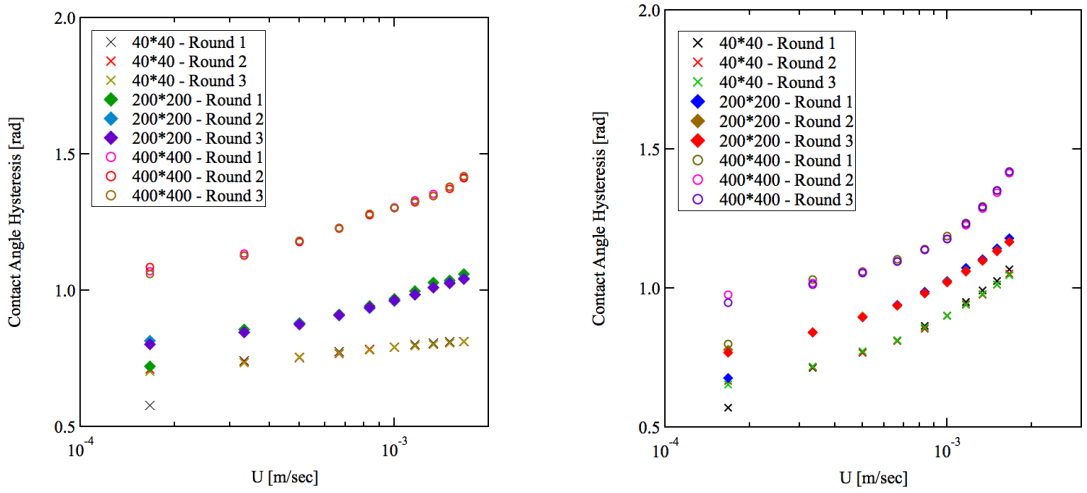

Figure 9.9: (a) Contact angle hysteresis of 10 wt% PEG/water on micro-textured (i.e. rough) Teflon plates. (b) Contact angle hysteresis of 20 wt% PEG/water on micro-textured Teflon plates.

The dynamics of receding motion of the liquid contact line on the rough Teflon plates, with Wenzel state of the equilibrium contact angle, were analyzed by applying both hydrodynamics theory and molecular-kinetic theory. The free fitting parameter for analysis with hydrodynamics theory was only the slip length. The free fitting parameters for analysis with molecular-kinetic theory were K_w and λ which are the frequency of the molecular displacement at equilibrium and the average distance between two adjacent adsorption sites, respectively. Figure 9.10 shows the fitting analysis on the forced receding motion of the liquid contact line for both PEG/water mixtures (i.e. 10 wt% and 20 wt%) on the rough Teflon plate with mesh size 40 × 40. The molecular-kinetic theory was the best appropriate model to describe the dependency of the

receding dynamic contact angle to the liquid contact line velocity for both PEG/water mixtures on rough (i.e. micro-textured) Teflon plates with mesh sizes of 40×40.

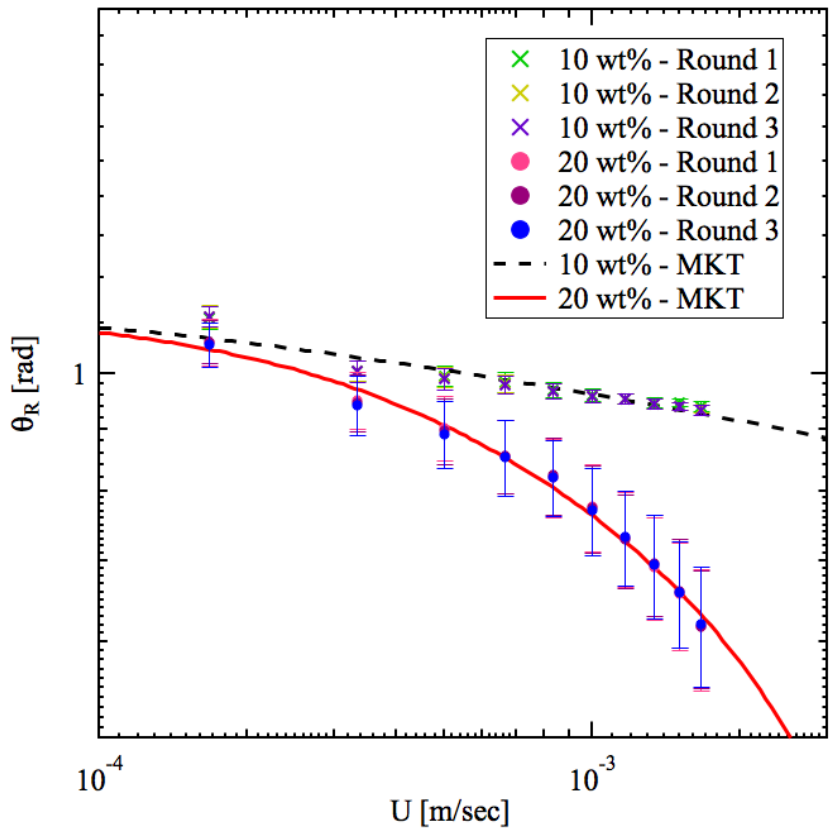

Figure 9.10: Fitting analysis on spreading dynamics for receding motion of PEG/water mixtures on micro-textured (i.e. rough) Teflon plates roughened with mesh size 40×40:

10 wt% PEG/water fitted with molecular-kinetic theory: $\theta_{0R} = 1.1335 \pm 0.0298 \left[\text{rad}\right]$,

$\lambda = \left[1.6705 \times 10^{-9} \pm 1.5 \times 10^{-10}\right]\left[\text{m}\right]$, $K_w = \left[40820 \pm 23000\right]\left[\text{Hz}\right]$;

20 wt% PEG/water fitted with molecular-kinetic theory: $\theta_{0R} = 1.1335 \pm 0.0298 \left[\text{rad}\right]$,

$$\lambda = \left[9.6481\times10^{-10} \pm 4.4\times10^{-11}\right]\left[\mathrm{m}\right],\ K_w = \left[1.8952\times10^{5} \pm 6.89\times10^{4}\right]\left[\mathrm{Hz}\right].$$

Figure 9.11 shows the fitting analysis on the forced receding motion of the liquid contact line for both PEG/water mixtures (i.e. 10 wt% and 20 wt%) on the micro-textured (i.e. rough) Teflon plates with mesh sizes of 200×200. The molecular-kinetic theory was a more appropriate model to describe the dependency of the receding dynamic contact angle on the liquid contact line velocity for both PEG/water mixtures on the rough Teflon plates with mesh sizes of 200×200.

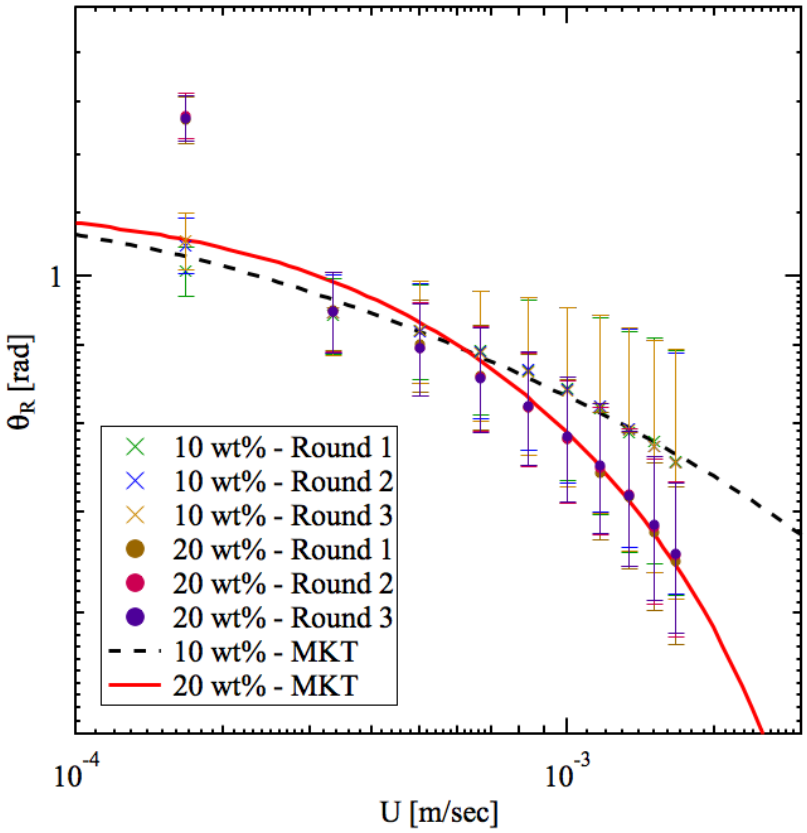

Figure 9.11: Fitting analysis on spreading dynamics for receding motion of PEG/water mixtures on micro-textured (i.e. rough) Teflon plates patterned with mesh size 200×200:

10 wt% PEG/water fitted with molecular-kinetic theory: $\theta_{0R} = 1.1231 \pm 0.0496 \left[\text{rad}\right]$,

$\lambda = \left[1.2505 \times 10^{-9} \pm 5.47 \times 10^{-11}\right]\left[\text{m}\right]$, $K_w = \left[71065 \pm 4.88 \times 10^{4}\right]\left[\text{Hz}\right]$;

20 wt% PEG/water fitted with molecular-kinetic theory: $\theta_{0R} = 1.1231 \pm 0.0496 \left[\text{rad}\right]$,

$\lambda = \left[8.9397 \times 10^{-10} \pm 2.03 \times 10^{-10}\right]\left[\text{m}\right]$, $K_w = \left[3.0994 \times 10^{5} \pm 3.03 \times 10^{5}\right]\left[\text{Hz}\right]$.

Figure 9.12 shows the fitting analysis on the forced receding motion of the liquid contact line for both PEG/water mixtures (i.e. 10 wt% and 20 wt%) on the rough (i.e. micro-textured) Teflon plates with mesh sizes of 400×400. The molecular-kinetic theory was a more appropriate model to describe the dependency of the receding dynamic contact angle to the liquid contact line velocity for both PEG/water mixtures on the micro-textured Teflon plates with mesh sizes of 400×400.

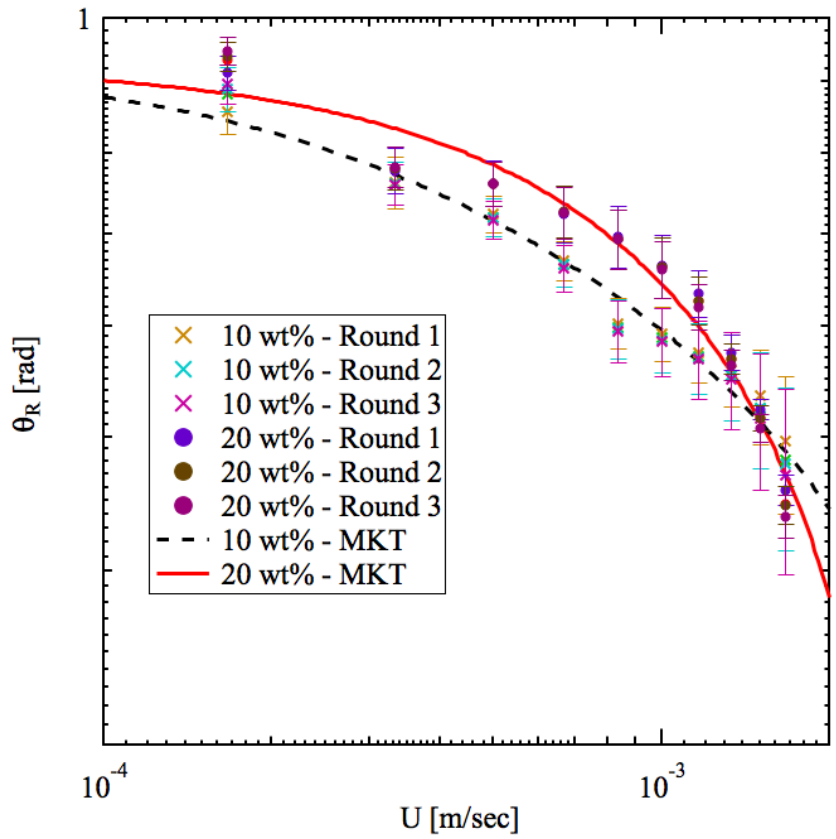

Figure 9.12: Fitting analysis on spreading dynamics for receding motion of PEG/water mixtures on micro-textured (i.e. rough) Teflon plates patterned with mesh size 400×400:

10 wt% PEG/water fitted with molecular-kinetic theory: $\theta_{0R} = 0.93126 \pm 0.0398 \left[\text{rad}\right]$,

$\lambda = \left[1.1773 \times 10^{-9} \pm 5.26 \times 10^{-11}\right]\left[\text{m}\right]$, $K_w = \left[1.0894 \times 10^{5} \pm 2.64 \times 10^{4}\right]\left[\text{Hz}\right]$;

20 wt% PEG/water fitted with molecular-kinetic theory: $\theta_{0R} = 0.93126 \pm 0.0398 \left[\text{rad}\right]$,

$\lambda = \left[8.4466 \times 10^{-10} \pm 1.8 \times 10^{-10}\right]\left[\text{m}\right]$, $K_w = \left[5.7604 \times 10^{5} \pm 5.43 \times 10^{5}\right]\left[\text{Hz}\right]$.

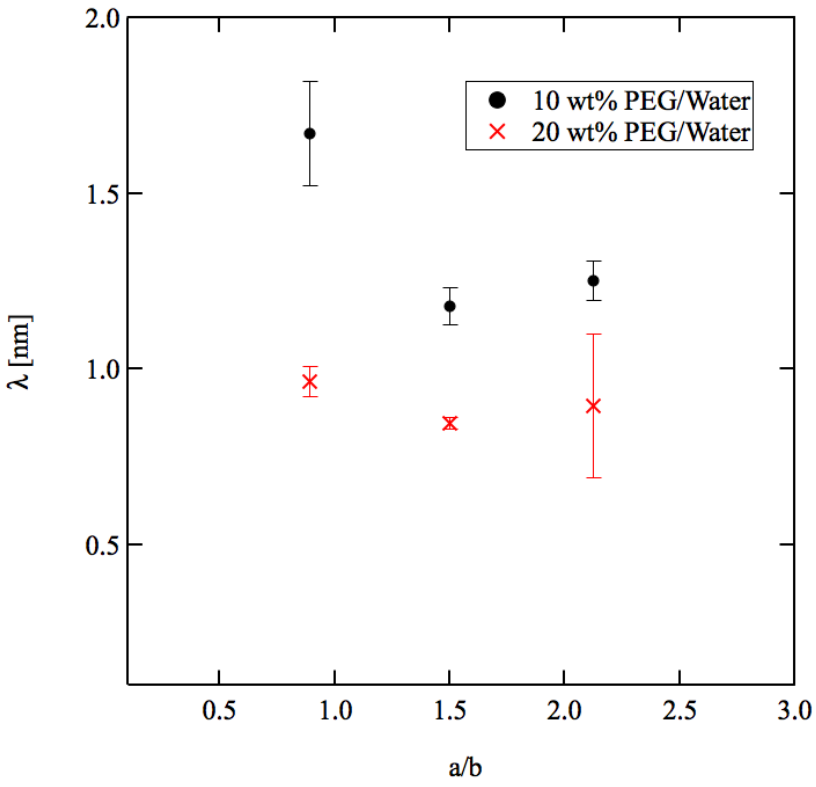

Figure 9.13: Plot of λ, average molecular-displacement at three-phase contact line, versus (a/b), ratio of micro-post width over micro-post distance.

The average molecular displacement at the vicinity of the three-phase contact line (i.e. average distance between adsorption sites on the solid surface) shown by λ, obtained from fitting analyses, depends on the size of the roughness and the distance between them. Figure 9.13 illustrates the dependency of the average distance between adsorption sites, λ, obtained from fitting analysis from all of our experimental results on the ratio of the roughness width (i.e. roughness size) over the roughness distance, a/b. Molecular-displacement, λ, has a stronger dependency on the dynamic viscosity of fluid as illustrated by figure 9.13. The value for λ decreases for higher dynamic viscosity for the same rough surface. This signifies that the increase in the dynamic viscosity of the liquid makes the resisting force between the liquid

molecules larger hence lowering the average displacements of the liquid molecules at the vicinity of the liquid contact line.

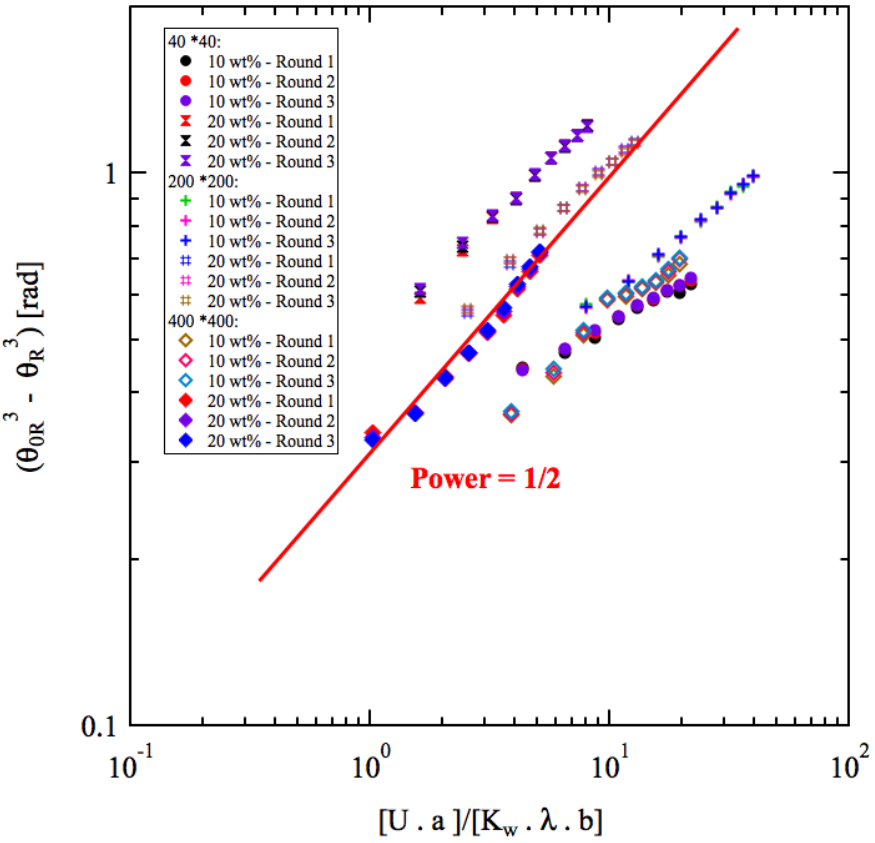

Figure 9.14: Alternative form for describing the spreading dynamics for receding motion of all PEG/water mixtures on all rough Teflon plates.

The theoretical analysis has been done showing the dependency of the receding dynamic contact angle on the relative significance of macroscopic scale of flow to the microscopic scale of flow. This consisted of introducing a non-dimensional variable shown as a parameter $\left(U\,a\right)/\left(K_{w}\,\lambda\,b\right)$. Figure 9.14 shows the dependency of $\theta_{0R}^{3} - \theta_{R}^{3}$ on the non-dimensional variable

$(U\,a)/(K_w\,\lambda\,b)$. As is illustrated by figure 9.10, the functionality of $\theta_{0R}^3 - \theta_R^3$ to the non-dimensional variable $(U\,a)/(K_w\,\lambda\,b)$ follows the power law as shown in (9.6).

$$(\theta_{0R}^3 - \theta_R^3) \sim \left\{\left(\frac{U}{K_w \lambda}\right)\left(\frac{a}{b}\right)\right\}^{1/2} . \tag{9.6}$$

The possibility of existence of large slip length occurring along the roughness on the rough Teflon surfaces during the forced receding motion may cause the power law of ½ for the relation between difference of the cube of the receding dynamic contact angle and the equilibrium receding contact angle with the liquid contact line velocity as shown in (9.6) for the case of the Wenzel state of the equilibrium contact angle. In comparison, Rothstein and his co-workers have obtained different power law based on the optical method [153] for the case of the Cassie-Baxter state of the equilibrium contact angle which was the power of 1/3. The difference of power law between the Wenzel state of the equilibrium contact angle and the Cassie-Baxter state of the equilibrium contact angle is due to the fact that there is a larger solid/liquid interface for the case of the Wenzel state compared to the case of the Cassie-Baxter state where there is very small area of solid/liquid interface. This fact causes the reduction in the shear force hence reduction the power law dependency of the receding dynamic contact angle to the contact line velocity.

9.5 Conclusions

Experimental investigations on the dynamics of spreading on the rough Teflon plates, with the Wenzel state of the equilibrium contact angle, have been performed using the force spreading mechanism with Tensiometer. The working fluids were two mixtures of PEG/water with weight ratios of 10 wt% and 20 wt%. The controlled-rough Teflon plates were prepared by patterning

three different mesh sizes on smooth Teflon plates. The spreading dynamics of both PEG/water mixtures on all three rough Teflon plates have been investigated using hydrodynamics theory and molecular-kinetic theory showing the dependency of the dynamic contact angle on the liquid contact line velocity. The existence of roughness on smooth Teflon surfaces have important impact on the dynamic contact angles (i.e. both advancing and receding).

The advancing dynamic contact angle was independent of the liquid contact line velocity for controlled-rough surfaces with the Wenzel state of the equilibrium contact angle as it also has been observed for the case of the Cassie-Baxter state of the equilibrium contact angle by Rothstein and his co-workers [153]. This signifies the fact that the presence of the roughness on the hydrophobic surface makes the advancing dynamic contact angle independent of the liquid contact linen velocity no mater on what type of the equilibrium state is (i.e. the Cassie-Baxter state or the Wenzel state). This can be due to the impact of the pinning force on the roughness of the micro-textured (i.e. rough) Teflon surfaces. The larger density of roughness causes the increase in the constant value of the advancing dynamic contact angle. The receding dynamic contact angle was dependent on the liquid contact line velocity. The receding dynamic contact angle decreases as the liquid contact line velocity increases for all experimental results. The increase on the density of roughness on the rough surface influences on the value of the receding dynamic contact angle to decrease. The density of roughness on the rough surfaces has no influence on the slope of the variation of the contact angle hysteresis versus the liquid contact line velocity.

The hydrodynamics theory was not appropriate model to describe the dynamics of receding motion for the forced receding motion on rough surfaces with the Wenzel state of the equilibrium contact angle as it has been also concluded by Rothstein and his co-workers [153]

for the case of the forced receding motion on rough surfaces with the Cassie-Baxter state of the equilibrium contact angle. This is caused by the effect of pinning and presence of partial slip-condition along the rough surface.

The molecular-kinetic theory was found to be the best model to describe the dynamics of the receding motion of the liquid contact line on the rough Teflon plates, with the Wenzel state of the equilibrium contact angle. An empirical relation between the receding dynamic contact angle and the non-dimensional parameter, which shows the relative significance of the macroscopic scale to the microscopic scale, has been introduced. We have obtained an empirical power law relation between the receding dynamic contact angle and the non-dimensional parameter with power of one-half, which was higher than the power law obtained by Rothstein and his co-workers for the case of the Cassie-Baxter state of the equilibrium contact angle [153].

CHAPTER 10

Spreading of Emulsions on a Solid Substrate

This chapter was taken with slight modification from the article "Spreading of emulsions on a solid substrate", published in Journal of Coatings Technology and Research [162].

10.1 Abstract

The wettability of emulsions is a prominent factor with a broad impact in an extensive variety of industrial applications ranging from the petroleum to cosmetic industries. Surprisingly, there is no comprehensive study of emulsion spreading to date. In this work, the spreading of water/silicone oil emulsions on glass substrates was investigated. The emulsions were prepared with varying volume fractions of water dispersed in silicone oil, with addition of small amounts of surfactant to stabilize the emulsion structure. The time dependent variation of dynamic contact angle, base diameter, and the spreading rate of the emulsion droplets were studied. The effect of water/silicone oil weight percentage as well as the droplet size and dispersed phase bubble size were also investigated. The weight percentage of water/silicone oil emulsion and droplet size did not have a significant impact on the spreading dynamics; however the dispersed phase bubble size affected the spreading dynamics substantially. The coarsening of the dispersed phase

bubbles was the key factor in the distinct spreading behavior of emulsions compared to pure liquids.

Key words: dynamic contact angle, base diameter, coarsening, dispersed phase bubble, continuous phase region

10.2 Introduction

When a liquid droplet is deposited on a solid substrate, it spreads uniformly and axi-symmetrically until it reaches its equilibrium [1]. There has been considerable attention on the spreading phenomena both experimentally [16,45,49,50,53,57,58,88,97,] and theoretically [3,52,59,70,79,88,91]. The radius of the pure liquid droplet varies based on the $1/10^{th}$ power law while spreading on the solid substrate [16,70,88] and the dynamic contact angle of the pure liquid droplet follows the Hoffman-Voinov-Tanner (HVT) law which relates the dynamic contact angle of the droplet to Capillary number during its spreading [16,70,88].

$$\theta_d^3 \propto Ca = \frac{\mu U}{\sigma} \tag{10.1}$$

Equation 10.1 refers to the spreading of liquid on a solid surface where the complete wetting occurs (The equilibrium static contact angle goes to zero after complete wetting). The spreading of emulsions is expected to be substantially different compared to pure liquids due to its complex structure. An emulsion is a mixture of two or more liquids that are normally immiscible. In an emulsion consisting of two different liquids, one is dispersed phase and the other is continuous phase [152]. The wettability and stability of emulsions are important parameters with a broad impact on a great variety of industrial applications ranging from petroleum industry, cosmetic

industry, printing and coating technology [152]. For example, all facial cosmetic products are types of emulsions and their spreading on the skin is a very influential parameter for skin treatments. Despite the extensive variety of applications, there is no comprehensive study of emulsion spreading to date. There has only been one paper on the subject of spreading of emulsions, which was from Forester et al. 2001 regarding the spreading of water-silicone oil on a smooth horizontal solid substrate [41]. This is mostly due to the complex structure of the emulsions and non-homogeneity of the dispersed phase bubbles in size and their distribution through the continuous phase liquid in the emulsion structure. Their focus was on the leading edge of the continuous phase region. In their experimental investigation, they measured the radius of the leading edge of the continuous phase as well as the variation of the width of the advancing continuous phase region versus time. Both follow the $1/10^{th}$ power law, which is not surprising since the continuous phase region includes the pure silicone oil and it is supposed to spread as a pure liquid. Based on that they have claimed that the increase of dynamic interline radius versus time also follows the $1/10^{th}$ power law. We have investigated on the spreading and wettability of emulsions on solid substrates. Emulsions were prepared the same way as Forester et al. 2001 with different weight percentage of water, silicone oil, and small amounts of surfactant. Single drops of emulsions with different weight percentage were placed on glass substrates. We show here that for the variation of contact angle, base diameter, and contact line of the drops as a function of time, the emulsion spreading follows the HVT law as it was claimed by Forester et al. 2001.

10.3 Materials and Methods

10.3.1 Sample Preparation

The chemical constituents that were used to prepare emulsion samples were Deionized water, silicon oil with kinematic viscosity of 10 cst and a regular soap as a surfactant to stabilize the emulsion. Emulsion samples were prepared based on different volume fractions of the DI water as a dispersed phase in the silicone oil as a continuous phase and a small amount of soap as a surfactant to stabilize the structure of emulsion the same way as Forester et al. 2001 prepared their emulsion samples. The total volume of each prepared sample of emulsion was 150 mL. In each emulsion sample, 2% v/v (volume ratio of total volume) was the regular soap. The emulsion samples were made based on the different weight percentages of volume ratio of water added to the silicon oil. The emulsions were made for 40%, 50%, and 60% v/v of DI water dispersed in the silicone oil. First, the desired amount of silicone oil was added into the 200 mL beaker and then 2% v/v of soap was added to the beaker. Then the beaker was placed on a magnetic stirrer with a magnetic stirring bar inside the beaker. The desired amount of DI water was added to the sample contained in the 200 mL beaker and was mixed with the sample using the magnetic stirring bar inside the sample. The DI water was added to the sample during the sample preparation in 0.5 mL increments. After each addition of DI water to the sample, the beaker was moved around at least 7 times manually such that the magnetic stirring bar was in contact with the wall of the beaker continually. After all the desired amount of DI water was added to the sample, the sample continued to be stirred for an additional 5 minutes. Then after 24 hours of leaving the sample still to stabilize into a two-phase region, the observational experiments were done using the top portion of the sample, which was the stabilized emulsion mixture.

10.3.2 Experimental Technique

Observation of the spreading of emulsions on solid substrates was conducted with Drop Shape Analyzer (DSA 100), Krüss GMBH. A glass substrate with dimensions of 50×24×0.15 mm^3 (VWR micro-cover glass) was cleaned with acetone, methanol and DI water successively, and then plasma cleaned with Plasma Cleaner (PDC-32g) for 7 minutes. The emulsion droplet was deposited manually with negligible impact velocity on the glass substrate, which was placed on the stage inside the chamber following two steps. First, the emulsion was extracted from the beaker into the syringe of 2 mL size by pumping the emulsion into the syringe using the metal syringe plunger and then the syringe filled with emulsion was placed in the syringe holder of the DSA 100 in downward direction. A single emulsion droplet was deposited on the glass substrate manually with zero impact velocity by pushing through the syringe by the syringe plunger and through the 0.5mm inner diameter injection needle with the needle very close to the surface of the glass substrate. The High-speed CCD camera capable of recording 90 fps from side view of droplet was used as a visualization technique to study droplet evolution during spreading. Drop shape analyzer using the Laplace-Young method measured the base diameter and contact angle of the emulsion drop. In this method, a profile of sessile drop in the region of the baseline was fitted by the Young-Laplace equation. From the fitted parameters, the slope of the three-phase contact point and the baseline were first determined and then used to determine the contact angle. Consequently, base diameter was defined as the distance between left and right contact points at the three-phase contact region. Since the fast spreading stage happens very quickly we also did the observation from top view for spreading of the emulsion droplet with 60% v/v of dispersed phase water on a smooth horizontal glass substrate using the high-speed camera Phantom 663

capable of recording 36000 fps for a resolution of 256 pixels by 256 pixels to capture the details of the spreading within a three second window of fast spreading stage.

10.4 Results and Discussion

The experiments were done on emulsion droplets with three weight percentages. Figures 10.1, 10.2, and 10.3 show the variation of base diameter, left and right contact points at the three-phase contact line from side view observation during the spreading of emulsion on the glass substrate for 40% v/v, 60% v/v with large dispersed phase water bubbles, and 60% v/v with small dispersed phase bubbles, respectively. The volume of the 40% v/v emulsion droplet is 2.56 μL and the volume of the 60% v/v emulsion droplet with small dispersed phase water bubbles is 2.42 μL and the volume of the 60% v/v emulsion droplet with large dispersed phase water bubbles is 2.97 μL. Spreading of the emulsion droplets happened in three consecutive stages. We observed the sudden fast spreading of emulsion droplets (stage 2) occurred for all of them after being deposited on the glass substrate after an interval of time to stay still on the glass substrate in the form of spherical cap or spread very slowly (stage 1). This procedure happened for all emulsion droplets in a matter of a few seconds. The reason for this was the coalescence of the dispersed phase water bubbles behind the intermediate dynamic contact line region where the continuous phase region separated from the emulsion due to the demarcation of dispersed phase bubbles. Based on the small magnitude of the Ohnesorge number, Oh, and small magnitude of the characteristic length of the drop compared to the capillary length, the liquid spherical cap formed on the solid surface when each emulsion droplet was spreading on smooth horizontal glass substrate [57]. For stage 2 where sudden fast spreading happens due to coarsening of the

dispersed phase water bubbles, the inertia term in the momentum equation balances with the capillary term [57]. Capillary term can be defined based on the pressure jump across the bubble due to surface tension, σ, and curvature of the bubble, $\frac{\partial^2 h}{\partial x^2}$ where h is the characteristic height of the free interface between emulsion droplet and the air. The inertia term can be defined as the convective term, $\rho u \frac{\partial u}{\partial x}$, and the capillary term can be represented as $\frac{\partial p}{\partial x}$.

By balancing the capillary term with the convective inertial term [22,57] and using scaling analysis and applying the assumption of constant droplet volume constraint, the power law relation for the time variation of droplet radius can be obtained.

$$R(t) \sim \left(\frac{\sigma V}{\rho \pi} \right)^{1/6} t^{1/3} \tag{10.2}$$

We also observed that the spreading on the left contact point and right contact point of the droplet is not the same and one of them is significantly faster than the other. This is due to the non-uniform distribution of the dispersed phase water bubbles inside the water-silicon oil emulsion. Hence the left and right contact lines have a substantial difference in spreading rate. In experiments, we noticed that the size of the dispersed phase water bubbles is not the same everywhere. The size of the dispersed phase bubble has an important effect on the speed of the fast spreading region as it is shown in Figures 10.2 and 10.3. As the size of the dispersed phase bubbles are larger behind the intermediate dynamic contact line, the coarsening of the bubbles would produce additional driving force on the leading edge of the continuous phase region (three-phase dynamic contact line) to move faster in the fast spreading stage. Figure 10.4 shows the actual picture of the emulsion droplet when deposited on the glass substrate during the experiment and also a schematic of the picture. This non-homogeneity of the sizes of the

dispersed phase water bubbles influence on the spreading rates of the contact points of right and left sides.

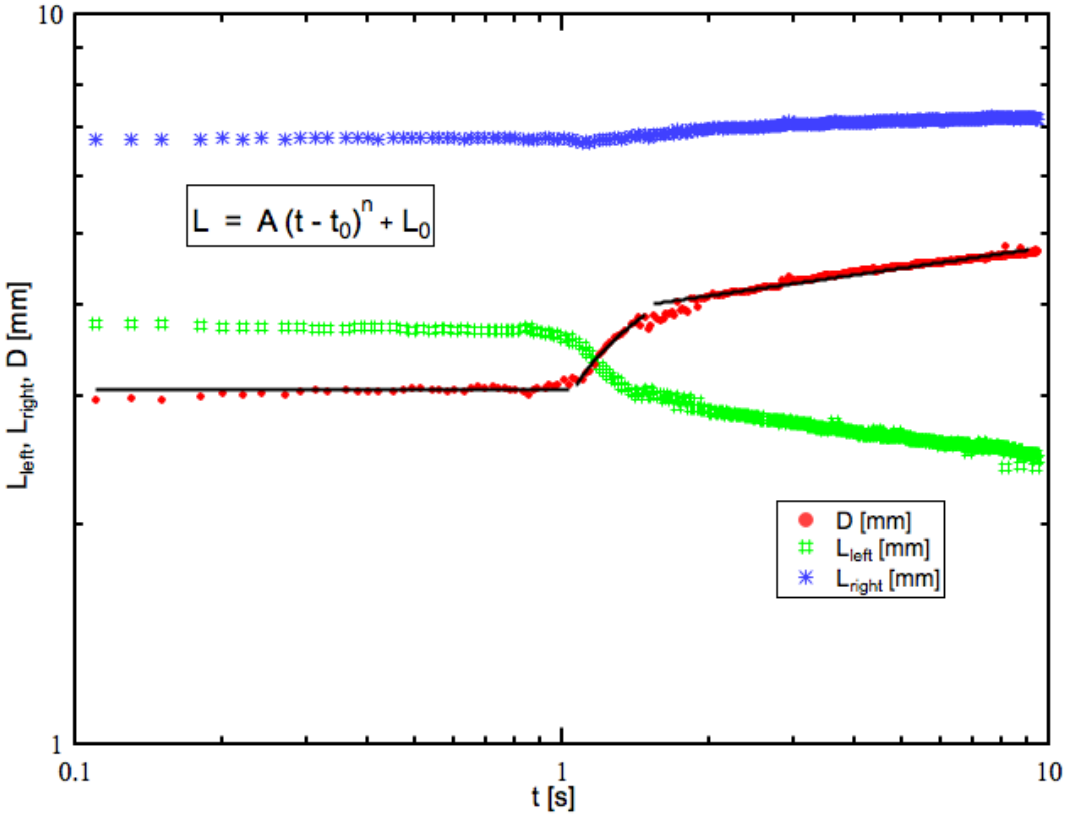

Figure 10.1: The variation of base diameter, left contact point and the right contact point at the three-phase contact line in time. 40% v/v with large dispersed phase bubbles; stage1: (A = 0.0042 ± 0.000 mm/sec^n, t_0 = -691.1 ± 636 sec, L_0 = 3.050 ± 0.006 mm, n = 0.1 ± 0.00); stage 2: (A = 2.5766 ± 0.52 mm/sec^n, t_0 = 0.92871 ± 0.0864 sec, L_0 = 1.7658 ± 0.521 mm, n = 0.333 ± 0.000); stage 3: (A = 2.237 ± 0.032 mm/sec^n, t_0 = 1.457 ± 0.035 sec, L_0 = 1.98 ± 0.040 mm, n = 0.1 ± 0.000).

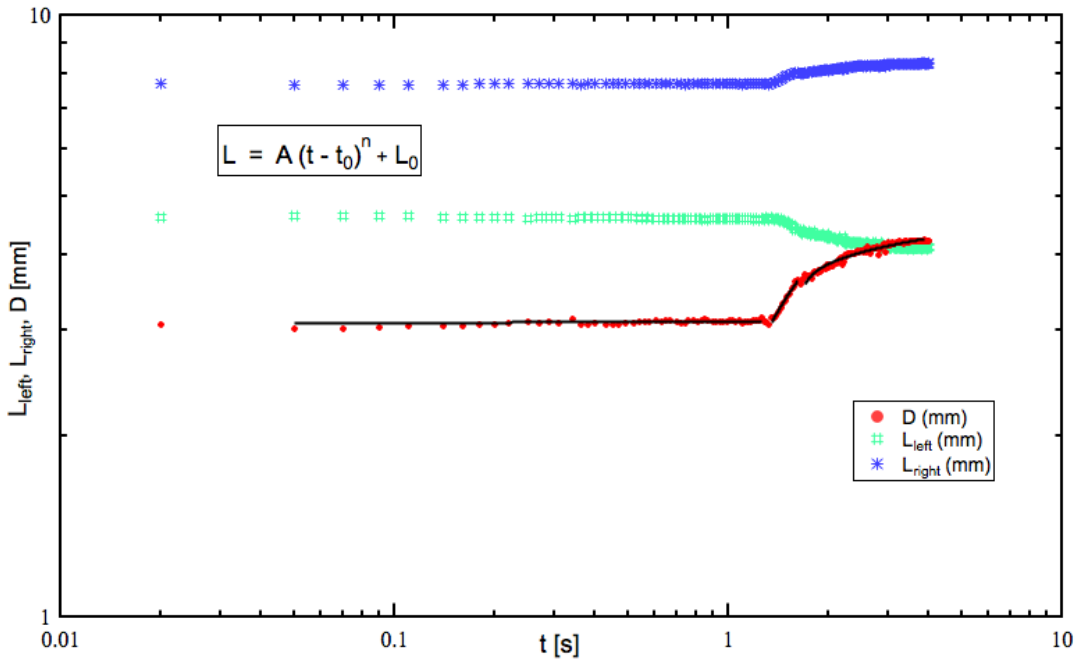

Figure 10.2: The variation of base diameter, left contact point and the right contact point at the three-phase contact line in time. 60% v/v with large dispersed phase bubbles; stage 1: ($A = 1.3632 \pm 3.14$ mm/sec^n, $t_0 = -47.156 \pm 16.2$ sec, $L_0 = 1.0823 \pm 4.64$ mm, $n = 0.1 \pm 0.000$); stage 2: ($A = 4 \pm 0$ mm/sec^n, $t_0 = 0.92787 \pm 0.0334$ sec, $L_0 = 0.090763 \pm 0.0672$ mm, $n = 0.333 \pm 0.000$); stage 3: ($A = 2.2098 \pm 0.341$ mm/sec^n, $t_0 = 1.6152 \pm 0.155$ sec, $L_0 = 1.8538 \pm 0.341$ mm, $n = 0.1 \pm 0.000$).

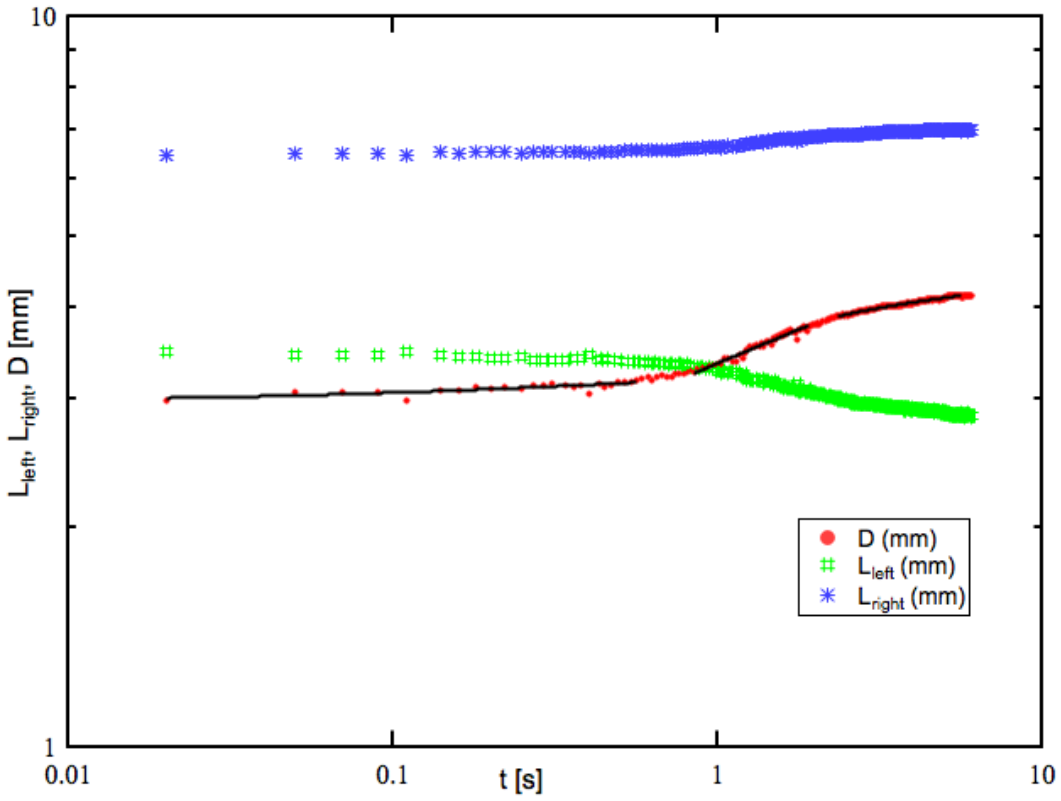

Figure 10.3: The variation of base diameter, left contact point and the right contact point at the three-phase contact line in time. 60% v/v with small-dispersed phase bubbles; stage1: (A = 0.764 ± 0.353 mm/sec^n , t_0 = -0.038 ± 0.093 sec, L_0 = 2.431 ± 0.337 mm, n = 0.1 ± 0.00); stage 2: (A = 1.522 ± 0.34 mm/sec^n, t_0 = 0.276 ± 0.33 sec, L_0 = 1.987 ± 0.511 mm, n = 0.333 ± 0.000); stage 3: (A = 1.592 ± 0.06 mm/sec^n, t_0 = 1.480 ± 0.080 sec, L_0 = 2.317 ± 0.072 mm, n = 0.1 ± 0.000).

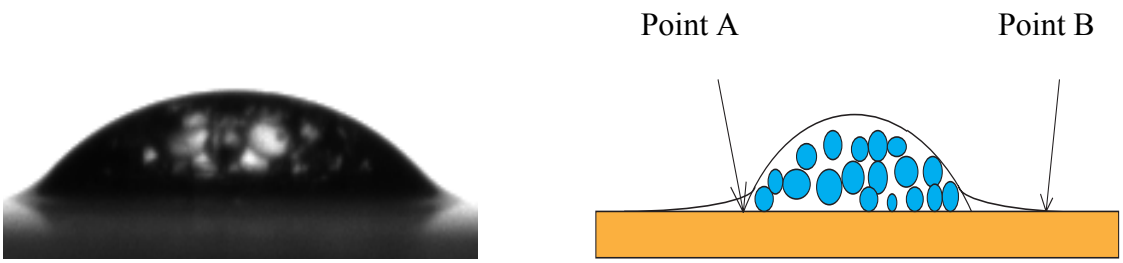

(a) (b)

Figure 10.4: (a) Actual picture of emulsion droplet and (b) schematic of the emulsion droplet when deposited on the glass substrate. Intermediate dynamic contact line is shown with point A in 2D side view and three-phase contact line or leading edge of the continuous phase region is shown with point B in 2D side view.

The variation of dynamic contact angle at the three-phase contact line region versus time was also investigated. We found that the variation of dynamic contact angle versus time follows the exponential form. Figure 10.5 shows the variation of the dynamic contact angle at the three-phase contact line region as a function of time for the spreading of emulsion with 60% v/v of dispersed phase water.

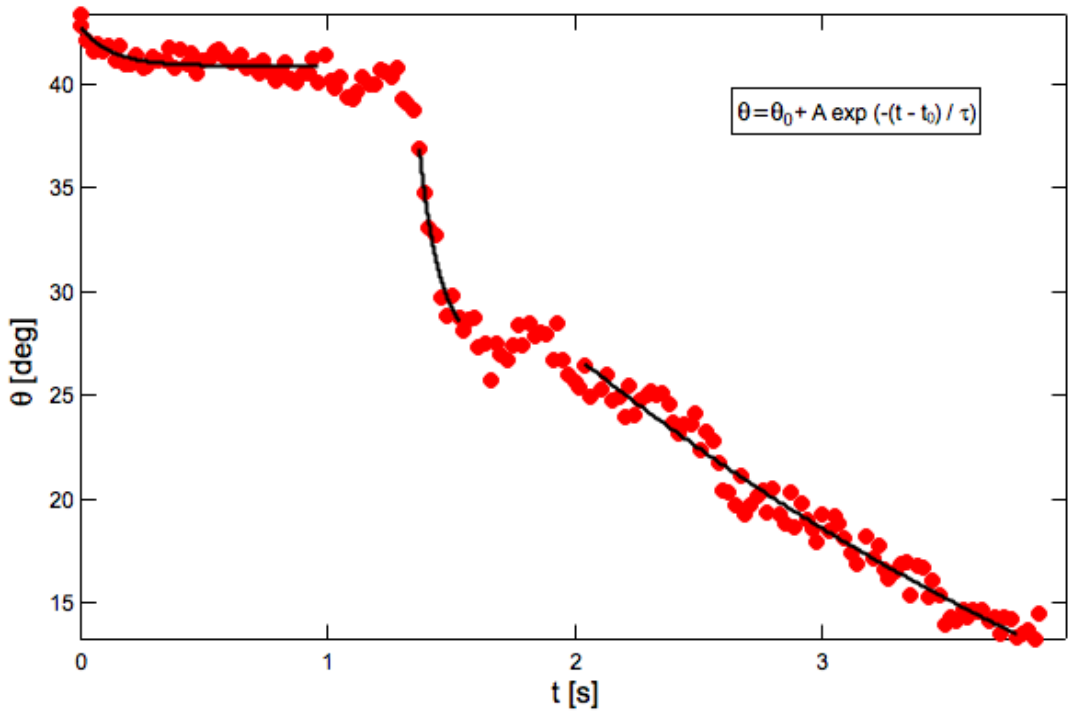

Figure 10.5: The variation of dynamic contact angle at three-phase contact line as a function of time in the exponential form; stage 1: (θ_0 = 40.887 ± 0.093 deg, A = 1.845 ± 0.261 deg, τ = 0.125 ± 0.037 sec, t_0= 0 sec) stage 2: (θ_0 = 27.107 ± 2.17 deg, A = 9.792 ± 1.98 deg, τ = 0.086 ± 0.041 sec, t_0= 1.37 sec); stage 3: (θ_0 = -7.149 ± 9.5 deg, A = 33.699 ± 9.31 deg, τ = 3.568 ± 1.28 sec, t_0= 2.04 sec).

We observed from top view to see how the dispersed phase water bubbles interact and what was actually going on inside the emulsion in the vicinity of intermediate contact line. We found out that coarsening of the dispersed phase bubbles effect on the motion of the leading edge of the continuous phase with introducing additional driving force to the leading edge of the continuous phase region. The movie that can be found in the supplementary materials shows the spreading of the emulsion droplet with 60% v/v of dispersed phase water on a smooth horizontal glass

substrate from top view using the High Speed Camera Phantom 663. The spreading of the emulsion included some rigid body motion of the droplet during the spreading due to the huge difference in local additional driving force due to the coarsening of the dispersed phase water bubbles in the vicinity of the intermediate dynamic contact line, which separates the emulsion part of the droplet from the continuous phase region of the droplet. Figure 10.6 shows the plot of variation of radius of curvature of the upside region of the emulsion droplet versus time from just before the coarsening of the dispersed phase bubbles on the upside region of the droplet until some time after that coarsening.

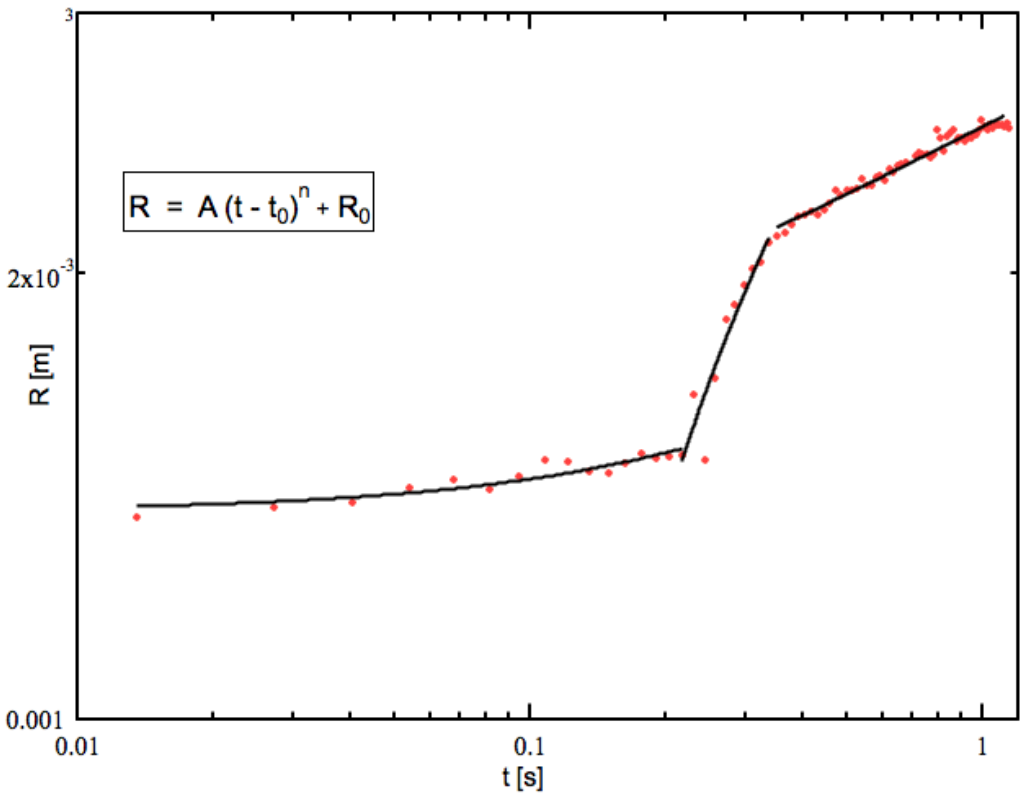

Figure 10.6: The radius of curvature of upside region of the emulsion droplet with 60% v/v of dispersed phase water versus time; stage 1: ($A = 0.0042 \pm 0$ m/sec^n, $n = 0.1 \pm 0$, $t_0 = -0.510 \pm 0.075$ sec, $R_0 = -0.003 \pm 0.000$ m); stage 2: ($A = 0.004965 \pm 0.00627$ m/sec^n, $n = 0.333 \pm 0$, $t_0 = 0.089314 \pm 0.336$ sec, $R_0 = -0.0010015 \pm 0.00531$ m); stage 3: ($A = 0.0042 \pm 0$ m/sec^n, $n = 0.1 \pm 0$, $t_0 = -0.092 \pm 0.020$ sec, $R_0 = -0.002 \pm 0.000$ m).

10.5 Conclusions

The sharp spreading stage is due to the coarsening of the dispersed phase bubbles, which were demarcated behind the intermediate dynamic contact line separating the continuous phase region from the emulsion mixture. Non-axisymmetric spreading in the dynamic contact line at the three-phase contact region is due to non-uniform distribution of bubbles and non-homogeneity of the

dispersed phase water bubble size within the emulsion. Tanner's law based on the $1/10^{th}$ power law (equation 10.3) is almost valid before and after the stage of fast spreading in evolution of base diameter versus time at the leading edge of the continuous phase region.

(10.3)

The variation of the dynamic contact angle at the three-phase contact line versus time behaves in the exponential form (equation 10.4)

$$y = y_0 + A\exp\left(\frac{-\left(t - t_0\right)}{\tau}\right) \tag{10.4}$$

As the size of the dispersed phase bubble increases the exponential decrease of the intermediate dynamic contact angle in time increases. This unusual behavior of the spreading of the emulsions on glass substrates is due to the coarsening of the emulsion. Spreading of the emulsions depend on several parameters which we could not control during the experiments. As we mentioned earlier two of the most important parameters are the distribution of the dispersed phase water bubbles and the heterogeneity of the dispersed phase water bubbles' sizes within the continuous phase region, which we could not control in our experiments. Another important factor, which is very crucial for the spreading of emulsions, is the exact volume fraction of the dispersed phase water bubbles within the silicone oil. The volume fractions that we measured are based on the volume fractions of the emulsion samples before becoming stabilized. However, the emulsion samples became separated into two phases of the pure silicone oil phase and the emulsion phase after being stabilized.

CHAPTER 11

Effect of Viscosity on Contact Angle Measurement Using Tensiometer

11.1 Motivation

The only disadvantage of the Tensiometer is the fact of neglecting the viscous force in force measurement method applied on the plate's surface during advancing and receding motion in the pool of highly viscous liquid. Hence that factor makes the Tensiometer to loose its extent of flexibility for being used for experiments with highly viscous liquids. Due to this fact, there are also some limitations on the range of the speeds for doing the measurements of dynamic contact angles using Tensiometer. To be able to apply the Tensiometer in dynamic contact angles measurements for high speeds and for any large viscous liquids, one will have to consider the effect of the viscous force due to the velocity gradient in the region close to the surface of the plate.

11.2 Viscous Model for Tensiometer

The region close to the surface of the solid substrate during the immersion/withdrawal in the pool of the liquid where there is a velocity gradient is termed the viscous boundary layer. Figure 11.1 illustrates the schematic of the viscous boundary layer formed on the solid flat plate during the immersion of the plate in the pool of viscous liquid.

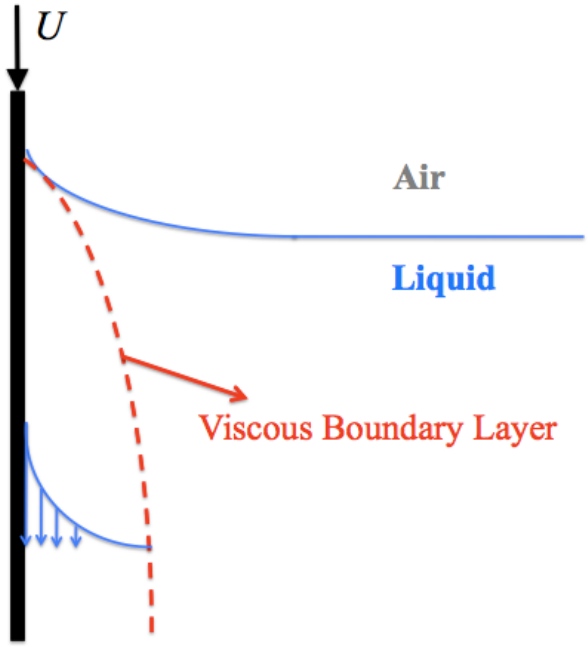

Figure 11.1: The schematic of the viscous boundary layer formed on the plate during its immersion inside a pool of viscous liquid.

A model that signifies the effect of the viscous force on the plate during force calculation has been obtained for the case of low Reynolds number flow of a solid flat plate into the pool of viscous liquid by applying the boundary layer theory.

In the analysis the following assumptions have been applied:

1. Steady state flow

2. Incompressible fluid

3. Creeping flow (Low Reynolds number flow)

The viscous model analysis was carried out for the situation of two-dimensional flow of a viscous liquid near a corner of a solid plate with angle of the corner to be 180^o. This problem is similar to the Taylor problem. The solid flat plate has width, w, thickness, t, and length, l. In this case, the solid flat plate is immersing with constant speed, U, into a pool of viscous liquid through the interface of the liquid/air as illustrated in figure 11.2. In the polar-coordinate system shown in equation 11.2, the velocity in the radial direction, r, is u_r, and the velocity in the θ direction is u_θ.

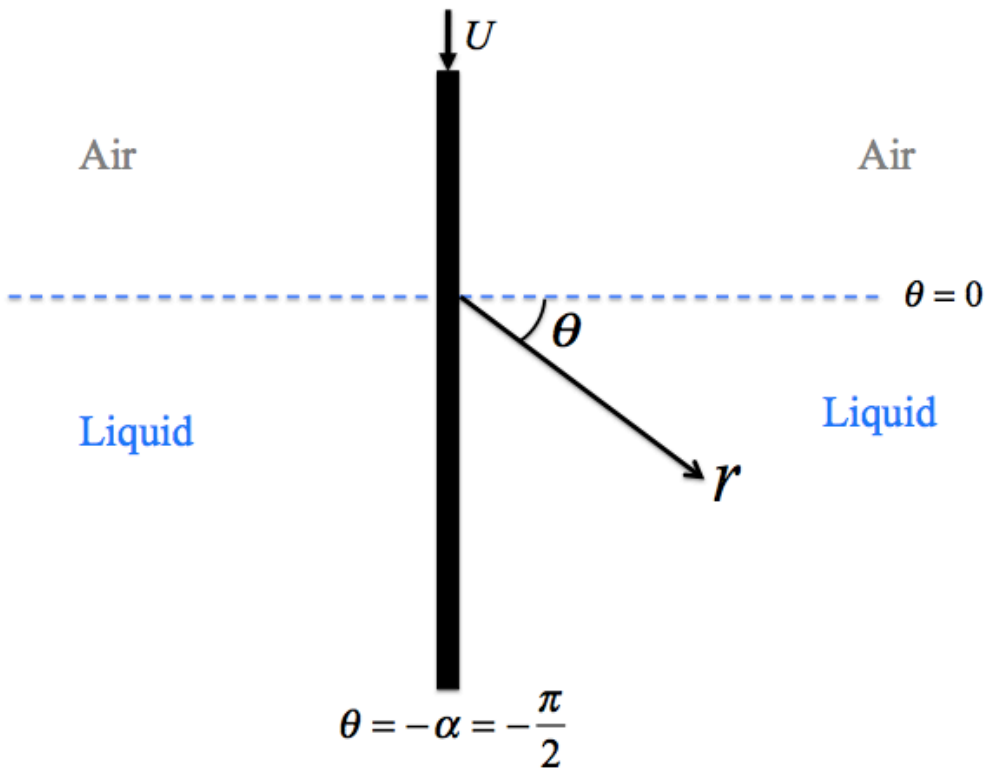

Figure 11.2: Immersion of the solid flat plate into a pool of viscous liquid in a polar coordinate system $\left(r,\theta\right)$.

The following boundary conditions applied on this problem in cylindrical coordinate system.

The no-slip boundary condition along the solid/liquid interface is shown in equation 11.1.

$$u_r = U \qquad\qquad \theta = -\alpha = -\frac{\pi}{2} \tag{11.1}$$

The no-flow through boundary condition along the solid/liquid interface is shown in equation 11.2.

$$u_\theta = 0 \qquad\qquad \theta = -\alpha = -\frac{\pi}{2} \tag{11.2}$$

The shear stress, $\tau_{r\theta}$, in the polar coordinate system which is zero along the liquid/air interface (i.e. shear-free condition along the liquid/air interface) as shown in equation 11.3.

$$\tau_{r\theta} \equiv \frac{1}{r}\left(\frac{\partial u_r}{\partial \theta}\right) = 0 \qquad\qquad \theta = 0 \tag{11.3}$$

The no-flow through boundary condition along the liquid/air interface is described in equation 11.4.

$$u_\theta = 0 \qquad\qquad \theta = 0 \tag{11.4}$$

The stream function, ψ, for the flow configuration in polar coordinate system is described in equation 11.5.

$$\psi = U\,r\left(\sin\alpha\,\cos\alpha - \alpha\right)^{-1}\left[\sin\alpha\left(\theta\,\cos\theta\right) - \left(\alpha\,\cos\alpha\right)\sin\theta\right] \tag{11.5}$$

The radial component of velocity is defined based on the stream function as shown in equation 11.6:

$$u_r = \frac{1}{r}\frac{\partial \psi}{\partial \theta} \tag{11.6}$$

The radial component of velocity along the solid/liquid interface is defined as follows:

$$\left(u_r\right)_{\alpha=\frac{\pi}{2}} = \frac{1}{r}\left(\frac{\partial \psi}{\partial \theta}\right)_{\alpha=\frac{\pi}{2}} \tag{11.7}$$

Taking the derivative of stream function in its general form (i.e. equation 11.5), we can obtain the following form:

$$\frac{\partial \psi}{\partial \theta} = \left(\frac{-Ur}{\alpha}\right)\left(\cos\theta - \theta\sin\theta\right) \tag{11.8}$$

By substituting $\alpha = \frac{\pi}{2}$ into equation 11.9:

$$\left(\frac{\partial \psi}{\partial \theta}\right)_{\alpha=\frac{\pi}{2}} = \left(\frac{-2Ur}{\pi}\right)\left(\cos\theta - \theta\sin\theta\right) \tag{11.9}$$

Then the radial component of the velocity for the situation illustrated in figure 11.2 (i.e. $\alpha = \frac{\pi}{2}$) can be obtained by substituting equation 11.9 into equation 11.7:

$$\left(u_r\right)_{\alpha=\frac{\pi}{2}} = \frac{1}{r}\left(\frac{\partial \psi}{\partial \theta}\right)_{\alpha=\frac{\pi}{2}} = \frac{-2U}{\pi}\left(\cos\theta - \theta\sin\theta\right) \tag{11.10}$$

The shear stress in general can be defined based on the tangential derivative of the radial component of the velocity in polar coordinate system as follows:

$$\left(\tau_{r\theta}\right) = \frac{\mu}{r}\left(\frac{\partial u_r}{\partial \theta}\right) \tag{11.11}$$

The shear stress for the situation in figure 11.2 is defined as follows:

$$\left(\tau_{r\theta}\right)_{\alpha=\frac{\pi}{2}} = \frac{\mu}{r}\left(\frac{\partial u_r}{\partial \theta}\right)_{\alpha=\frac{\pi}{2}} \tag{11.12}$$

Hence, the general form of the shear stress for the situation shown in figure 11.2 is shown as follows:

$$\left(\tau_{r\theta}\right)_{\alpha=\frac{\pi}{2}} = \frac{\mu}{r}\left(\frac{\partial u_r}{\partial \theta}\right)_{\alpha=\frac{\pi}{2}} = \left(\frac{2\mu U}{r\pi}\right)\left(2\sin\theta + \theta\cos\theta\right) \tag{11.13}$$

As a result, the shear stress along the solid/liquid interface for the situation shown in figure 11.2 is describes as follows:

$$\left(\tau_{r\theta}\right)_{\alpha=-\frac{\pi}{2},\theta=\frac{\pi}{2}} = \left[\frac{\mu}{r}\left(\frac{\partial u_r}{\partial \theta}\right)\right]_{\alpha=-\frac{\pi}{2},\theta=\frac{\pi}{2}} = \left(\frac{2\mu U}{r\pi}\right)\left(2\sin\left(-\frac{\pi}{2}\right) - \frac{\pi}{2}\cos\left(-\frac{\pi}{2}\right)\right) \tag{11.14}$$

By simplifying the equation 11.15, the shear stress along the solid/liquid interface is defined as:

$$\left(\tau_{r\theta}\right)_{\alpha=-\frac{\pi}{2},\theta=\frac{\pi}{2}} = \frac{-4\mu U}{r\pi} \tag{11.15}$$

The total drag applied on the solid flat plate due to the viscous shear stress is obtained by integrating the viscous shear stress, shown in equation 11.15, over the surface area of the solid flat plate as shown in equation 11.17:

$$F_{viscous} = 2\left(w+t\right)\int_{\varepsilon}^{x}\left[\left(\tau_{r\theta}\right)_{\alpha=-\frac{\pi}{2},\theta=\frac{\pi}{2}}\right]dr = 2\left(w+t\right)\int_{\varepsilon}^{x}\left(\frac{-4\mu U}{r\pi}\right)dr \tag{11.16}$$

In equation 11.17, the cut-off length, ε is very small, $\varepsilon \ll 1$.

After taking the integration across the boundaries shown in equation 11.17, the total viscous drag applied on the solid flat plate is shown in equation 11.18.

$$F_{Viscous} = \left(\frac{-8\left(w+t\right)\mu U}{\pi} \right)\left(\ln\left(\frac{x}{\varepsilon} \right) \right) \tag{11.17}$$

In the measurements of dynamic contact angles using Tensiometer for the case of high viscous liquids, the viscous drag, $F_{viscous}$, should be added to the equation of the force balance that is used to calculate the dynamic contact angle.

For the situation of the advancing motion in which the solid flat plate immerses into the pool of the viscous liquid, the equation of the force balance should as follows:

$$F_{measured} - F_{Capillary} + F_{Bouyancy} - F_{gravity} + F_{viscous} = 0 \tag{11.18}$$

Figure 11.3 illustrates the schematic of the directions of the forces applied on the solid flat plate during the advancing motion.

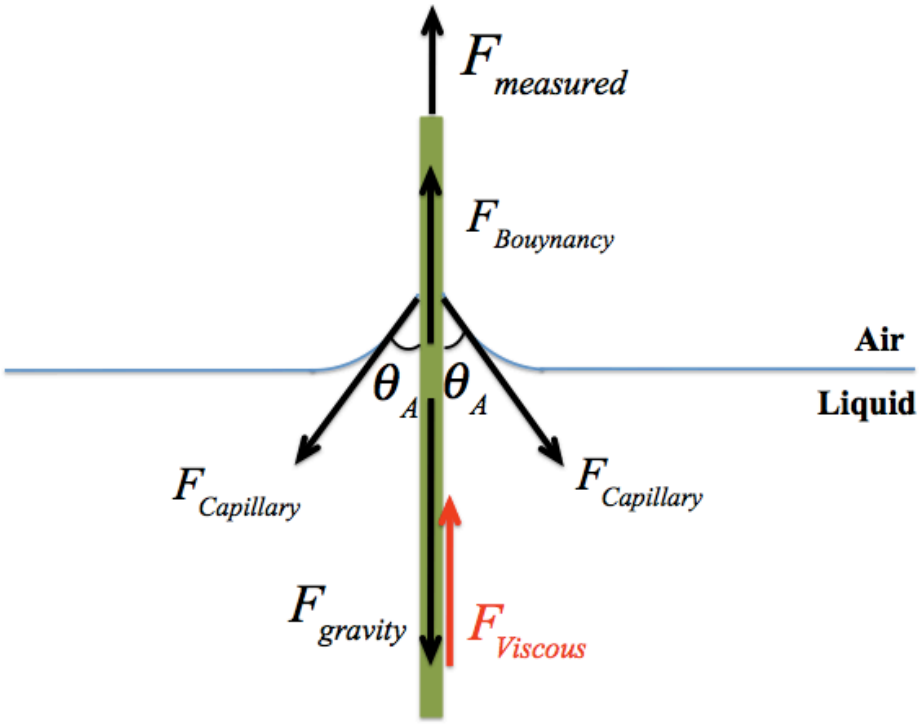

Figure 11.3: Schematic of the advancing motion of the solid flat plate into the pool of the liquid.

For the situation of the receding motion in which the solid flat plate withdrawals from the pool of the viscous liquid, the equation of the force balance should as follows:

$$F_{measured} - F_{Capillary} + F_{Bouyancy} - F_{gravity} - F_{viscous} = 0 \qquad (11.19)$$

Figure 11.4 illustrates the schematic of the directions of the forces applied on the solid flat plate during the receding motion.

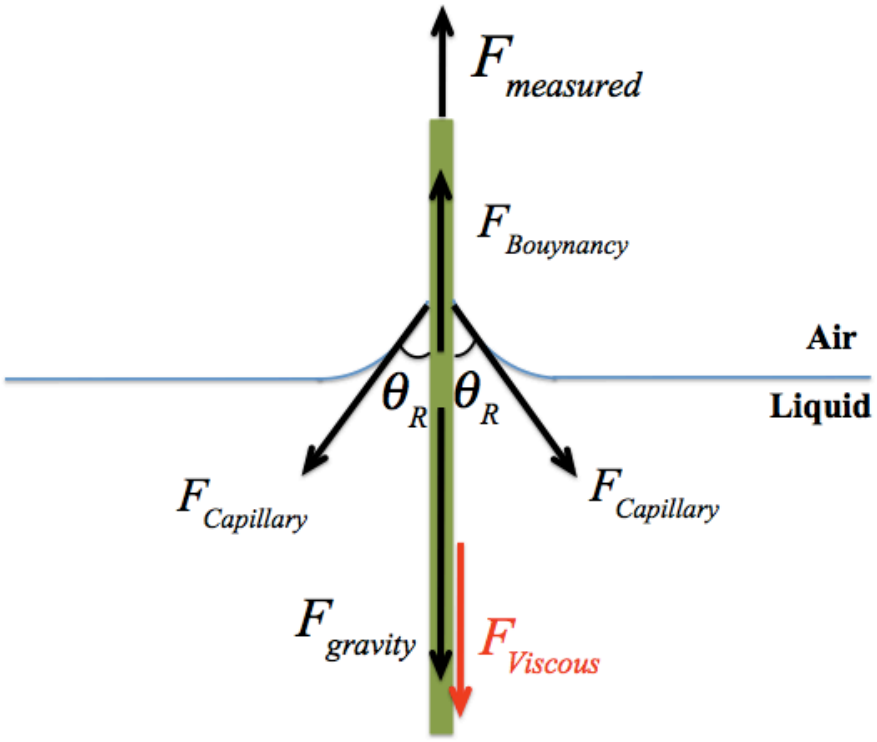

Figure 11.4: Schematic of the receding motion of the solid flat plate from the pool of the liquid.

We have to note that direction of viscous force is always in a direction opposing the motion of the solid flat plate. In equations 11.18 and 11.19, the sign of the measured force, $F_{measured}$, depends on the weight of the solid plate and the value of the dynamic contact angle. For example, for the situation of advancing motion where the advancing dynamic contact angle is larger than 90^o, then the capillary force would be in upward direction and that may make the measured force to be in downward direction.

11.3 Experiment

To show the significance of the role of the viscous force on the dynamic contact angle measurement using Tensiometer, the experiments have been done for three liquids with very distinct dynamic viscosities. During the experiments with Tensiometer, the dynamic contact angles have been also measured applying optical method. In optical method, the SLR Canon camera observed and recorded the shapes of the menisci of the liquids at the liquid contact line and then the dynamic contact angle have been measured using the ImageJ. The values of the dynamic contact angle obtained from Tensiometer, $\theta_{Tensiometer}$, have been compared with the values of dynamic contact angle obtained from optical method, $\theta_{Optical}$.

Figure 11.5 shows the dependency of the advancing dynamic contact angle to the contact line velocity obtained from the Tensiometer and the optical method for the immersion of the glass substrate inside the pool of the silicone oil 100 cSt. It shows that for speeds up to 400 mm/min, the results obtained from Tensiometer match with the results obtained from the optical method. But for speeds beyond 400-mm/min, $\theta_{Tensiometer}$ is different from $\theta_{Optical}$, since the velocity gradient becomes very large for the thin boundary layer formed on the surface of the solid flat plate that makes the viscous force important in calculation of the dynamic contact angle.

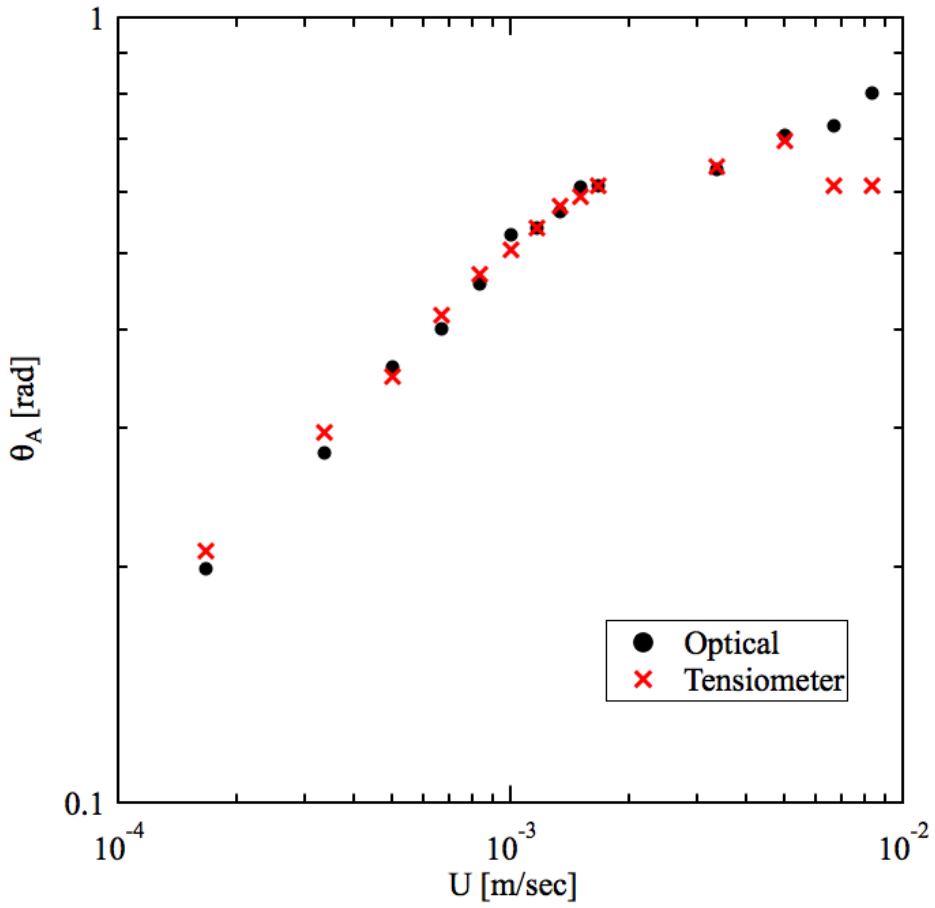

Figure 11.5: The plots of the advancing dynamic contact angle versus the liquid contact line speed for the advancing motion of the silicone oil 100 cSt on the glass substrate.

Figure 11.6 shows the dependency of the advancing dynamic contact angle to the contact line velocity obtained from the Tensiometer and the optical method for the immersion of the glass substrate inside the pool of the glycerin. It shows that the results obtained from Tensiometer, $\theta_{Tensiometer}$, do not match with the results obtained from the optical method, $\theta_{Optical}$ for any speed since the dynamic viscosity of the glycerin is very large subsequently the effect of the viscous force is prominent factor for dynamic contact angle measurement for any speed.

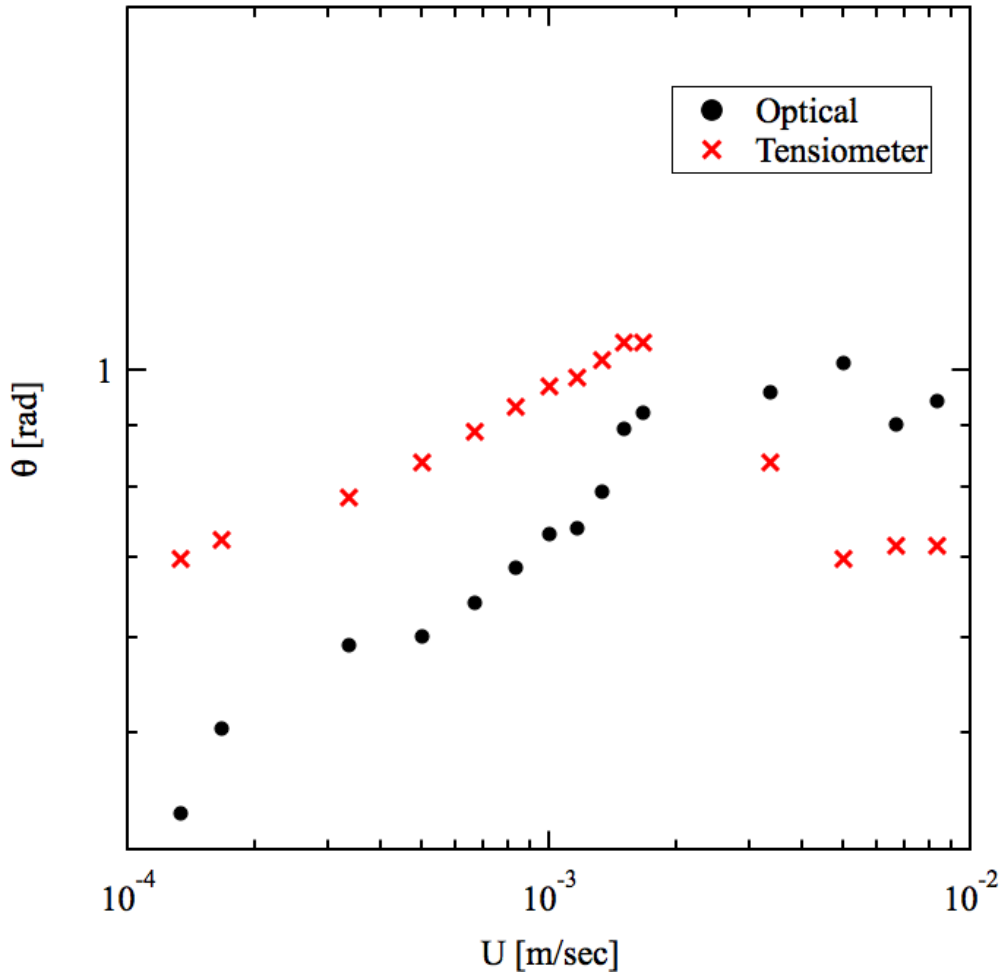

Figure 11.6: The plots of the advancing dynamic contact angle versus the liquid contact line speed for the advancing motion of the glycerin on the glass substrate.

Figure 11.7 shows the dependency of the advancing dynamic contact angle to the contact line velocity obtained from the Tensiometer and the optical method for the immersion of the glass substrate inside the pool of the silicone oil 10000 cSt. Similarly, it shows that the results obtained from Tensiometer, $\theta_{Tensiometer}$, do not match with the results obtained from the optical method, $\theta_{Optical}$ for any speed since the dynamic viscosity of the silicone oil 10000 cSt is very large. Due

to this fact, it is important to include the effect of the viscous force for dynamic contact angle measurement for any speed.

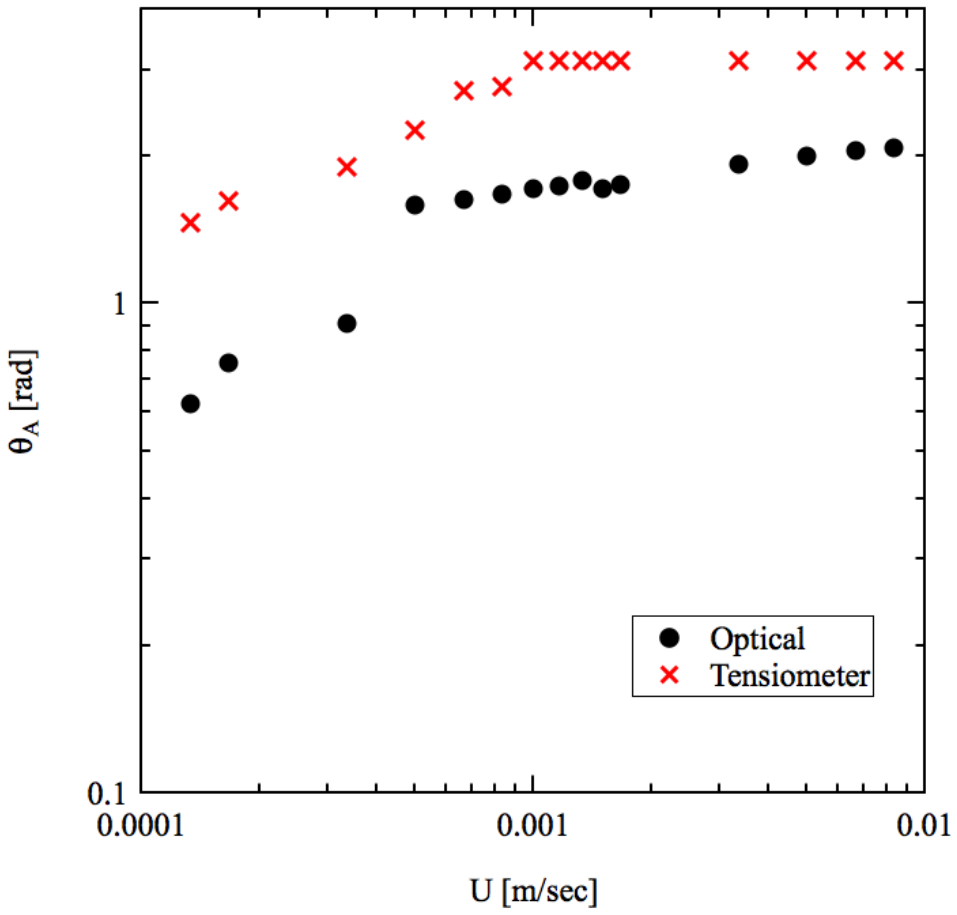

Figure 11.7: The plots of the advancing dynamic contact angle versus the liquid contact line speed for the advancing motion of the silicone oil 10000 cSt on the glass substrate.

To illustrate the significance of the relative importance of the viscous force to the capillary force on the difference between the results obtained from Tensiometer compared to the results obtained from the optical method, the ratio $\theta_{Optical}/\theta_{Tensiometer}$ versus Capillary number was

investigated. Figure 11.8 shows the dependence of the ratio $\theta_{Optical}/\theta_{Tensiometer}$ to the Capillary number for the dip coating (i.e. forced spreading) of silicone oil 100 cSt, silicone oil 10000 cSt, and glycerin on the glass substrate. Based on the fitting analysis, it has been found out that the dependency of the ratio $\theta_{Opitcal}/\theta_{Tensiometer}$ on the Capillary number, Ca, follows the 1/5 power law for liquids with large dynamic viscosities (i.e. glycerin and silicone oil 10000-cSt).

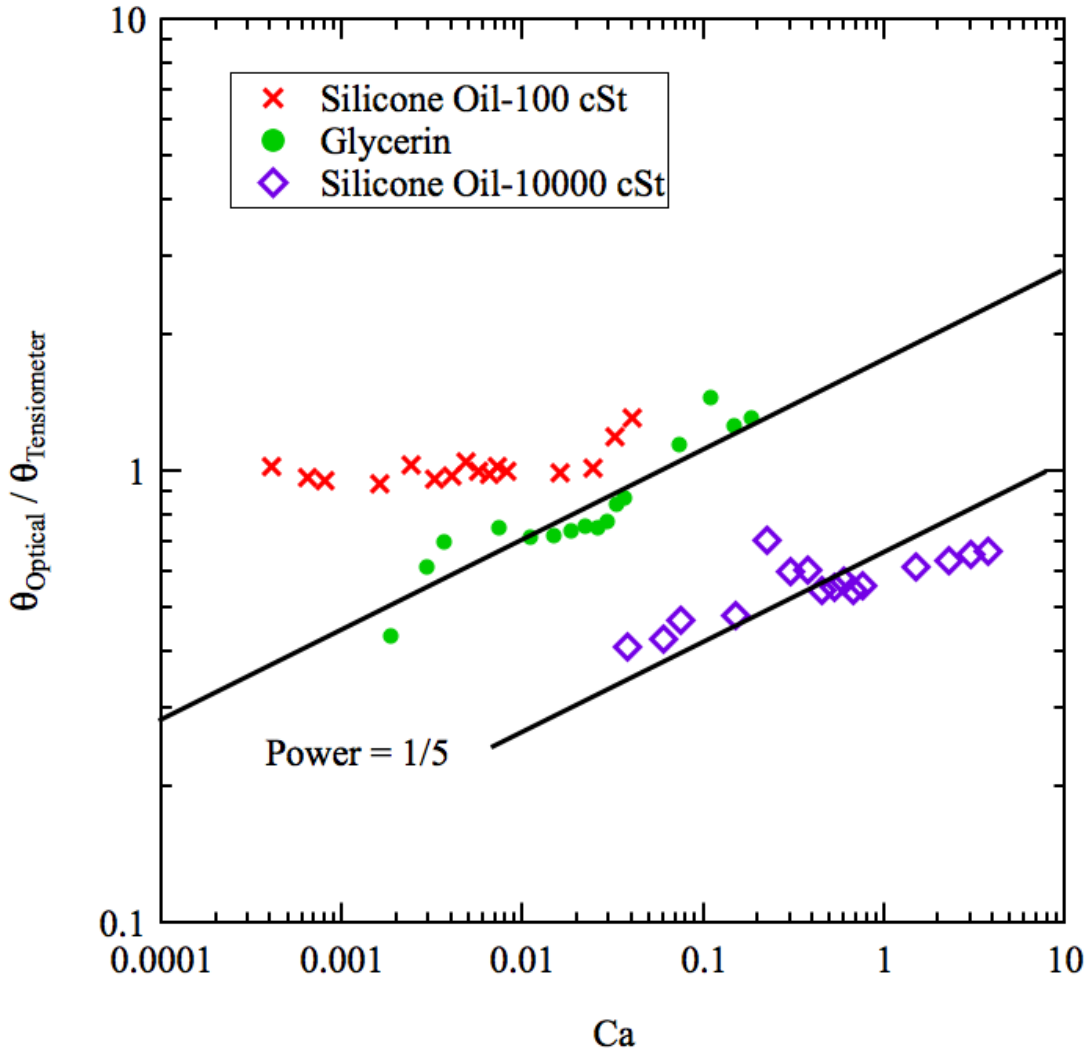

Figure 11.8: The plot of ratio of the results obtained from Tensiometer over the results obtained from the optical method versus Capillary number for dip coating experiments on silicone oil 100 cSt, silicone oil 10000 cSt, and glycerin on glass substrate.

The only challenge in applying the viscous force described in equation 11.17 is the ratio, $\frac{x}{\varepsilon}$, which can be itself a function of the speed of the liquid contact line and physical properties of the liquid. Hence the investigation has been done on the dependency of the ratio $\frac{x}{\varepsilon}$ to the Capillary number that signifies the relative importance of the viscous force to the capillary force. In this

research, it has been assumed that x to be defined as the Capillary length and ε to be defined as the cut-off length. The dynamic contact angles were obtained from the optical method for the speeds of the liquid contact line for which the experiments have been done and $F_{measured}$ values were the values of the measured force obtained from Tensiometer force sensor for the corresponding dynamic contact angles obtained from the optical method. Then the dependence of the ratio $\frac{x}{\varepsilon}$ to the Capillary number, $Ca = \left(\mu U\right)/\sigma$, was obtained by considering the other known parameters to be known in the equation 11.18. Figure 11.9 shows the dependence of the ration $\frac{x}{\varepsilon}$ on the Capillary number for the experiment of dip coating of glass substrate into the pool of the glycerin.

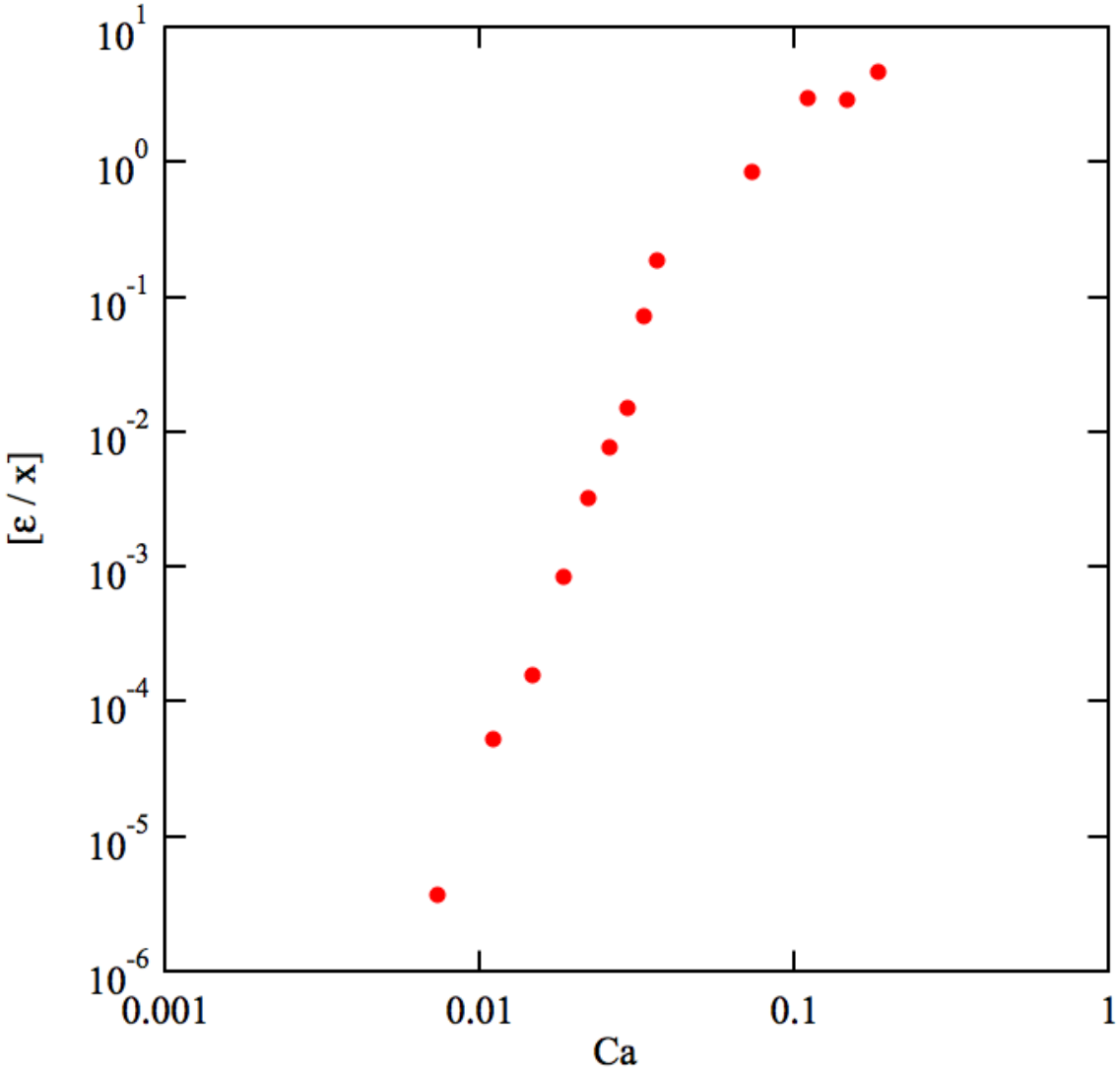

Figure 11.9: The forced spreading (i.e. dip coating) of the glass substrate in to the pool of glycerin.

As it is shown in the figure 11.9, the dependency of the ratio $\frac{x}{\varepsilon}$ on the Capillary number can be defined by power law. For the low Capillary number region over which the cut-off-length is very

smaller than the Capillary length, the dependency follows the 6-power law and beyond the low Capillary number range, over which the cut-off-length is the same size or greater than the Capillary length, the dependency follows the 2-power law.

APPENDICES

Appendix A:

Derivation of hydrodynamics theory based on dimensional analysis can be shown as follows.

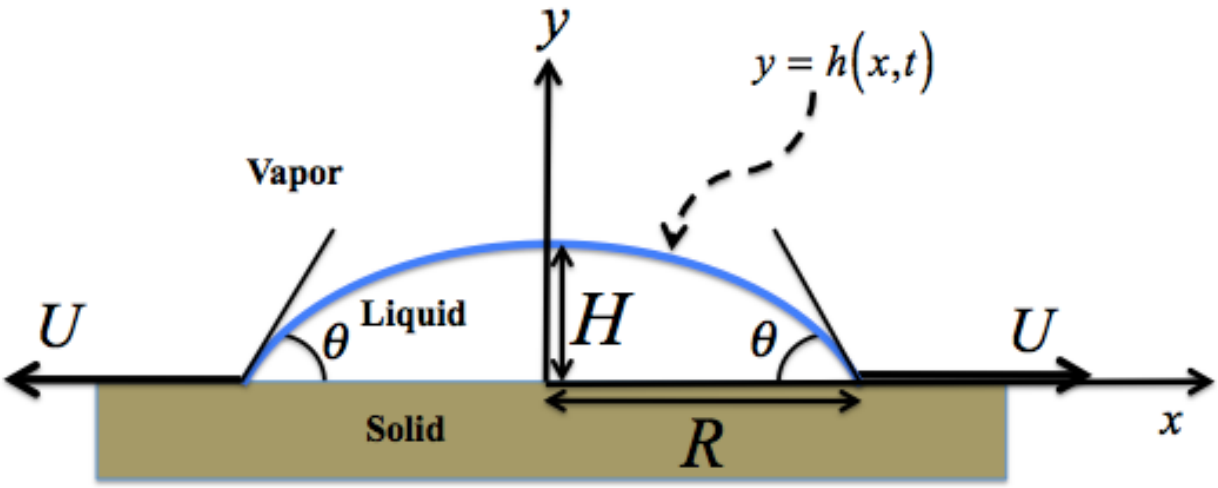

Figure A.1: The schematic picture of the liquid droplet on a solid surface.

Navier-Stokes equations by applying creeping flow approximation, which is known as the Stokes equation.

$$\mu \nabla^2 u \approx \nabla p \tag{A.1}$$

Laplace pressure of the liquid droplet, p, can be defined based on the curvature of the liquid droplet. In equation A.1, μ is the dynamic viscosity of the liquid.

$$p \equiv \sigma \frac{\partial^2 y}{\partial x^2} \tag{A.2}$$

In equation A.2, σ is the surface tension of the liquid.

The Stokes equation can be written for two-dimensional flow as follows:

$$\mu \frac{\partial^2 u}{\partial y^2} \approx \sigma \frac{\partial}{\partial x} \frac{\partial^2 y}{\partial x^2} \tag{A.3}$$

Applying the following dimensional analysis on the Stokes equation, the relation between the size of the liquid droplet (i.e. the radius of the liquid droplet) as a function of time can be obtained as follows:

$$x \approx R \qquad y \approx H \qquad u \equiv U \approx \frac{R}{t} \tag{A.4}$$

$$\mu \frac{\frac{R}{t}}{H^2} \approx \sigma \frac{1}{R} \frac{H}{R^2} \tag{A.5}$$

$$R^4 \approx \frac{\sigma}{\mu} H^3 t \tag{A.6}$$

The volume of the spherical cap, V, of the liquid droplet on the solid surface is described based on the radius of the liquid droplet and the height of the liquid droplet at its center.

$$V \equiv \frac{\pi R^2 H}{2} \tag{A.7}$$

$$R^4 \approx \frac{\sigma}{\mu} \left(\frac{2V}{\pi R^2} \right)^3 t \tag{A.8}$$

$$R^{10} \approx \left(\frac{8 \sigma V^3}{\pi^3 \mu} \right) t \tag{A.9}$$

$$R \approx \left(\frac{8 \sigma V^3}{\mu \pi^3} \right)^{1/10} t^{1/10} \tag{A.10}$$

$$R(t) \propto t^{\frac{1}{10}} \tag{A.11}$$

The relation between the dynamic contact angle, θ, and Capillary number, Ca, can also be obtained using dimensional analysis.

$$\mu \nabla^2 u \approx \nabla p \tag{A.12}$$

$$p \equiv \sigma \frac{\partial^2 y}{\partial x^2} \tag{A.13}$$

$$\mu \frac{\partial^2 u}{\partial y^2} \approx \sigma \frac{\partial}{\partial x} \frac{\partial^2 y}{\partial x^2} \tag{A.14}$$

$$x \equiv R \qquad y \equiv H \qquad u \equiv U \tag{A.15}$$

$$\mu \frac{U}{H^2} \approx \sigma \frac{H}{R^3} \tag{A.16}$$

$$\tan\theta \equiv \frac{H}{R} \tag{A.17}$$

$$\theta \approx \tan\theta \tag{A.18}$$

$$\frac{\mu U}{\sigma} \approx \left(\frac{H}{R} \right)^3 \approx \theta^3 \tag{A.19}$$

$$\theta \approx \left(\frac{\mu U}{\sigma} \right)^{\frac{1}{3}} \equiv Ca^{\frac{1}{3}} \tag{A.20}$$

$$\theta \propto Ca^{\frac{1}{3}} \tag{A.21}$$

Appendix B:

The following values have been applied to calculate the Ohnesorge number, Oh, and the characteristic length of the droplet.

$$Oh = \frac{\mu}{\sqrt{\rho R \sigma}}$$

$$\mu = 0.00432 \left[\text{Pa.sec} \right]$$

$$\sigma \approx 22 \left[\text{mN/m} \right]$$

$$R \approx \left(V \right)^{1/3} \approx 1.375 \left[\text{mm} \right]$$

$$\rho \approx 902.8 kg / m^3$$

$$Oh \approx 7.14 \times 10^{-4} \ll 1$$

$$l_{cap} = \sqrt{\frac{\sigma}{\rho g}} = \sqrt{\frac{22 \times 10^{-3} \left[\text{N/m} \right]}{\left(902.8 \left[\text{kg/m}^3 \right] \right) \left(9.81 \left[\text{m/sec}^2 \right] \right)}} \approx 1.576 \left[\text{mm} \right]$$

$$R < l_{cap}$$

Hence, based on the small magnitude of the Ohnesorge number and small magnitude of the characteristic length of the drop compared to the capillary length, the liquid spherical cap forms on the solid surface when droplet is spreading on solid surface by referring to Kavehpour, Ovryn and McKinley. And the driving force is Capillary and Resisting force is Inertia based on the Table 3 of Kavehpour et al. (2002) [57]. Based on these conclusions, inertia term in Navier-Stokes equation can be balanced with the pressure gradient term using the Laplace pressure term to define the pressure and applying the scaling analysis we could obtain equation 2 that we mentioned in the manuscript.

Inertia terms can be represented as $\rho\frac{\partial u}{\partial t}$ due to the unsteadiness effect or $\rho u\frac{\partial u}{\partial x}$, due to the convective effect.

Capillary term can be represented as $\frac{\partial p}{\partial x}$.

Applying the scaling analysis on the unsteady inertia term, convective inertia term, capillary term (due to Laplace pressure term defined by surface tension and curvature of the dispersed phase bubbles), we get the following terms.

$$\rho\frac{\partial u}{\partial t}\sim\rho\frac{U}{t} \tag{1}$$

$$\rho u\frac{\partial u}{\partial x}\sim\rho\frac{U^2}{R} \tag{2}$$

$$p=\sigma\frac{\partial^2 h}{\partial x^2}\sim\sigma\frac{h}{R^2} \tag{3}$$

$$\frac{\partial p}{\partial x}\sim\sigma\frac{h}{R^3} \tag{4}$$

Characteristic velocity defined based on the radius of the droplet and time of spreading.

$$U\sim\frac{R}{t} \tag{5}$$

Volume of the droplet based on applying the assumption of the thin cylindrical shape of droplet at any time of spreading (applying lubrication assumption):

$$V=\pi R^2 h \tag{6}$$

Hence we can get the following relation:

$$\frac{h}{R^3}=\frac{V}{\pi R^5} \tag{7}$$

By balancing the unsteady inertia term with the capillary term:

$$\rho \frac{\partial u}{\partial t} \sim \frac{\partial p}{\partial x} \tag{8}$$

Based on the scaling analysis obtained earlier, the equation (8) can be written as:

$$\rho \frac{U}{t} \sim \sigma \frac{h}{R^3} \tag{9}$$

Applying equation (5) into equation (9):

$$\rho \frac{R}{t^2} \sim \sigma \frac{h}{R^3} \tag{10}$$

Combining equations (10) and equation (7):

$$\rho \frac{R}{t^2} \sim \frac{\sigma V}{\pi R^5} \tag{11}$$

Hence we get the following relation between the dynamical radius of droplet with time:

$$R^6 \sim \left(\frac{\sigma V}{\rho \pi} \right) t^2 \tag{12}$$

$$R \sim \left(\frac{\sigma V}{\rho \pi} \right)^{1/6} t^{1/3} \tag{13}$$

$$\begin{aligned} R &\sim t^{\frac{1}{3}} \\ R &\sim t^{0.333} \end{aligned} \tag{14}$$

By balancing the convective inertia term and the capillary term:

$$\rho u \frac{\partial u}{\partial x} \sim \frac{\partial p}{\partial x} \tag{15}$$

Based on the scaling analysis obtained earlier, the equation (15) can be written as:

$$\rho \frac{U^2}{R} \sim \frac{\sigma h}{R^3} \tag{16}$$

Combining equation (5), equation (7), and equation (16):

$$\rho \frac{R}{t^2} \sim \frac{\sigma V}{\pi R^5} \tag{17}$$

Hence we get the following relation between the dynamical radius of droplet with time:

$$R^6 \sim \left(\frac{\sigma V}{\rho \pi} \right) t^2 \tag{18}$$

$$R \sim \left(\frac{\sigma V}{\rho \pi} \right)^{\frac{1}{6}} t^{\frac{1}{3}} \tag{19}$$

$$R \sim t^{\frac{1}{3}} \tag{20}$$

As a result, we can conclude that for the stage 2 of the variation of the base diameter versus time, the 1/3 power law would be a good approximation and also it fitted very well with the experimental results.

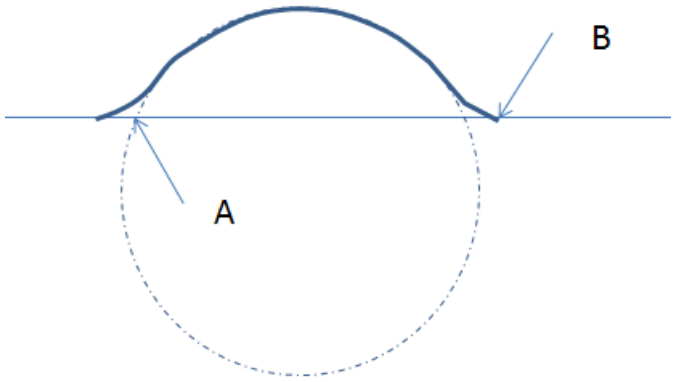

Figure B.1: The schematic representation of the liquid contact line (i.e. denoted by point B) and the “intermediate dynamic liquid contact line” (i.e. denoted by point A).

The contact line we refer to is point **B** in the drawing shown above as shown in figure B.1. Since we used the Young-Laplace equation for fitting the parameters to obtain the slopes of the contact points at the three phase contact points (left and right contact points in the side view). By “intermediate dynamic contact line” we mean point A in 2D side view as illustrated in figure B.1. By “three-phase contact line” or “leading edge of the continuous phase” we mean point B in 2D side view. All the plots that we included in the manuscript are corresponding to the “three-phase contact line” or “leading edge of the continuous phase” which correspond to point B in 2D side view.

REFERECES

1. D. Bonn, J. Eggers, J. Indekeu, J. Meunier, and E. Rolley "Wetting and spreading." *Rev. Mod. Phys.*, **81**(2): 739-805, 2009.

2. T. Young "An Essay on the Cohesion of Fluids" *Phil. Trans. R. Soc. Lond.*, **95**: 65-87, 1805.

3. P. G. de Gennes "Wetting: statics and dynamics" *Rev. Mod. Phys.*, **57**(3): 827-863, 1985.

4. J. W. Gibbs "The Scientific Papers of J. Willard Gibbs" **1**: Thermodynamics, Dover, New York, 1961.

5. R. E. Johnson "Conflicts between Gibbsian Thermodynamics and Recent Treatments of Interfacial Energies in Solid-Liquid-Vapor" *J. Phys. Chem.,* **63**(10): 1655-1658, 1959.

6. X. F. Yang "Equilibrium contact angle and intrinsic wetting hysteresis" *Appl. Phys. Lett.,* **67**(15): 2249-2251, 1995.

7. R. E. Johnson, JR., R. H. Dettre, and D. A. Brandreth "Dynamic Contact Angles and Contact Angle Hysteresis" *J. Colloid Interf. Sci.,* **62**(2): 205-212, 1977.

8. M. E. R. Shanahan "Simple Theory of "Stick-Slip" Wetting Hysteresis" *Langmuir*, **11**(3): 1041-1043, 1995.

9. C. W. Extrand and Y. Kumagai “An Experimental Study of Contact Angle Hysteresis” *J. Colloid Interf. Sci.,* **191**: 378-383, 1997.

10. C. W. Extrand and Y. Kumagai “Liquid-Drops on an Inclined Plane–The Relation Between Contact Angles, Drop shape, and Retentive Force” *J. Colloid Interface Sci.,* **170**: 515-521, 1995.

11. P. G. de Gennes, F. Brochard-Wyart, and D. Quere “Capillarity and wetting phenomena: drops, bubbles, pearls, waves” Springer, New York, 2004.

12. R. N. Wenzel “Resistance of Solid Surfaces to Wetting by Water” *Ind. Eng. Chem.,* **28**(8): 988-994, 1936.

13. S. Baxter and A. B. D. Cassie “8-The Water Repellency of Fabrics and a New Water Repellency Test” *J. Textile Inst.,* **36**: T67, 1945.

14. A. B. D. Cassie and S. Baxter “Wettability of porous surfaces” *Trans. Faraday Soc.*, **40**: 546-551, 1944.

15. R. J. Hansen and T. Y. Toong “Interface Behavior as One Fluid Completely Displaces Another from a Small-Diameter Tube” *J. Colloid Interf. Sci.*, **36**(3): 410-413, 1971.

16. R. L. Hoffman "A Study of Adavncing Interface 1. Interface Shape in Liquid-Gas Systems" *J. Colloid Interf. Sci.*, **50**(2): 228-241 ,1975.

17. M. Bracke, F. De Voeght, and P. Joos “The kinetics of wetting: the dynamic contact angle” *Prog. Coll. Pol. Sci. S*, **79**: 142-149, 1989.

18. G. R. Zvan, L. J. Douglas, and S. F. Kistler “A Novel Method for Dynamic Contact Angle Measurement” *International symposium on Coating Process Science & Technology.* Spring National Meeting, New Orleans, LA, 1992.

19. M. N. Esmail and M. T. Ghannam “Air Entrainment and Dynamic Contact Angles in Hydrodynamics of Liquid Coating” *Can. J. Chem. Eng.*, **68** (2): 197-203, 1990.

20. S. F. Kistler and J. C. Berg “Wettability: Hydrodynamics of Wetting”, Marcel Dekker, New York, **49**: 311-429, 1993.

21. G. Berteloot, C.-T. Pham, A. Daerr, F. Lequeux, and L. Limat “Evaporation-induced flow near a contact line: Consequences on coating and contact angle” *EPL-Europhys. Lett.*, **83**: 140031-140035, 2008.

22. J. Ashmore, A. Q. Shen, H. P. Kavehpour, H. A. Stone and G. H. McKinley "Coating flows of non-Newtonian fluids: weakly and strongly elastic limits." *J. Eng. Math.,* **60**(1): 17-41, 2008.

23. M. Schneemilch, R. A. Hayes, J. G. Petrov, and J. Ralston ”Dynamic Wetting and Dewetting of a Low-Energy Surface by Pure Liquids” *Langmuir*, **14**: 7047-7051, 1998.

24. T. D. Blake and M. Bracke “Experimental evidence of nonlocal hydrodynamic influence on the dynamic contact angle” *Phys. Fluids*, **11**(8): 1995-2007, 1999.

25. K. M. Smyth and K. K. Varanasi “Wetting Hysteresis and Droplet Roll Off Behavior on Superhydrophobic Surfaces”, Bachelor of Science degree Thesis at Massachusetts Institute of Technology, 2010.

26. H. Li, M. Paneru, R. Sedev, and J. Ralston “Dynamic Electrowetting and Dewetting of Ionic Liquids at a Hydrophobic Solid-Liquid Interface” *Langmuir*, **29**: 2631-2639, 2013.

27. W. C. Nelson, P. Sen, and CJ Kim “Dynamic Contact Angles and Hysteresis under Electrowetting-on-Dielectric” *Langmuir*, **27**: 10319-10326, 2011.

28. M. J. Vega, C. Gouttiere, D. Seveno, T. D. Blake, M. Voue, and J. De Coninck “Experimental Investigation of the Link between Static and Dynamic Wetting by Forced Wetting of Nylon Filament” *Langmuir*, **23**: 10628-10634, 2007.

29. J. G. Petrov, J. Ralston, M. Schneemilch, and R. A. Hayes “Dynamics of Partial Wetting and Dewetting in Well-Defined Systems”, *J. Phys. Chem. B*, **107**: 1634-1645, 2003.

30. J. G. Petrov, J. Ralston, M. Schneemilch, and R. A. Hayes “Dynamics of Partial Wetting and Dewetting of an Amorphous Fluoropolymer by Pure Liquids” *Langmuir*, **19**: 2795-2801, 2003.

31. W. Xiao-dong, P. Xiao-feng, and W. Bu-xuan "Effect of Solid Surface Properties on Dynamic Contact Angles" *Heat Trans. Asian Res.*, **35**(1): 1-12, 2006.

32. A. Mohammad Karim and H. P. Kavehpour "Spreading of emulsions on a solid substrate" *J. Coat. Technol. Res.*, **11**(1): 103-108, 2014.

33. B. S. Kennedy and R. Burley "Dynamic Fluid Interface Displacement and Prediction of Air Entrainment" *J. Colloid Interf. Sci.*, **62**(1): 48-62, 1976.

34. J. T. Korhonen, T. Huhtamaki, O. Ikkala, and R. H. A. Ras "Reliable Measurement of the Receding Contact Angle" *Langmuir*, **29**: 3858-3863, 2013.

35. A. T. Paxson and K. K. Varanasi "Self-similarity of contact line depinning from textured surfaces" *n. comms.*, **2482**: 1-8, 2013.

36. S. Semal, M. Voue, M. J. de Ruijter, J. Dehuit, and J. De Coninck "Dynamics of Spontaneous Spreading on Heterogeneous Surfaces in a Partial Wetting Regime" *J. Phys. Chem. B*, **103**: 4854-4861, 1999.

37. J. Ralston, M. Popescu, and R. Sedev "Dynamics of Wetting from an Experimental Point of View" *Annu. Rev. Mater. Res.*, **38**: 23-43, 2008.

38. K. K. Varanasi, T. Deng, M. F. Hsu, N. Bhate “Design of Superhydrophobic Surfaces for Optimum Roll-off and Droplet Impact Resistance”, *ASME,* 1-9, 2008.

39. M. Cachile, A. M. Cazabat, S. Bardon, M. P. Valignat, and F. Vandenbrouck “Spontaneous spreading of surfactant solutions on hydrophilic surfaces” *Colloid. Surface.,* **159**: 47-56, 1999.

40. R. A. Hayes and J. Ralston “Forced Liquid Movement on Low Energy Surfaces” *J. Colloid. Interf. Sci.*, **159**: 429-438, 1993.

41. J. E. Forester, J. M. Sunkel and J. C. Berg "Spontaneous spreading of emulsions on solid surfaces: Morphology and dynamics" *J. Appl Polym. Sci.*, **81**(7): 1817-1825, 2001.

42. S. Semal, M. Voue, and J. De Coninck “Dynamics of Spontaneous Spreading on Energetically Adjustable Surfaces in a Partial Wetting Regime” *Langmuir*, **15**: 7848-7854, 1999.

43. A. C. Zettlemoyer “Hydrophobic Surfaces” *J. Colloid Interf. Sci.*, **28**(3/4): 343-369, 1968.

44. S. Sikalo, H. –D. Wilhelm, I. V. Roisman, S. Jakirlic, and C. Tropea “Dynamic contact angle of spreading droplets: Experiments and simulations” *Phys. Fluids*, **17**: 062103 , 2005.

45. J. D. Chen and N. Wada "Wetting Dynamics of the Edge of a Spreading Drop" *Phys. Rev. Lett.,* **62**(26): 3050-3053, 1989.

46. L. M. Hocking and A. D. Rivers “The spreading of a drop by capillary action” *J. Fluid Mech.*, **121**: 425-442, 1982.

47. R. J. Hansen and T. Y. Toong “Dynamic Contact Angle and Its Relationship to Forces of Hydrodynamic Origin” *J. Colloid Interf. Sci.*, **37**(1): 196-207, 1971.

48. P. G. Petrov and J. G. Petrov “Comparison of the static and dynamic contact angle hysteresis at low velocities of the three-phase contact line” *Colloid. Surface.*, **61**: 227-240, 1991.

49. P. Ehrhard “Experiments on isothermal and non-isothermal spreading” *J. Fluid Mech.,* **257**: 463-483, 1993.

50. A. M. Cazabat and M. A. C. Stuart "Dynamics of Wetting: Effects of Surface Roughness" *J. Phys. Chem.,* **90**(22): 5845-5849, 1986.

51. H. P. Kavehpour “An Interferometric Study of Spreading Liquid Films” Thesis, Massachusetts Institute of Technology, 2003.

52. A. Oron, A., S. H. Davis, and S. G. Bankoff "Long-scale evolution of thin liquid films." *Rev. Mod. Phys.*, **69**(3): 931-980, 1997.

53. G. McHale, M. I. Newton, S. M. Rowan, and M. Banerjee "The spreading of small viscous stripes of oil" *J. Phys. D: Applied Phys.*, **28**(9): 1925-1929, 1995.

54. H. P. Kavehpour, B. Ovryn, and G. H. McKinley ”Microscopic and Macroscopic Structure of the Precursor Layer in Spreading Viscous Drops” *Phys. Rev. Lett.*, **91**(19): 1961041-1961044, 2003.

55. H. E. Seebergh and J. C. Berg “A comparison of force and optical techniques for the measurement of dynamic contact angles” *Chem. Eng. Sci.*, **47**(17/18): 4468-4470, 1992.

56. E. B. Dussan V., E. Rame, and S. Garoff “On indentifying the appropriate boundary conditions at a moving contact line: an experimental investigation” *J. Fluid Mech.*, **230**: 97-116, 1991.

57. P. Kavehpour, B. Ovryn and G. H. McKinley "Evaporatively-driven Marangoni instabilities of volatile liquid films spreading on thermally conductive substrates." *Colloid. Surface. a.*, **206**(1-3): 409-423, 2002.

58. H. E. Huppert "The propagation of two-dimensional and axisymmetric viscous gravity currents over a rigid horizontal surface” *J. Fluid Mech.,* **121**: 43-58, 1982.

59. H. P. Greenspan "On the motion of a small viscous droplet that wets a surface" *J. Fluid Mech.*, **84**: 125-143, 1978.

60. P. G. Petrov and J. G. Petrov “A Combined Molecular-Hydrodynamic Approach to Wetting Kinetics” *Langmuir*, **8**: 1762-1767, 1992.

61. H. Eyring, *Cold Spring Symposia on Quantitative Biology*, **3**, 1935.

62. E. B. Dussan V. "The moving contact line: the slip boundary condition" *J. Fluid Mech.,* **77**: 665-684, 1976.

63. C. G. Ngan and E. B. Dussan V. "On the dynamics of liquid spreading on solid surfaces" *J. Fluid Mech.*, **209**: 191-226, 1989.

64. L. M. Hocking "A moving fluid interface. Part 2. The removal of the force singularity by a slip flow" *J. Fluid Mech.,* **79**: 209-229, 1977.

65. M. J. de Ruijter and J. De Coninck, and G. Oshanin "Droplet Spreading: Partial Wetting Regime Revisited" *Langmuir*, **15**: 2209-2216, 1999.

66. C. Huh and S. G. Mason "The steady movement of a liquid meniscus in a capillary tube", *J. Fluid Mech.*, **81**: 401-419, 1977.

67. T. D. Blake and J. M. Haynes "Kinetics of liquid/liquid displacement" *J. Colloid Interf. Sci.*, **30**: 421-423, 1969.

68. T. D. Blake and J. C. Berg "Wettability: Dynamic Contact Angles and Wetting Kinetics", Marcel Dekker, New York, **49**: 251-309, 1993.

69. E. B. Dussan and S. H. Davis “On the motion of a fluid-fluid interface along a solid surface” *J. Fluid Mech.*, **65**: 71-95, 1974.

70. O. V. Voinov "Hydrodynamics of Wetting" *Izvestiya Akademii Nauk SSSR, Mekhanika Zhidkosti i Gaza*, (5): 714-721, 1976.

71. R. G. Cox “The dynamics of the spreading of liquids on a solid surface. Part 1. Viscous flow” *J. Fluid Mech.,* **168**: 169-194, 1986.

72. L. Landau and B. Levich “Dragging of a Liquid by a Moving Plate” *Acta Physicochim. U.R.S.,* **17**(1-2): 42-54, 1942.

73. P. G. de Gennes “Deposition of Langmuir-Blodgett layers” *Coll. Polym. Sci.*, **264**: 463-465, 1986.

74. C. Huh and L. E. Scriven “Hydrodynamic Model of Steady Movement of a Solid/Liquid/Fluid Contact Line”, *J. Colloid Interf. Sci.*, **35**(1): 85-101, 1971.

75. S. Glasstone, K. J. Laidler, and H. J. Eyring “The Theory of Rate Processes”, McGraw-Hill, New York, 1941. Papers cited there, especially, Powell, R. E., Roseveare, W. E., and Eyring, H., *Ind. Eng. Chem.*, **33**, 430, 1941.

76. H. J. Ensikat, P. Ditsche_Kuru, C. Neinhuis, and W. Barthlott “Superhydrophobicity in perfection: the outstanding properties of the lotus leaf”, *Beilstein J. Nanotechnol.,* **2**: 152-161, 2011.

77. A. L. Yarin “Drop Impact Dynamics: Splashing, Spreading, Receding, Bouncing…” *Annu. Rev. Fluid Mech.*, **38**: 159-192, 2006.

78. J. S. Rowlinson and B. Widom “Molecular Theory of Capillarity” Oxford: Clarendon, 1982.

79. L. M. Hocking "Rival contact-angle models and the spreading of drops" *J. Fluid Mech.,* **239**: 671-681, 1992.

80. M. J. Davis and S. H. Davis “Droplet spreading: Theory and experiments” *C. R. Phys.*, **14**: 629-635, 2013.

81. E. B. Dussan “On the Spreading of Liquids on Solid Surfaces: Static and Dynamic Contact Lines” *Ann. Rev. Fluid Mech.*, **11**: 371-400, 1979.

82. L. Leger and J. F. Joanny “Liquid spreading” *Rep. Prog. Phys.*, 431-486, 1992.

83. A. E. Seaver and J. C. Berg “Spreading of a Droplet on a Solid Surface” *J. Appl. Polym. Sci.*, **52**: 431-435, 1994.

84. T. D. Blake “The physics of moving wetting lines” *J. Colloid Interf. Sci.*, **299**: 1-13, 2006.

85. A. Eddi, K. G. Winkels, and J. H. Snoeijer “Short time dynamics of viscous drop spreading” *Phys. Fluids*, 1-19, 2012.

86. D. Seveno, A. Vaillant, R. Rioboo, H. Adao, J. Conti, and J. De Coninck “Dynamics of Wetting Revisited” *Langmuir*, **25**(22): 13034-13044, 2009.

87. J. H. Snoeijer and B. Andreotti “Moving Contact Lines: Scales, Regimes, and Dynamical Transitions” *Annu. Rev. Fluid Mech.*, **45**: 269-292, 2013.

88. L. H. Tanner "The spreading of silicone oil drops on horizontal surface” *J. Phys. D: Appl. Phys.*, **12**(9): 1473-1484 ,1979.

89. L. W. Schwartz “Modeling and simulation of wetting and spreading phenomena for thin liquid films” *Anziam J.*, **49**: C69-C84, 2007.

90. Jean-Baptiste Dupont, D. Legendre “Numerical simulation of static and sliding drop with contact angle hysteresis” *J. Comput. Phys.*, **229**: 2453-2478, 2010.

91. L. M. Hocking "The Spreading of a Thin Drop by Gravity and Capillarity" *Q. J. Mech. Appl. Math.*, **36**: 55-69, 1983.

92. J. J. Thalakkottor and K. Mohseni “Analysis of Boundary Slip in a Flow with an Oscillating Wall” *Phys. Rev. E*, **87**: 0330181-03301810, 2013.

93. C. J. Hirasaki and S. Y. Yang “Dynamic contact line with disjoining pressure, large capillary numbers, large angles and pre-wetted, precursor, or entrained films” *Contact Angle, Wettability and Adhesion*, **2**: 1-30, 2002.

94. E. O. Tuck and L. W. Schwartz “A Numerical and Asymptotic Study of Some Third-Order Ordinary Differential Equations Relevant to Draining and Coating Flows” *SIAM Review*, **32**(3): 453-469, 2001.

95. N. Sedighi, S. Murad, and S. K. Aggarwal “Molecular dynamics simulations of spontaneous spreading of a nanodroplet on solid surfaces” *Fluid Dyn. Res.,* **43**: 1-22, 2011.

96. J. Eggers and H. A. Stone “Characteristic lengths at moving contact lines for a perfectly wetting fluid: the influence of speed on the dynamic contact angle” *J. Fluid Mech.*, **505**: 309-321, 2004.

97. P. Levinson, A. M. Cazabat, M. A. C. Stuart, F. Heslot, and S. Nicolet "The spreading of a macroscopic droplets" *Rev. Phys. Appl.,* **23**(6): 1009-1016, 1988.

98. W. Barthlott and C. Neinhuis “Purity of the sacred lotus, or escape from contamination in biological surfaces”, *Planta*, **202**, 1-8, 1997.

99. L. Gao, T. J. McCarthy, and X. Zhang "Wetting and Superhydrophobicity" *Langmuir,* **25**(24): 14100-14104, 2009.

100. A. Nakajima "Design of hydrophobic surfaces for liquid droplet control" *NPG Aisa Mater.*, **3**: 49-56, 2011.

101. Y. Pomeau and J. Vannimenus "Contact Angle on Heterogeneous Surfaces: Weak Heterogeneities" *J. Colloid Interf. Sci.*, **104**(2): 477-488, 1985.

102. M. L. Heck and D. V. Papavassiliou "Effects of Hydrophobicity-Inducing Roughness on Micro-Flows" *Chem. Eng. Commun.*, **200**: 919-934, 2013.

103. K. M. Smyth, A. T. Paxson, H. Kwon, and K. K. Varanasi "Visualization of contact line motion on hydrophobic textures" *Surface Innovations*, 1(S12): 84-91, 2013.

104. M. von Bahr, F. Tiberg, and V. Yaminsky "Spreading dynamics of liquids and surfactant solutions on partially wettable hydrophobic substrates" *Colloid. Surface.*, **193**: 85-96, 2001.

105. A. Lafuma and D. Quere "Superhydrophobic states" *nat. mater.*, **2**: 457-460, 2003.

106. B. He, J. Lee, and N. A. Patankar "Contact angle hysteresis on rough hydrophobic surfaces" *Colloid. Surface.*, **248**: 101-104, 2004.

107. J. F. Joanny and P. G. de Gennes "A model for contact angle hysteresis" *J. Chem. Phys.,* **81**(1): 552-562, 1984.

108. V. S. Kumar K, B. A. Puthenvettil "Shape and motion of drops in the inertial regime" *Preceedings of the 13th Asian Congress of Fluid Mechanics*, Dhaka, Bangladesh, 2010.

109. D. Oner and T. J. McCarthy "Ultrahydrophobic Surfaces. Effects of Topography Length Scales on Wettability" *Langmuir*, **16**: 7777-7782, 2000.

110. P. Van Remoortere and P. Joos "The Kinetics of Wetting: the Motion of a Three Phase Contactline in A Capillary" *J. Colloid Interf. Sci.*, **141**(2): 348-359, 1991.

111. O. Benichou, M. Cachile, A. M. Cazabat, C. Poulard, M. P. Valignat, F. Vandenbrouck, and D. Van Effenterre "Thin films in wetting and spreading" *Adv. Colloid Interface*, **100-102**: 381-398, 2003.

112. J. Lopez, C. A. Miller, and E. Ruckenstein "Spreading kinetics of liquid drops on solids" *J. Colloid. Interf. Sci.*, **56**: 460-468, 1976.

113. E. Saiz and A. P. Tomsia "Atomic dynamics and Marangoni films during liquid-metal spreading" *nat. mater.*, **3**: 903-909, 2004.

114. E. Saiz and A. P. Tomsia "Kinetics of high-temperature spreading" *Curr. Opin. Solid St. M.*, **9**: 167-173, 2005.

115. E. Saiz, A. P. Tomsia, N. Rauch, C. Scheu, M. Ruehle, M. Benhassine, D. Seveno, J. de Coninck, and S. Lopez-Esteban "Nonreactive spreading at high temperature: Molten metals and oxides on molybdenum" *Phys. Rev. E*, **76**: 0416021-04160215, 2007.

116. M. J. de Ruijter, T. D. Blake, and J. De Coninck "Dynamic Wetting Studied by Molecular Modeling Simulations of Droplet Spreading" *Langmuir*, **15**: 7836-7847, 1999.

117. P. Roach, N. J. Shirtcliffe, and M. I. Newton "Progress in Superhydrophobic Surface Development" *Soft matter*, **4**: 224-240, 2008.

118. J. D. Chen "Experiments on a spreading drop and its contact angle on a solid" *J. Colloid Interf. Sci.*, **122**: 60-72, 1988.

119. J. A. Marsh, S. Garoff, and E. B. Dussan V. "Dynamic Contact Angles and Hydrodynamics near a Moving Contact Line" *Phys. Rev. Lett.*, **70**(18): 2778-2781, 1993.

120. V. M. Starov "Spreading of droplets of nonvolatile liquids over a flat solid surface" *Colloid J. USSR*, **45**: 1009-1015, 1983.

121. P. Ehrhard and S. H. Davis “Non-isothermal spreading of liquid drops on horizontal plates” *J. Fluid Mech.*, **229**: 365-388, 1991.

122. H. Kamusewitz, W. Possart, and D. Paul “The relation between Young’s equilibrium contact angle and the hysteresis on rough paraffin wax surfaces” *Colloid. Surface.*, **156**: 271-279, 1999.

123. P. Neogi “Bead formation near the contact line in forced spreading” *Chem. Eng. Sci.*, **65**: 4572-4578, 2010.

124. A. Chawla, G. Buckton, K. M. G. Taylor, J. M. Newton, and M. C. R. Johnson “Wilhelmy plate contact angle data on powder compacts: considerations on plate perimeter” *Eur. J. Pharm. Sci.*, **2**: 253-258, 1994.

125. G. Zografi and B. A. Johnson “Effects of surface roughness on advancing and receding contact angles” *Int. J. Pharm.*, **22**: 159-176, 1984.

126. D. P. Hoult “Oil Spreading on the Sea” *Annu. Rev. Fluid Mech.*, 341-368, 1972.

127. B. M. Weon and J. H. Je “Self-Pinning by Colloids Confined at a Contact Line” *Phys. Rev. Lett.*, **110**: 0283031-0283035, 2013.

128. F. Brochard-Wyart and P. G. de Gennes "Dynamics of partial wetting" *Adv. Colloid Interface*, **39**: 1-11, 1992.

129. M. Ramiasa, J. Ralston, R. Fetzer, and R. Sedev "Contact Line Friction in Liquid-Liquid Displacement on Hydrophobic Surfaces" *J. Phys. Chem. C*, **115** (50): 24975-24986, 2011.

130. J. M. Gomba and G. M. Homsy "Analytical Solutions for Partially Wetting Two-Dimensional Droplets" *Langmuir*, **25**(10): 5684-5691, 2009.

131. R. Goodwin and G. M. Homsy "Viscous flow down a slope in the vicinity of a contact line" *Phys. Fluids A-Fluid*, **3**(4): 515-528, 1991.

132. J. G. Petrov and P. G. Petrov "Molecular-Hydrodynamic Description of Langmuir-Blodgett Deposition" *Langmuir*, **14**: 2490-2496, 1998.

133. D. M. Anderson and S. H. Davis "The spreading of volatile liquid droplets on heated surfaces" *Phys. Fluids*, **7**(2): 248- 265,1995.

134. M. Benhassine, E. Saiz, A. P. Tomsia, and J. De Coninck "Nonreactive spreading at high-temperature revisited for metal systems via molecular dynamics" *Langmuir*, **25**: 11450-11458, 2009.

135. L. W. Schwartz, D. Roux, J. J. Cooper-White "On the shapes of droplets that are sliding on a vertical wall" *Physica D*, **209**: 236-244, 2005.

136. J. F. Oliver and S. G. Mason "Liquid spreading on rough metal surfaces" *J. Mater. Sci.*, **15**: 431-437, 1980.

137. C. Dorrer and J. Ruhe "Some thoughts on superhydrophobic wetting" *soft matter*, **5**: 51-61, 2009.

138. B. Bhushan and Y. C. Jung "Wetting study of patterned surfaces for superhydrophobicity" *Ultramicroscopy*, **107**: 1033-1041, 2007.

139. R. E. Johnson, Jr. and R. H. Dettre "Contact Angle Hysteresis. III. Study of an Idealized Heterogeneous Surface" *J. Phys. Chem.*, **68**(7): 1744-1750, 1964.

140. S. Rafai, D. Sarker, V. Bergeron, J. Meunier, and D. Bonn "Superspreading: Aqueous Surfactant Drops Spreading on Hydrophobic Surfaces" *Langmuir*, **18**: 10486-10488, 2002.

141. H. Gelderblom, A. G. Marin, H. Nair, A. van Houselt, L. Lefferts, J. H. Snoeijer, and D. Lohse "How water droplets evaporate on a superhydrophobic substrate" *Phys. Rev. E*, **83**: 0263061-0263066, 2011.

142. M. K. Chaudhury and G. M. Whitesides "How to Make Water Run Uphill" *Science*, **256**(5063): 1539-1541, 1992.

143. D. Quere and P. Aussillous "Non-Stick Droplets" *Chem. Eng. Technol.*, **25**(9): 925-928, 2002.

144. D. Quere "Non-sticking drops" *Rep. Prog. Phys.*, **68**: 2495-2532, 2005.

145. P. Collet, J. De Coninck, F. Dunlop, and A. Regnard "Dynamics of the Contact Line: Contact Angle Hysteresis" *Phys. Rev. Lett.*, **79**(19): 3704-3707, 1997.

146. A. Nakajima, K. Hashimoto, and T. Watanabe "Recent studies on super-hydrophobic films" *Monatsh. Chem.*, **132**(1): 31-41, 2001.

147. G. McHale, N. J. Shirtcliffe, and M. I. Newton "Super-hydrophobic and super-wetting surfaces: Analystical potential?" *Analyst*, **129**: 284-287, 2004.

148. I. P. Parkin and R. G. Palgrave "Self-cleaning coatings" *J. Mater. Chem.*, **15**: 1689-1695, 2005.

149. M. Callies and D. Quere "On water repellency" *Soft Matter*, **1**: 55-61, 2005.

150. X. Feng and L. Jiang “Design and Creation of Superwetting/Antiwetting Surfaces” Adv. Mater., **18**: 3063-3078, 2006.

151. A. Solga, Z. Cerman, B. F. Striffler, M. Spaeth, and W. Barthlott “The dream of staying clean: Lotus and biomimetic surfaces” *Bioinsp. Biomim.*, **2**: 126-134, 2007.

152. P. Becher “Emulsions: Theory and Practice” *American Chemical Society*, Washington D.C., 2001.

153. J. H. Kim, H. P. Kavehpour & J. P. Rothstein “Dynamic contact angle measurements on superhydrophobic surfaces.” *Phys. Fluids*, **27**: 032107, 2015.

154. D. Song, R. J. Daniello & J. P. Rothstein “Drag reduction using superhydrophobic sanded Teflon surfaces.” *Exp. Fluids*, **55**: 1783, 2014.

155. J. Ou, B. Perot & J. P. Rothstein “Laminar drag reduction in microchannels using ultrahydrophobic surfaces.” *Phys. Fluids,* **16**: 4635-4643, 2004.

156. R. J. Daniello, N. E. Waterhouse & J. P. Rothstein “Drag reduction in turbulent flows over superhydrophobic surfaces.” *Phys. Fluids*, **21**: 085103, 2009.

157. M. Apel-Paz & A. Marmur “Spreading of liquids on rough surfaces.” *Colloid. Surface.* **146**: 273-279, 1999.

158. A. M. Cazabat & M. A. Cohen Stuart "Dynamics of wetting on smooth and rough surfaces." *Prog. Coll. Pol. Sci. S.* **74**: 69-75, 1987.

159. S. J. Kim, J. Kim, M. W. Moon, K. R. Lee, & H. Y. Kim "Experimental study of drop spreading on textured superhydrophilic surfaces." *Phys. Fluids* **25**: 092110, 2013.

160. J. F. Oliver & S G. Mason "Microspreading studies on rough surfaces by scanning electron microscopy." *J. Colloid. Interf. Sci.* **60**: 480-487, 1977.

161. A. Mohammad Karim & H. P. Kavehpour "Dynamics of spreading on ultra-hydrophobic surfaces." *J. Coat. Technol. Res.* **12**(5): 959-964, 2015.

162. A. Mohammad Karim & H. P. Kavehpour "Spreading of emulsions on a solid substrate." *J. Coat. Technol. Res.* **11**(1): 103-108, 2014.

163. T. D. Blake, J. C. Femandez-Toledano, G. Doyen, and J. De Coninck "Forced Wetting and Hydrodynamic Assist." *Phys. Fluids* (In Press).